AN ABSTRACT OF THE THESIS OF

Peter J. Wampler for the degree of Master of Science in Geology

presented on April 13, 1994.

Title: Geology, Hydrothermal Alteration, and Geographic Information System Analysis of the Zortman Mine Area, Montana

Redacted for Privacy

Abstract approved: _____

John H. Dilles

The Zortman and Landusky mines together comprise one of the largest gold occurrences in northeast-central Montana. As of January, 1993, the combined Zortman and Landusky mines had proven and probable reserves of 96,355,000 tons, grading 0.018 ounces of gold per ton, totalling 1,776,000 contained ounces of gold. Zortman and Landusky are exceptional epithermal deposits in that they are spatially associated with shallowly emplaced silicic-alkalic, porphyritic, granitic intrusions of Paleocene age.

Geologic mapping within a 14 square kilometer area surrounding the Zortman Mine identified several silicic porphyry intrusive complexes shallowly emplaced, during multiple intrusive episodes, into Archean crystalline rocks and Paleozoic sedimentary rocks. Whole rock geochemical compositions of the unaltered porphyries surrounding the Zortman Mine indicate that the porphyries are

unaltered and apparently post-mineralization. Whole rock geochemical analysis of the least altered porphyries yielded 64 to 68 weight percent SiO_2, 3 to 6 weight percent K_2O, and 5 to 6 weight percent Na_2O; whereas potassically altered samples yielded 65 to 69 weight percent SiO_2, 9 to 12 weight percent K_2O, and 0.1 to 1.1 weight percent Na_2O. North-northwest striking shear zones, which have strike lengths ranging in the hundreds of meters, localize epithermal mineralization. Prominent joint sets measured in outcrop include north-northwest-, north-south-, and east-west-striking joints. Master joints, often visible only in aerial photography and satellite imagery, are relatively common in the porphyritic intrusive rocks and may have controlled hydrothermal mineralization locally.

Widespread potassium metasomatism, characterized by replacement of feldspars by adularia + sericite, and replacement of mafic minerals by sericite, is common surrounding the mine area and encloses all zones of economic mineralization. An initial widespread weak sericite + pyrite alteration is characterized by partial replacement of primary sanidine and plagioclase feldspars by sericite $\pm$ quartz $\pm$ pyrite $\pm$ adularia(?) $\pm$ fluorite(?) $\pm$ calcite $\pm$ quartz(?), and replacement of mafic minerals by sericite $\pm$ pyrite.

Weak sericite + pyrite alteration appears to predate shear-zone-controlled adularia + pyrite alteration and adularia + jarosite overgrowth veins. The overgrowth veins are similar to adularia overgrowth veins described at the Round Mountain epithermal gold deposit in Nevada. Pervasive adularia + pyrite alteration occurs central to a larger zone of overgrowth adularia + jarosite alteration. Pervasive adularia + pyrite alteration is characterized by complete (>90 volume

percent) replacement of primary plagioclase and potassium feldspar phenocrysts by adularia, 2 to 10 volume percent pyrite addition, and no apparent change in SiO_2 content. Mafic minerals are typically either completely destroyed, or are completely altered to sericite. Increasing degrees of alteration, observable in thin section and whole rock geochemical analyses, are commonly not conspicuous in hand sample. Both open-space- and replacement-type adularia veins were observed in thin section. Veins tend to be dominated by quartz in the groundmass, and often contain adularia only when passing through potassium or plagioclase feldspar phenocrysts. Minerals which occur within adularia veins include quartz, pyrite, jarosite, sericite, hematite, and fluorite.

Propylitic alteration occurs only in dikes emplaced late in the intrusive sequence, after adularia and sericite alteration, and is characterized by chlorite + calcite + pyrite ± epidote replacing mafic minerals, and albite(?) ± quartz ± epidote ± sphene replacing plagioclase and potassium feldspar phenocrysts.

Mineralization likely occurred during at least two stages. Stage I mineralization is characterized by subeconomic (<0.005 ounces of gold per ton) disseminated gold/silver mineralization likely associated with widespread weak sericite + pyrite alteration. Stage II mineralization is a more consistently economic (>0.02 ounces of gold per ton), shear-zone-controlled mineralization, associated with adularia alteration. Stage II mineralization likely consisted of an early phase in which adularia + pyrite + gold were deposited and a main stage in which adularia + jarosite + gold were deposited. It is unclear from the present study whether main Stage II mineralization and alteration represents a distinct event or the waning stage

of the pervasive adularia + pyrite + gold mineralizing event. Gold in grab samples, soil samples, and exploration drilling show a strong correlation between gold mineralization and pervasive adularia alteration and adularia overgrowth veining, characterized by elevated K_2O/Na_2O ratios as a result of potassium metasomatism.

A geographic information system was used to analyze geochemical, geophysical, geologic data from a roughly 14 square kilometer area surrounding the Zortman Mine area, both to assess its utility as an exploration tool and to delineate potential exploration targets. Analyses were done at three levels of resolution, progressing from small areas with the most complete data, to larger areas with less complete data.

Based on empirical correlations and the geologic model developed for the area, the geographic information system was used to create several derivative maps which delineated areas with high potential for undiscovered mineralization. The most useful derivative map, estimating gold potential, was created by proportionally weighting gold in rock samples, gold in soil samples, mapped faults, and inverse distance to exploration drill holes. Several areas were identified which had high potential based on the analysis criteria. In several locations, the areas of high potential coincide with mineralized trends mapped in and around the Zortman Mine area. Other geographic information system analyses performed during the study generated maps showing the best place to build roads based on Landsat imagery and terrain analysis, areas of iron oxide based on Landsat imagery, and areas of anomalous metal suites in soils.

Geographic information system analysis is a useful tool for exploration; however, it clear that familiarity of the analyst with the data sets and the associated underlying assumptions are critical to effective analysis. Several complex and expensive geographic information system programs were tested in the initial stages of this study, before a relatively inexpensive program named IDRISI was chosen. IDRISI proved to be an easy to use and effective program, able to fulfill many of the needs of property-scale exploration and geographic information system analysis, especially when the analysis involves Landsat or other raster-based data.

Geology, Hydrothermal Alteration, and Geographic Information System Analysis of the Zortman Mine Area, Montana

by

Peter J. Wampler

A THESIS

submitted to

Oregon State University

in partial fulfillment of
the requirements for the
degree of

Master of Science

Completed April 13, 1994

Commencement June 1994

APPROVED:

Redacted for Privacy

Associate Professor of Geosciences in charge of major

Redacted for Privacy

Head of department of Geosciences

Redacted for Privacy

Dean of Graduate School

Date thesis is presented April 13, 1994

Thesis completed by Peter J. Wampler

ACKNOWLEDGEMENTS

This research was made possible through the generous funding of Zortman Mining Incorporated and Pegasus Gold Corporation. Special thanks go to Charlie Russell and Joan Gabelman for many stimulating discussions about the geology and alteration of the Zortman Mine area. I would also like to thank my wife, Leslie, for her support while I was going through the three-year gestation period in producing this child, and for numerous hours of help in compiling this manuscript. I could not have done it without her. Thanks also go to John Dilles for his willingness to spend time whenever my wheels were spinning out-of-control, and for his thorough reviews of my text. I would also like to thank Cy Field and A. Jon Kimerling for serving on my thesis committee. Credit is also due to Gary Lynch of the Oregon Department of Geology and Mineral Industries for his flexibility in allowing me to complete my research while still working full time.

TABLE OF CONTENTS

LIST OF FIGURES

LIST OF TABLES

LIST OF PLATES

GEOLOGY, HYDROTHERMAL ALTERATION, AND GEOGRAPHIC INFORMATION SYSTEM ANALYSIS OF THE ZORTMAN MINE AREA, MONTANA

INTRODUCTION

The Zortman Mine area has been producing metals sporadically since the late 1800's. Between 1884 and 1985, an estimated 727,414 ounces of gold were produced from the combined Zortman and Landusky mines (Hastings, 1988). Prior to 1979, the Zortman Mine ore production was predominantly from underground workings which followed high grade (>0.1 ounces of gold per ton) shear zones. Between 1979 and 1990, approximately 800,000 ounces of gold were produced from large open-pit, heap-leach operations which processed the low-grade ore surrounding the high grade shear zones. As of January 1993, the combined Zortman and Landusky mines had proven and probable reserves of 96,355,000 tons, grading 0.018 ounces per ton gold, and total reserves of 1,776,000 ounces of gold (Pegasus Gold Inc., 1992).

Exploration activity surrounding the Zortman and Landusky mine areas has been aggressive since the mid-1980's. Extensive reverse circulation drilling, as well as stream sediment sampling; soil and rock geochemical analyses; and geophysical, geological, and satellite imagery surveys have been conducted to locate additional ore bodies. The present study integrates existing data with new field data, collected during the summers of 1991 and 1992, and laboratory studies, to gain a better understanding of the geology, alteration, and genesis of the Zortman gold deposit. The knowledge gained and models developed are then used to estimate areas with a

high probability of containing buried ore bodies using a geographic information system (GIS). A GIS is a computer program or set of computer programs which enable the integration of geographically referenced data.

The Zortman and Landusky mines comprise one of the largest gold occurrences in northeast-central Montana. Various workers have proposed that the mines are of epithermal origin. However, they are exceptional epithermal deposits because they are spatially associated with shallowly emplaced Paleocene silicic-alkalic porphyritic intrusions. The current study describes and maps the hydrothermal alteration and geology surrounding the Zortman gold deposit in an attempt to better understand the genesis of the deposit and predict the location of undiscovered ore bodies.

Data for GIS analysis were compiled into a raster-based GIS named IDRISI. The GIS was used as a tool in manipulating, integrating, and analyzing the data sets. Based on empirical models, maps of gold mineralization potential were prepared to locate areas which hold high potential for undiscovered mineralization. Similar studies utilizing a GIS in gold exploration have proven successful on a regional scale (Bonham-Carter, et al., 1988; Watson, et al., 1989).

Location and Regional Geology

The Zortman Mine is located in northeast-central Montana, near the core of the Little Rocky Mountains. The Little Rocky Mountains are an isolated, roughly circular range which rises 2,500 feet above the surrounding plains. The project area

includes approximately five square miles surrounding the Zortman Mine (see Figure 1).

The Little Rocky Mountains are the eroded remnant of a large Paleocene intrusive complex which bowed up overlying Paleozoic and Mesozoic sediments. Precambrian amphibolites and gneisses crop out in the core of the range, leading early workers to suggest that many of the plutons are laccolithic (Emmons, 1908; Richardson, 1973). However, Dyson (1938) interpreted the Precambrian rocks as roof pendants on top of a stock, rather than the exposed floor of a laccolith. The intrusive rocks are part of the Montana Alkalic Petrographic Province of Central Montana as defined by Larsen (1940). Knechtel (1959) mapped the geology and described the stratigraphy and intrusive phases of the Little Rocky Mountains, concentrating mainly on the stratigraphy of the sedimentary rocks. The range is flanked by gently to steeply dipping Mesozoic and Paleozoic limestones, shales, sandstones, and dolomites, which unconformabley overlie Precambrian rocks. The core of the range consists of Paleocene porphyritic syenites and quartz monzonites. K-Ar dating of orthoclase feldspar and fission-track dating of apatites in quartz monzonite yielded ages of 60 to 64 million years (Marvin et al., 1980).

The lack of well-developed megascopic metasomatism and/or thermal alteration led Wilson and Kyser (1988) to suggest that the contacts between the sedimentary and intrusive rocks are largely structural. However, Russell (1990) suggested that the low water content of the porphyries may explain the lack of extensive contact metasomatism aureoles. In addition, the sinuous nature of many of

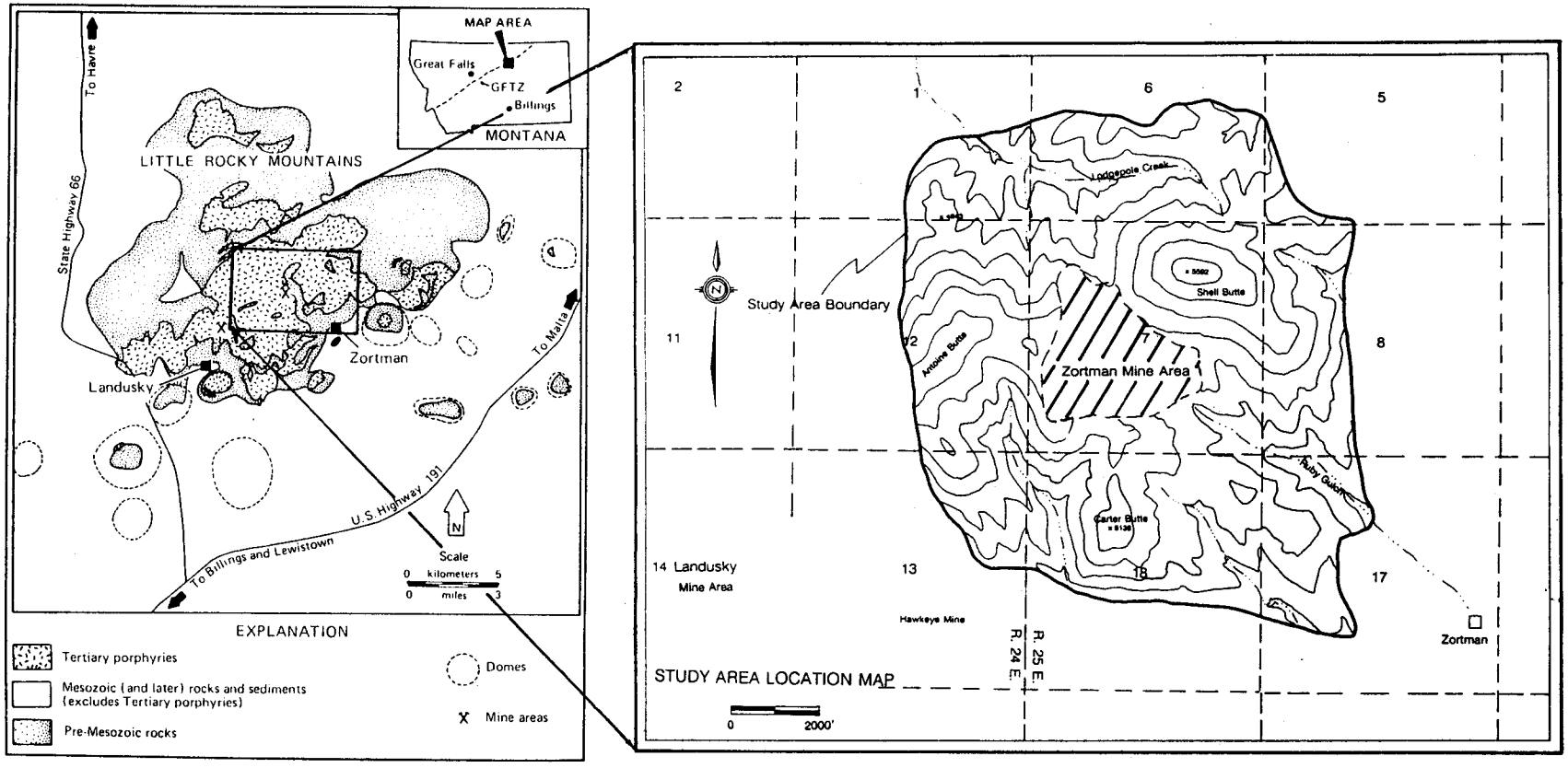

Figure 1. Location map (modified after Russell, 1991).

the contacts, as well as a lack of good exposures of bounding fault surfaces, suggest that many of the contacts are intrusive rather than structural. The inferred shallow depth of emplacement of the intrusions may explain, at least in part, the low degree metasomatism developed in the country rocks.

Ore Deposit Geology

The term "epithermal" was first used by Lindgren (1933) to describe hydrothermal ore deposits which form at shallow depths (< 1 km) and low temperatures (50° to 300°C). Epithermal deposits are hosted by many different rock types. However, sediment- and volcanic-hosted types are by far the most common. Epithermal deposits are thought to be related to hydrothermal fluids derived from, or heated by, nearby hypabyssal or subvolcanic intrusions, although the location of the source plutons is commonly problematic.

Volcanic-hosted epithermal deposits have been subdivided into adularia-sericite and acid-sulfate types by Heald et al. (1987). The adularia-sericite type is characterized by introduced adularia and sericite, local quartz-sericite alteration, and supergene alunite; whereas the acid-sulfate type is characterized by hypogene alunite, advanced argillic alteration, and no adularia. The Zortman gold deposit, although similar in many respects to other adularia-sericite epithermal gold deposits, differs in that it is hosted primarily in hydrothermally altered porphyritic syenites and quartz monzonites (minor ore occurs in Precambrian amphibolites and Paleozoic sediments) rather than volcanic lithologies. The Zortman deposit is similar to typical porphyry

copper deposits in terms of its host rock, widespread alteration, and disseminated mineralization; however, the lack of significant base metals and apparent lack of large-scale alteration halos distinguishes it from other base metal porphyry deposits. Russell (1991) suggested that the Zortman gold deposit is a structurally controlled epithermal deposit superimposed upon a pre-existing porphyry system. Further, he proposed that low P_{H20} in the porphyries, as indicated by a hornblende-aegerine-augite assemblage instead of a hornblende-biotite assemblage, hindered the development of extensive alteration, hydrofracturing, and mineralization zoning common in many other copper porphyry systems. Phase diagrams from Naney (1983) indicate, however, that the crystallization of horneblende before biotite at 2 kb pressure and a temperature of approximately 750 to 875°C requires a P_{H2O} of greater than 4 weight percent. Therefore, since the dominant assemblage contains hornblende, it is likely that the water content was greater than 4 weight percent.

Mineralization is localized along major north-northwest-striking shear zones associated with adularia, quartz, pyrite, and locally fluorite. K-Ar dates of illites, which are associated with gold mineralization according to Wilson and Kyser (1988), yielded dates which ranged from 57.6 to 67.8 million years (Wilson and Kyser, 1988). The most reliable dates place the alteration between 57.6 and 62.3 million years, indicating that gold mineralization occurred within 4 million years of the emplacement of the porphyries, at 60 to 64 million years. Trace amounts of galena, sphalerite, and chalcopyrite occur within the Zortman deposit, but in concentrations much lower than is typical of base-metal porphyry systems. The overall metal

assemblage is dominated by gold and silver occurring as native gold, native silver or electrum, tellurides, and sulfosalts (Russell, 1991; Dyson, 1939). This metal assemblage is typical of an epithermal gold deposit, and not a porphyry hydrothermal system.

Dyson (1939), Rogers and Enders (1982), Enders and Rogers (1983), Hastings (1988), and Wilson and Kyser (1988) all noted that the hydrothermal alteration of the Zortman deposit has many features in common with an epithermal system. The mineral assemblage and overall distribution of alteration and mineralization are similar to the adularia-sericite type of epithermal deposit described by Heald et al. (1987). Adularia was not identified in previous petrological studies, although geochemical analyses performed by Wilson (1987) were unusually rich in K_2O. Sodium/potassium weight percentage ratios in many of the altered porphyries are very low (<0.1), suggesting potassium metasomatism rather than an initial alkalic magma composition as advocated by Wilson and Kyser (1988). Petrologic work performed by this author has identified adularia, a low-temperature potassium feldspar with a highly disordered structural state, in veinlets and as replacements of plagioclase and igneous potassium feldspars along veinlet margins. Bailey (1974) noted secondary orthoclase associated with quartz veins and as overgrowths on primary orthoclase in the Alder Gulch area to the south of the Zortman Mine. Bailey concluded, based on textural evidence, that the secondary orthoclase was a deuteric/late magmatic alteration product. However, he also noted an association between high K_2O percentages and introduced quartz and pyrite; an association

which would argue for potassium metasomatism related to mineralization rather than deuteric/late magmatic alteration.

The well-developed shear zones of the Zortman deposit have been noted by virtually every worker who has studied the area. Gold grades in the Zortman Mine are highest along a N20°W-striking shear zone which extends for 1,800 meters along strike. Low grade ore extends up to 300 meters on both sides of the shear zone and may correlate with the limits of overgrowth adularia veining (see Alteration section). Russell (1991) has suggested a possible link between the northeast-striking Great Falls Tectonic Zone described by O'Niell and Lopez (1985; Figure 1, inset), and the northeast-striking structures controlling mineralization at the nearby Landusky Mine. The northwest trend in the Zortman Mine may bear some, as yet undetermined, relation to the northeast regionally extensive Great Falls Tectonic Zone.

Objectives and Methods of Research

The objective of this study was two-fold. The initial objective was to describe the hydrothermal wallrock alteration and geology of the Zortman deposit, relying somewhat on information collected by previous workers, but predominantly on newly acquired data from detailed mapping and petrographic observations. Of particular importance were detailed descriptions of alteration mineralogy, vein assemblages, cross-cutting relationships, and structural controls on mineralization.

The data collected were compared and contrasted to the epithermal and porphyry gold deposit models to develop a model for the genesis of the deposit.

Geologic and alteration data were collected and interpreted to build a geologic model for ore formation and to provide a basis for using a GIS to integrate the existing database of geophysical, geological, geochemical, and remote sensing data. The data, constrained by the geologic model, were then manipulated within the GIS to produce gold potential maps.

Alteration and geologic mapping of a roughly five-square mile area surrounding the Zortman Mine was completed at a scale of at 1 inch = 400 feet (see Plates 1 and 4). A local coordinate system used by Zortman Mining Inc. was used to reference samples, outcrops, and other data. This coordinate system is used periodically in the text to describe locations; refer to Plate 1 for sample locations and coordinates. A limited amount of mapping and sampling at a scale of 1 inch = 20 feet was performed in the open pits in order to develop a better understanding of the details of alteration associated with the mineralization. This mapping recorded sulfide mineralization, rock silicate alteration mineralogy and its spatial distribution, orientations of faults and veins, and the spatial distribution and temporal relations between the different rock types. Samples were collected during mapping for petrologic studies, geochemical analyses of ore metals, and trace element geochemical analysis. Thin sections provided by Zortman Mining Inc. personnel were examined prior to fieldwork to develop a strategy for field identification of alteration assemblages. Examination of thin sections revealed at least some degree

of potassium metasomatism in the form of adularia-bearing veinlets and local replacement of plagioclase and potassium feldspars along veinlet margins. One of the primary objectives of the project was to better define and describe the magnitude and nature of this previously undescribed adularia alteration. Close examination of feldspars in thin section and chemical analyses of feldspars by electron microprobe were useful in differentiating individual alteration events and their respective mineral assemblages. Detailed field descriptions of outcrops were essential to allow reinterpretation after laboratory analyses and petrologic examinations were complete.

The completed geology and alteration maps were digitized and edited with AutoCAD, a computer drafting program compatible with most GIS software. Output in digital format was then fed into the raster-based GIS, IDRISI. A local 1,000-foot by 1,000-foot grid system surveyed by mine personnel served as the grid control for the GIS. Separate layers were maintained for major components such as structure, rock types, air photo linears, and alteration. Gold values, determined by atomic absorption performed by Zortman Mining Inc. laboratory, from over 200 reverse circulation drill holes, 300 rock samples, and over 100 stream sediment samples, already in digital {x,y,Au value} format, were added as separate layers. A commercial laboratory analyzed 3,000 soil samples for metals. Aeromagnetic, induced polarization, and Very Low Frequency (VLF) data were digitized by hand, and/or directly imported from diskettes. Landsat thematic mapper imagery, consisting of data for seven spectral bands was imported, creating a separate data layer for each spectral band. Spectral band ratios were compared with areas of

known hydrothermal alteration and mineralogy in order to isolate individual hydrous alteration minerals and their areal extent.

After the data sets were compiled into the GIS, derivative maps were produced by combining and overlaying different data layers. Areas of high potential for gold mineralization were outlined in a separate report provided to Zortman Mining Inc. (Wampler, 1992).

GEOLOGY OF THE ZORTMAN MINE AREA

Several porphyritic intrusives, ranging in composition from quartz monzonite to trachyte, were mapped during the summers of 1991 and 1992. Intrusive rocks occur as stocks, dikes, and laccoliths intruding Paleozoic and Precambrian rocks. Figure 2 summarizes the relative age relationships between the intrusive units and the Paleozoic and Precambrian rocks.

Precambrian Rocks

Precambrian rocks, occurring predominantly as xenoliths and septa between intrusive bodies, comprise 21 percent of the area mapped. A whole rock rubidium/ strontium isochron date of an amphibolite by Peterman (1980) yielded an Archean age of approximately 2,550 million years. Lithologic field mapping units include the following: Precambrian undifferentiated (pCu), composed of various Precambrian rocks including biotite schist, augen gneiss, felsic gneiss, untextured granite, and, locally, quartzites with green micaceous material; Precambrian amphibolite (pCa), consisting of distinctive black amphibolites with abundant hornblende, biotite, and varying amounts of plagioclase, potassium feldspar, and quartz; Precambrian marble (pCm), consisting of coarse-grained, recrystallized, and variably dolomitic marble with local galena and chalcopyrite (< 1 percent) along fractures and as blebs. Locally, amphibolites are cut by mafic dikes or breccia pipes of unknown origin and age (i.e., sample PW269). Garnet/kyanite schist was identified in the northern portion of the map area. This is consistent with the observation made by Russell

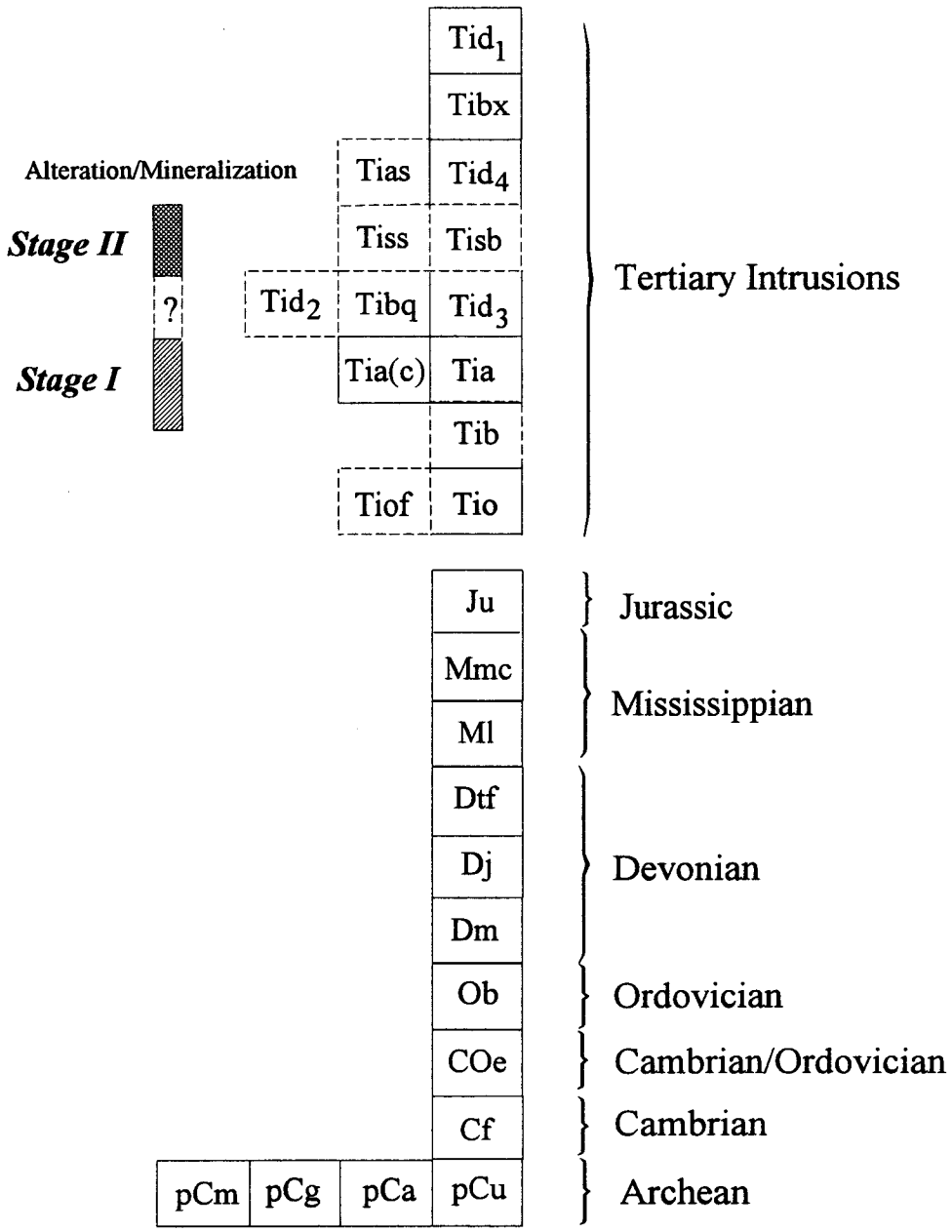

Figure 2. **Relative ages of intrusions. Dashed boxes indicate uncertainty in age relationship.**

(1984) that the metamorphic grade increases from south to north in the central portion of the Little Rocky Mountains.

Precambrian marble was found exclusively on north Antoine Butte and comprised 0.2 percent of the mapped area. The best exposure of Precambrian marble can be found at 7200E, 14800N (see Plate 1). Marble is spatially associated with skarn-like material and quartz veining. It is unclear whether the skarn-like material is of Precambrian or Tertiary age.

Garnet/Pyroxene "Skarn" Occurrences

The largest occurrence of skarn was mapped near Lodgepole Creek. The term skarn is used to refer to a coarse-grained calc-silicate rock which is spatially associated with marble; no genetic implications are intended. The skarn is composed of 50 to 60 percent red garnet (almandine?), 20 to 30 percent green pyroxene (diopside?), 5 to 10 percent plagioclase, and 5 to 10 percent quartz and accessory potassium feldspar, calcite, and magnetite. The origin and spatial relationships of the skarn are somewhat problematic (see Figure 3). The skarn is located near a pod of variably dolomitized marble, presumed to be Precambrian in age. The proximity of an apophysis of Antoine Butte porphyry north of the marble pod led to initial speculation that the apophysis was the source of metasomatic fluids which altered the dolomitic marble to garnet/pyroxene skarn. However, several field observations are inconsistent with this interpretation (refer to Figure 3):

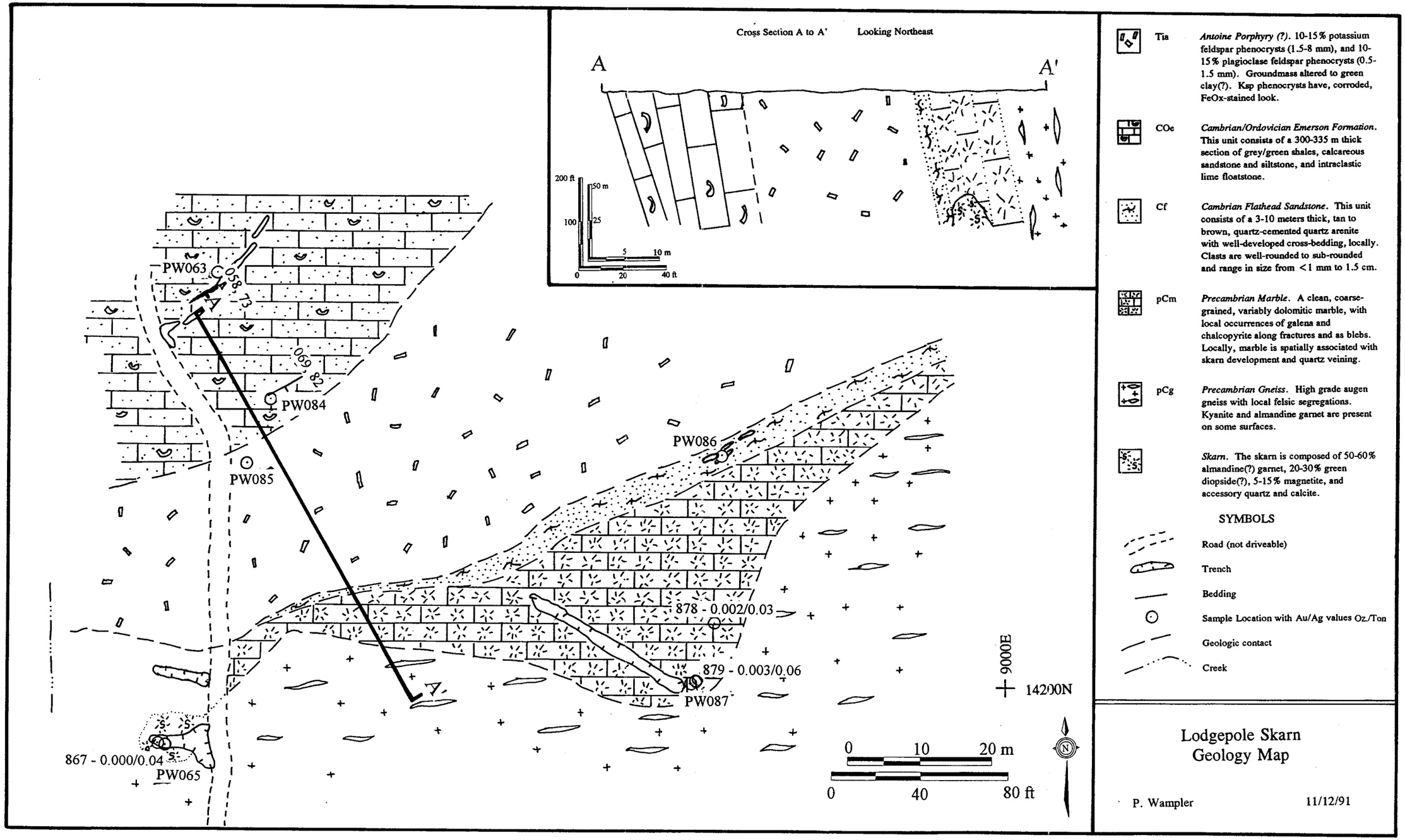

Figure 3. Lodgepole skarn geology map.

1. There is very little alteration in the marble located north or east of the skarn occurrence, even though the northeast portion of the marble is as close or closer to the apophysis of Antoine Butte porphyry.
2. There does not appear to be any zonation within the skarn body. The skarn is apparently a restricted pod within the southwest end of the marble, or perhaps is wholly within the gneiss(?).
3. The Emerson Formation, located 200 feet north of the skarn, is essentially unaltered even though it is in direct contact with the apophysis of Antoine Butte porphyry and contains abundant carbonate.
4. The texture of the skarn is distinct from other contact metasomatic skarns in that there is very little carbonate veining or mineral zonation. Pyroxene poikilitically encloses garnet and magnetite, a texture suggestive of higher temperatures than are commonly associated with contact metasomatic skarn.

One interpretation, which is consistent with the above observations, is that the skarn was formed prior to emplacement of the Tertiary pluton, perhaps during regional metamorphism. This would mean that the skarn's location near the Antoine Butte porphyry is coincidental (see Figure 3; inset). Walther and Wood (1986) point

out that under high-grade metamorphic conditions, marble has very low permeability as a result of its extreme ductility. It is possible that metamorphic fluids, present during the kyanite-stable metamorphism, simply followed the most permissive fluid pathway along the contact between the marble and the more competent high-grade metamorphic rocks, resulting in skarn formation along the marble/gneiss contact. This is consistent with the spatial relationships observed in the Lodgepole skarn occurrence, where skarn occurs at, or very near, the contact between marble and garnet/kyanite schists to the south. If the skarn formed during regional metamorphism, it is likely that similar skarn occurrences would be very small and restricted to pods of marble within Precambrian rocks.

If, on the other hand, this skarn was formed by Tertiary hydrothermal fluids, there is potential for unexposed skarn bodies at the marble/pluton contacts at depth. Geochemical analyses of the skarn, and other similar skarn occurrences, indicate they are not significantly anomalous in precious metals, but are weakly anomalous in base metals (see Table 1). Although the occurrence depicted in Figure 3 was the largest occurrence of skarn found within the map area, several pods of Precambrian marble were mapped on north Antoine Butte and could potentially host similar alteration which is not exposed at the surface.

Table 1. Geochemical analysis of garnet-pyroxene skarn.

Sample No.	Au (opt)	Ag (opt)	Au (ppb)	Ag (ppm)	Zn (ppm)	Mo (ppm)	Ni (ppm)	Co (ppm)	As (ppm)	Sb (ppm)	Cr (ppm)
PW065[1]			10	<5	<200	<2	51	27	5	<0.02	610
867[2]	0.000	0.04	0.0	0.1							
879[2]	0.003	0.06	9.4	0.2							
878[2]	0.002	0.03	0.3	0.1							

[1]Sample was analyzed for neutron activation by Bondar-Clegg and Company Ltd.
[2]Samples 867, 879, and 878 were analyzed both by atomic absorption by Zortman Mining Inc. laboratories (Au and Ag in opt) and by neutron activation by Bondar-Clegg (Au in ppb, Ag in ppm).

Paleozoic and Mesozoic Rocks

Paleozoic and Jurassic sedimentary rocks, although volumetrically minor, comprising 5 percent of the area mapped, provided critical stratigraphic control for determining fault displacements in the southeastern portion of the map. Although carbonates are abundant in the Paleozoic stratigraphy, metasomatic alteration is rare. The Paleozoic and Cretaceous units mapped are as follows; thicknesses are from a stratigraphic section measured in Lodgepole Creek by Russell (1984).

Flathead Sandstone (Cf)

The Flathead Sandstone (Cf) is composed of tan to brown, quartz-cemented quartz arenite. Locally, well-developed cross-bedding is preserved. Clasts are well-rounded to sub-rounded and range in size from < 1 mm to 1.5 cm. This unit has a total thickness of 10 to 15 meters (33 to 49 feet).

Emerson Formation (COe)

The Emerson Formation (COe) is composed of grey/green shales, calcareous sandstones and siltstones, and intraclastic lime floatstones with imbricated fragments. The total thickness is 335 meters (1,099 feet).

Bighorn Dolomite (Ob)

The Bighorn Dolomite (Ob) formation is composed of sugary, massive to thick-bedded, grey dolostone. The upper portion has ubiquitous star-shaped crinoid stems. It weathers to produce low, ragged cliffs with a hackly surface. It has a total thickness of 85 meters (279 feet).

Maywood Formation (Dm)

The Maywood formation (Dm) was not observed in the map area. It rarely forms prominent outcrops, and is composed of calcareous red to grey/green shales. It has a total thickness of 55 meters (180 feet).

Jefferson Limestone (Dj)

The Jefferson Limestone (Dj) formation is most easily recognized by the presence of stromatolites and silicified stromatolitic outlines. It is composed of medium- to dark-grey, massive to moderately thin-bedded, marly limestone. It has a total thickness of 131 meters (430 feet).

Three Forks Shale (Dtf)

Three Forks Shale (Dtf) forms a topographic low between the Jefferson Limestone and the Lodgepole Limestone. It is rarely exposed on the surface. It is composed of grey/green calcareous shales and sandy siltstones. It has a total thickness of 18 meters (59 feet).

Lodgepole Limestone (Ml)

Lodgepole Limestone (Ml) is the lower formation of the Madison Group. It is composed of thinly-bedded grey to dark-grey petroliferous grainstone with locally abundant fossil hash. Bryzoans and brachiopods are commonly present. It has a total thickness of 192 meters (630 feet).

Mission Canyon Limestone (Mmc)

Mission Canyon Limestone (Mmc) is the upper formation the Madison Group. It is composed of massive grey to light-grey limestone with extensive recrystallization, karst solution cavities, local chert nodules, and sparse fossils (predominantly crinoid stems). It has a total thickness of 125 meters (410 feet).

Jurassic Undifferentiated (Ju)

Jurassic Undifferentiated (Ju) includes the Rierdon, Swift, and Morrison formations and is composed of tan to brown arkosic sandstones. It has a total thickness of 106 meters (348 feet).

Petrography, Geometry, and Timing of Tertiary Intrusive Rocks

Thirteen intrusive units were differentiated for the purposes of mapping and are described below; these units intrude both Precambrian and Paleozoic lithologies. Many of these intrusions probably represent different phases of the same Paleocene intrusive event. Cross-cutting relationships are rare, making relative age relationships difficult to determine. K/Ar age dating of potassium feldspars from the Antoine Butte and Old Scraggy porphyries yielded ages of 63.9 $\pm$ 1.5 million years and 62.5 $\pm$ 1.8 million years, respectively (Marvin et al., 1980). The younger age for the Old Scraggy porphyry is somewhat suspect and may represent loss of radiogenic argon as a result of hydrothermal alteration during the emplacement of younger intrusives. K/Ar dating of potassium feldspars from an aegirine trachyte from the Landusky area yielded a somewhat younger age of 61.0 $\pm$ 2.1 million years (Marvin et al., 1980). Figure 2 summarizes the relative age relationships between the intrusive units, the Paleozoic rocks, and the Precambrian rocks. Table 2 summarizes the field and petrographic characteristics of the porphyries. The term potassium feldspar is used in the following descriptions to describe both sanidine and orthoclase feldspars. Determinations of 2V indicate that most of the potassium feldspar is sanidine. Observed variations in 2V from 5° to 80° may be due to cryptic replacement of magmatic feldspars by hydrothermal potassium feldspar.

Table 2. Summary of morphologic and petrologic characteristics of mapped intrusions.

Intrusion	Hand Sample			Petrographic Characteristics						
	Color	Key Texture/Feature	Erosion Resistance	Volume % Phenocrysts	Groundmass Size	Volume % Quartz	Volume % Plagioclase (mm)	Volume % Potassium Feldspar (mm)	Volume % Mafics (type)	Accessory Minerals
Tid_1	Green	Trachytic texture, color, lack of alteration	Moderate	25-30	0.025 mm		none	17.5-18	4-5 (aegirine augite)	sphene, melonite, apatite
Tibx	White/Light gray	Rounded clasts, rock flour/crystalline matrix	Low	40% fragments	rock flour		varies	varies	varies	1-3% pyrite, locally
Tias	Green/Gray	Equigranular to weakly porphyritic texture, propylitic alteration	Low(?)							
Tid_2	Dark gray/ Purple	Propylitic alteration, forms resistant fins	High	35-40	<0.01		23 (0.5-2)	15 (1-10)	1.5 (pyroxene), 0.8 (biotite)	quartz, sphene, amphibole(?)
Tiss	Tan	Lack of alteration, mafics often preserved	Low	25-30	0.06-0.08		10-15 (1-3)	5-10 (4-6)	2-5 (pyroxene)	1-3% pyrite
Tisb	White	Bleached appearance, uniform phenocryst size	Moderate	20-25	0.25-0.50		no large phenocrysts	20-25	2? (pyroxene)	
Tid_3	Black	Looks silicified, fractures into small fragments	High	10-20	<0.01	2-3		10-20		2-3% quartz
Tid_4	White/Tan	Large, tabular sanidine phenocrysts	High	20-30	<0.01		4-5 (0.5-2)	18-20 (5-25)	none preserved	
Tibq	White	Euhedral quartz bipyramids	Low	50-55	<0.01	2.5-7.5	25-30	15-17.5	1-1.5 (pyroxene?)	
Tia	White	uniformly pyritized	Low/ Moderate	15-45	<0.01-0.025	2-12	15-20	15-20	3-5 (pyroxene, amphibole)	sphene
Tia(c)	White/ Pinkish	>45% large, > 5 mm, potassium feldspar phenocrysts	Moderate	>45	0.05-0.5		15-20	>45	1-2 (pyroxene?)	
Tib	Green	Color, 1-3% pyrite, and fine-grained groundmass	Low	10-15	0.013	1-3	5-10	5-10		1-3% pyrite
Tio	White	5-15% embayed quartz "eyes"	Moderate/ High	35	0.025	1-2	12-17	10-15		
Tiof	White	Bleached white appearance	Low	10-15	<0.01		1-5 (<1 mm)	10-15	1-5 (aegirine augite?)	

Old Scraggy Fine-grained Porphyry (Tiof)

Old Scraggy fine-grained porphyry (Tiof) is volumetrically minor within the map area, comprising 0.8 percent of the area mapped. The Old Scraggy porphyry is a syenite porphyry with 10 to 15 percent phenocrysts consisting of 1.5 to 5 mm potassium feldspar; 1 to 5 percent needle-shaped mafics (aegerine-augite?), which are often altered to magnetite and iron-titanium oxides and hydroxides; plagioclase, if present, is very fine-grained (< 1 mm). The groundmass is aphanitic, < 0.01 mm, but appears to be made up of larger 0.1 mm groups of crystals, a texture similar to that observed locally in the Old Scraggy porphyry (Tio). The cause of the bimodal size distribution is unclear. It may be an annealing feature generated by the emplacement of younger intrusions. The porphyry fractures into 10 to 20 cm fragments, has a bleached white appearance in outcrop, and seldom stands up in relief. The best example of this porphyry can be found at approximately 13900E, 9150N. Although no cross-cutting relationships were observed which involved Old Scraggy fine-grained porphyry (Tiof), the close spatial relationship between Tiof and Tio, as well as the location of Tiof outward from the central mass of Tio, suggest that it could be a fine-grained border phase of the Tio.

Old Scraggy Porphyry (Tio)

Old Scraggy porphyry (Tio) occurs on the eastern boundary of the map area and is volumetrically minor within the area mapped, comprising 0.4 percent. Large

areas of Old Scraggy porphyry occur east of the map area near Old Scraggy Peak. It is a quartz monzonite porphyry with 35 volume percent phenocrysts consisting of 10 to 15 percent, 5 to 15 mm, poikilitic, potassium feldspar with inclusions of plagioclase commonly outlining growth zones; 12 to 17 percent, 2 to 4 mm, plagioclase phenocrysts; 1 to 2 percent, 5 to 10 mm, embayed quartz "eyes", often with iron-oxide/clay cores(?); and 0.5 to 1 percent, 0.5 to 1 mm, rectangular mafic sites, commonly occupied by light green clay (smectite?). The groundmass grains are approximately 0.025 mm but, as mentioned above, appear to be made up of larger 0.1 mm groups of crystals. The type locality and freshest example of Old Scraggy porphyry (Tio) can be found at 15350E, 7630N. Old Scraggy porphyry often forms prominent outcrops which are erosion resistant. The Old Scraggy porphyry is cut by dikes of Beaver porphyry, indicating it is older than that unit.

Beaver Porphyry (Tib)

Beaver porphyry (Tib) occurs only in the eastern portion of the map and comprises 0.5 percent of the map area. This unit may be equivalent to the Beaver porphyry mapped by Russell (1984). It consists of quartz monzonite porphyry with 10 to 15 percent phenocrysts dominated by 0.5 to 2 mm plagioclase, and 3 to 5 mm potassium feldspar; 1 to 3 percent, 1 to 2 mm, quartz phenocrysts; and 1 to 3 percent disseminated pyrite, typically unoxidized. The groundmass is aphanitic (0.013 mm) and green in color. The type example of this porphyry, as mapped for this study, can be found at 14900E, 9200N. Since no Beaver porphyry dikes were

observed to intrude Shell Butte porphyry, and because Beaver dikes appear to be cut by Shell Butte porphyry near the east side of Shell Butte (14500E, 11500N), they are presumed older than Shell Butte porphyry. Dikes of Beaver porphyry apparently cut Old Scraggy porphyry near 14500E, 11500N, indicating they are younger than that unit. Contacts were not observed between the Antoine Butte porphyry and Beaver porphyry. The presence of widespread sericite/illite alteration indicates that the Beaver porphyry was affected by Stage I mineralization (see Hydrothermal Alteration below).

Antoine Butte Porphyry (Undifferentiated) (Tia)

Antoine Butte porphyry (undifferentiated) (Tia) is volumetrically the most abundant porphyry, comprising 38 percent of the map area. It includes numerous porphyry variations, possibly emplaced at different times, found on Antoine Butte and southwest of the mine area, with phenocrysts ranging from fine-grained, 0.5 to 2 mm, to coarse-grained, up to 15 mm. Composition varies from monzonite porphyry to quartz monzonite porphyry with subequal amounts of 1 to 5 mm potassium feldspar phenocrysts and 0.5 to 1.5 mm plagioclase feldspar phenocrysts. Original ferromagnesian minerals are rarely preserved; however, mafic sites are present up to 5 percent, and likely originally contained both amphibole and pyroxene. The groundmass is aphanitic to aplitic and commonly has a seriate texture. Contacts with other intrusive units in the area are rare, but those observed are irregular and suggest a stock-like mode of emplacement. The Antoine Butte porphyry is the dominant host

for mineralization at the Zortman Mine and is altered in all observed exposures, indicating it was emplaced prior to, or during, Stage I mineralization. Porphyries with less than 45 percent large (>5 mm) phenocrysts were classified as Antoine Butte porphyry, while those with greater than 45 percent large phenocrysts were classified as the coarse-grained phase of the Antoine Butte porphyry.

Antoine Butte Porphyry (Coarse-grained phase) (Tia(c))

The coarse-grained phase of the Antoine Butte porphyry, Tia(c), is apparently transitional with the Antoine Butte porphyry, and has been called the Alabama porphyry by previous workers due to its prevalence in the Alabama Pit at the Zortman Mine. It occurs central to the area mapped as Antoine Butte porphyry, comprises 10 percent of the area mapped, and is similar to the Antoine Butte porphyry except that potassium feldspar phenocrysts are larger, equant to subequant, and more abundant (>45 percent by volume), giving it a "choked" appearance. The groundmass is made up of potassium feldspar and plagioclase from a wide range of size classes (0.5 to 5 mm). Quartz phenocrysts are present in amounts ranging from <1 to 5 percent. The large potassium feldspar phenocrysts often exhibit a distinct poikilitic texture enclosing plagioclase. Contacts with the main Antoine Butte porphyry mass range from moderately sharp, located to within 5 meters, to gradational over tens of meters. In one location (5200E, 8700N) an apophysis of the coarse-grained phase of the Antoine Butte porphyry appears to cut across the Antoine Butte porphyry, suggesting that the coarse phase of the Antoine Butte porphyry is

slightly younger than the main Antoine Butte porphyry phase. Both the Antoine Butte porphyry and its coarse-grained phase are intruded by several diking phases.

Bipyramidal Quartz-bearing Dikes (Tibq)

Bipyramidal quartz-bearing dikes (Tibq) comprise 0.2 percent of the map area and are altered in all observed occurrences. The dikes consist of quartz monzonite porphyry with 50 to 55 volume percent phenocrysts consisting of 2.5 to 7.5 percent, 2 to 4 mm, euhedral to subhedral, quartz bipyramids; 25 to 30 percent, 1 to 3 mm, plagioclase phenocrysts, 15 to 17.5 percent, potassium feldspar phenocrysts (sanidine); and 1 to 1.5 percent, 0.5 to 1.5 mm mafic sites (pyroxene?). The groundmass is grey and aphanitic, and contains less than 0.01 mm grains. Alteration is usually extensive, giving the rock a bleached appearance. Quartz bipyramids weather out in relief. The type location for bipyramidal quartz-bearing dikes is at 5800E, 12500N. Bipyramidal dikes strike north-northeast, roughly the same orientation as younger Tid_1 and Tid_3 dikes. Bipyramidal dikes were only observed to cut Antoine Butte porphyry. The fact that they are strongly potassically altered suggests that they are either pre- or syn-Stage II mineralization (see Alteration below), and likely older than Tid_2 dikes, which exhibit only minor propylitic alteration in all occurrences.

Fine-grained Dikes (Tid_3)

Fine-grained dikes (Tid_3) are volumetrically minor, comprising 0.1 percent of the map area and are interpreted to be intrusive breccia dikes. These dikes are typically pervasively potassically altered and variably silicified. They are composed of 10 to 20 percent, 0.5 to 1.5 mm, feldspar fragments and phenocrysts; and 2 to 3 percent grey, embayed(?) quartz phenocrysts in a rock flour matrix/groundmass. Phenocrysts have an irregular, fragmental texture. Outcrops are typically hard, manganese oxide-stained, and fractured into 10 to 15 cm fragments. Flow banding is common near the porphyry dike margins and may represent deformation which occurred during emplacement. The type locality for this unit occurs at the entrance to the Pink-Eye Pearl Mine on northeast Antoine Butte (7593E, 13093N). All mapped dikes strike north-northeast. The breccia dikes are likely either pre- or syn-Stage II mineralization.

Sanidine-bearing Dikes (Tid_4)

Sanidine-bearing dikes (Tid_4) comprise 0.4 percent of the area mapped. They consist of syenite porphyry with 20 to 30 volume percent phenocrysts consisting of 18 to 20 percent tabular, elongate, 5 to 25 mm sanidine; 4 to 5 percent plagioclase feldspar; 2 percent, 0.5 to 1 mm pyroxene. They have an aphanitic groundmass with a grain size less than 0.01 mm. The tabular potassium feldspar phenocrysts locally exhibit trachytic alignment. The type locality for this porphyry can be found

at 7900E, 13700N. Dikes are localized along the north-northwest trend of the Ruby shear zone suggesting that the shear zone was present prior to the emplacement of the dikes. The dikes are altered in the mine area and appear to have been present during mineralization. Tid_4 dikes were only observed cutting Antoine Butte porphyry, indicating that Tid_4 dikes are younger than the Antoine Butte porphyry.

Scraggy-Shell Porphyry (Tiss)

Scraggy-Shell porphyry (Tiss) occurs only in the northeast portion of the map area and comprises 8 percent of the mapped area. It consists of quartz monzonite porphyry with 25 to 30 volume percent phenocrysts consisting of 5 to 10 percent, glassy, equant, 4 to 6 mm, potassium feldspar phenocrysts; 10 to 15 percent, 1 to 3 mm, plagioclase feldspar phenocrysts; and 2 to 5 percent, 0.5 to 1 mm, blocky rectangular pyroxene sites commonly altered to iron-oxide + clays $\pm$ illite $\pm$ carbonate. The groundmass is aphanitic (0.06 to 0.08 mm) and typically contains 1 to 3 percent weathered pyrite sites. The freshest outcrop and type location for the Scraggy-Shell porphyry, can be found at approximately 13850E, 13300N. Only trace amounts of gold mineralization are hosted by the Scraggy-Shell porphyry, and alteration is relatively weak.

Shell Butte Porphyry (Tisb)

Shell Butte porphyry (Tisb) comprises 16 percent of the area mapped. It is a monzonite porphyry with 20 to 25 percent, 3 to 5 mm, potassium feldspar pheno-

crysts poikilitically enclosing plagioclase lathes. The groundmass has an aplitic, sugary texture averaging 0.25 to 0.50 mm, and typically consists of approximately 20 percent quartz, 20 percent potassium feldspar, and 40 to 60 percent plagioclase. Ferromagnesian minerals (pyroxene?) may be present up to 2 percent locally, but are largely absent, either due to an initial magmatic assemblage deficient in ferromagnesian minerals or alteration. Shell Butte porphyry characteristically has a bleached appearance in outcrop. The main Shell Butte stock has irregular boundaries and appears elongated in a north-northwest direction. Smaller plugs and stocks also occur south of the mine area, giving the Shell Butte intrusion an overall semi-circular shape. Dikes of Shell Butte porphyry cut Antoine Butte porphyry, indicating it is the younger of the two units. The widespread sericite/illite-pyrite alteration, common in the Antoine Butte porphyry, is largely absent in the Shell Butte porphyry. This indicates that the Shell Butte porphyry was spatially isolated during Stage I mineralization/alteration or post-dates it (overgrown adularia veinlets, typical of Stage II mineralization are common in the Shell Butte porphyry). Both the Beaver porphyry and the nearby Shell Butte porphyry are spatially isolated from the Antoine Butte porphyry, yet only the Beaver porphyry exhibits widespread alteration similar to that found in the Antoine Butte porphyry. It is difficult to envision a scenario whereby widespread alteration could affect the Beaver porphyry while leaving the Shell Butte porphyry unaffected.

Monzonite Porphyry (Tid_2)

Monzonite porphyry (Tid_2) dikes comprise 0.3 percent of the area mapped, and often form conspicuous erosion-resistant fins. The porphyries have 35 to 45 percent phenocrysts consisting of 15 percent, 1 to 10 mm, potassium feldspar (sanidine?); 23 percent, 0.5 to 2 mm, plagioclase feldspar; 1.5 percent, 1.5 mm, pyroxene; 0.8 percent, 0.12 mm, green biotite; a trace to 0.4 percent embayed quartz; and accessory sphene, amphibole(?) and rare earth element (REE) minerals such as monazite. The groundmass has a <0.01 mm grain size. The dikes are typically quite fresh, with ferromagnesian minerals locally altered to epidote, chlorite, and carbonate. They range in color from pinkish-grey to dark-grey. The grey dikes tend to be finer grained, while the pinkish-grey dikes have a wider range of phenocryst sizes, including large (>5 mm) phenocrysts. Many of the dikes exhibit flow banding near their margins. Tid_2 dikes crosscut and occur predominantly within the Antoine Butte porphyry, and its coarse-grained phase, Tia(c). One dike, designated as Tid_2, appears to cut Shell Butte porphyry, suggesting Tid_2 dikes are younger than Shell Butte porphyry. Intrusive breccia cuts a dike of Tid_2 in at least one location, indicating at least some of the intrusive breccias are younger than Tid_2.

Alder Gulch Syenodiorite (Tias)

Alder Gulch syenodiorite (Tias) was positively identified in only one location (approximately 8900E, 5500N). One of the occurrences tentatively identified as Alder Gulch syenodiorite is located at (approximately 7000E, 8700N). This unit is propylitically altered in all mapped occurrences. It is an equigranular syenodiorite with approximately 85 percent complexly zoned plagioclase feldspar; 2 to 5 percent potassium feldspar; 7 to 10 percent augite (altered to epidote + calcite + chlorite); 2 to 3 percent horneblende (altered to epidote + chlorite ± calcite); and trace sphene, biotite, and opaques (magnetite). The Alder Gulch syenodiorite intrudes Antoine Butte porphyry in all mapped occurrences. It is interpreted to be broadly contemporaneous with Tid_2 dikes; both mapped occurrences are near Tid_2.

Intrusive Breccia (Tibx)

Intrusive breccia (Tibx), occurs as irregularly shaped and roughly elliptical bodies. It comprises 0.7 percent of the area mapped. The intrusive breccias mapped for this study are matrix-supported, have rounded to sub-rounded clasts, and have a matrix of rock-flour of the same composition as the clasts. In some occurrences the intrusive breccia matrix appears to have a magmatic component, as evidenced by the presence of a fine-grained crystalline groundmass in some thin sections. Clasts generally reflect the composition of lithologies adjacent to the breccia occurrence. In cases where the intrusive breccia is adjacent to Precambrian rock, clasts include

Precambrian lithologies. Bryant and Metz (1966) defined an intrusive breccia as a breccia in which the composition of the clasts changed depending on the location of the breccia, whereas the composition of the rock-flour matrix was essentially the same throughout all occurrences. The breccias mapped for this study also have many aspects in common with the type of breccia referred to as "milled" or "pebble breccia" by Kents (1964). One intrusive breccia body clearly cuts across a dike of Tid_2 on south Carter Butte indicating it is younger than that unit (see Figure 4). This occurrence exhibited a sheeted zone at the upper limits of the pipe. No contact relationships were observed between Tid_1 and intrusive breccia; however, the fact that at least some of the intrusive breccia bodies are altered suggests they are older than Tid_1. One breccia mass, named the Medusa Breccia by Zortman Mining Inc. geologists, differs in that the matrix consists of brick-red gougey material with clasts(?) of pervasively silicified sedimentary rocks and porphyry. The silicification and brick-red hematitic staining suggest that the Medusa Breccia may be of hydrothermal origin, or at least have a significant hydrothermal component.

Trachyte Syenite Porphyry (Tid_1)

The youngest intrusive unit, trachyte syenite porphyry (Tid_1), is a volumetrically minor (0.01 percent of mapped area), northeast-trending dike of trachytic syenite porphyry with 25 volume percent phenocrysts consisting of 17.5 to 18 percent, 0.1 to 10 mm, potassium feldspar phenocrysts (sanidine); 4 to 5 percent, 0.5 to 1.2 mm, strongly-zoned, aegerine-augite; 1 to 1.5 percent, 0.25 to 1 mm,

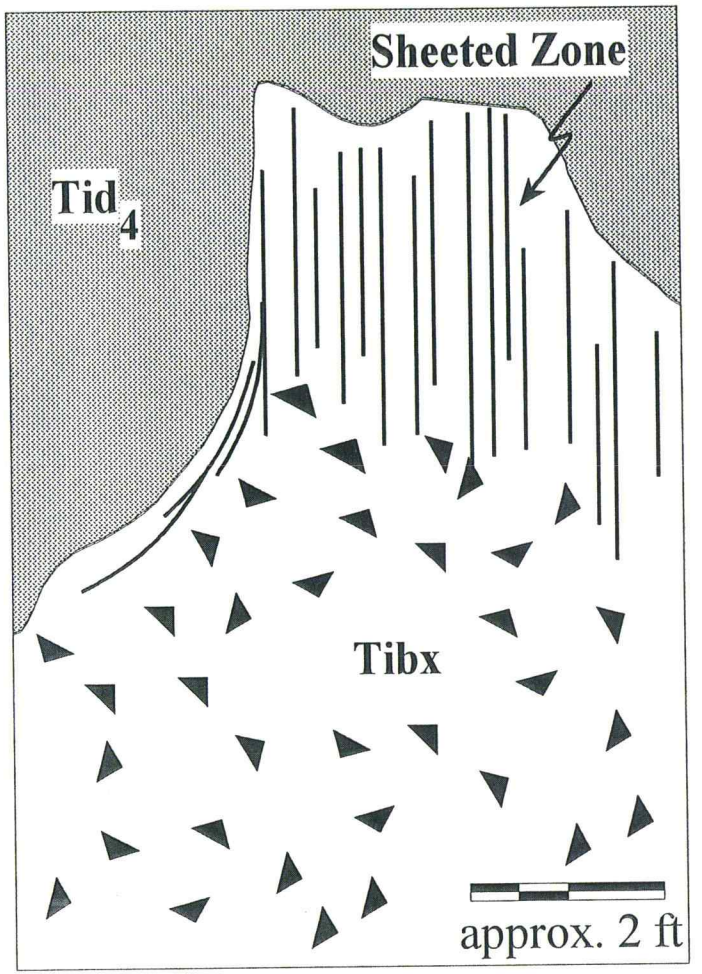

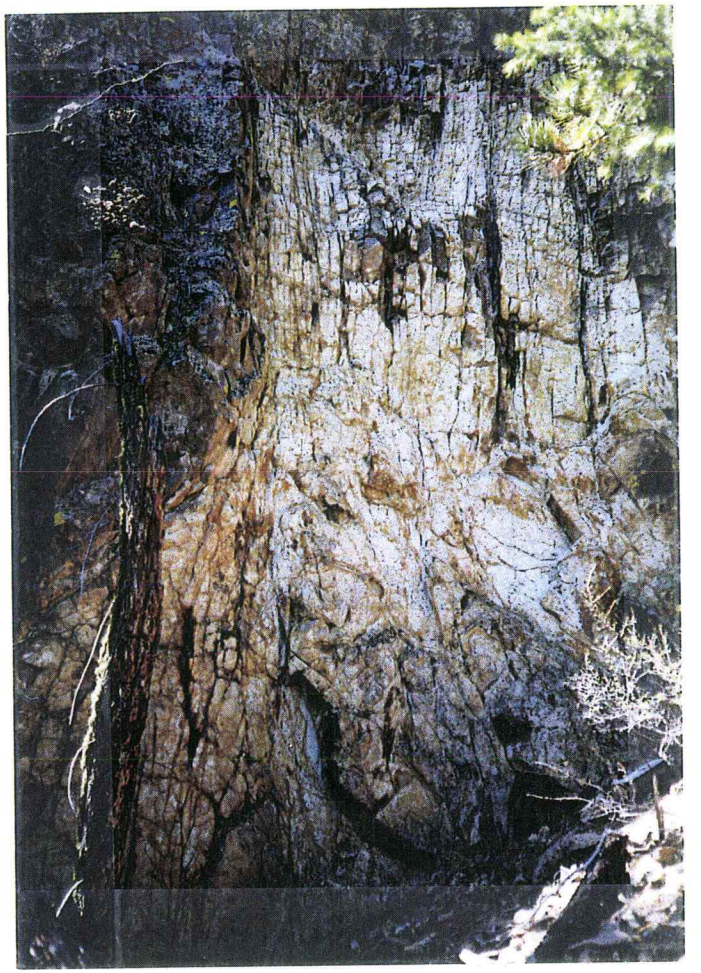

Figure 4. **Intrusive breccia occurrence. Note sheeted zone at the upper terminus of the breccia pod. The breccia is cutting a dike of Tid_4.**

elongate, sphene crystals; and <1 percent accessory brown melonite garnet and apatite. The aphanitic groundmass consists of trachytically aligned aegerine-augite intergrown with potassium feldspar, giving the rock an overall green appearance in hand sample. This unit may be equivalent to the tinguaite mapped by Richardson (1973) in the Landusky Mine area. Tid_1 dikes are unaltered in all mapped occurrences and cut Antoine Butte porphyry, establishing that Tid_1 dikes are both post-mineral and younger than the Antoine Butte porphyry. The Shell Butte porphyry, Tid_4, Tid_3, and intrusive breccia all show evidence of alteration and were likely emplaced prior to, or during, Stage II mineralization, and hence likely predate Tid_1. Tid_2 dikes are likely older than Tid_1 dikes since they are often propylitically altered.

Precambrian/Porphyry Contact Relationships

Large areas of Precambrian amphibolites crop out in the core of the range, leading early workers to suggest that many of the Paleocene porphryritic intrusives are laccolithic, and underlain by a Precambrian "floor" (Emmons, 1908; Richardson, 1973). However, Dyson (1938) interpreted the Precambrian rocks as roof pendants on top of stock-like intrusions, rather than the exposed floor of a laccolith. Brasher, Coolbough, and Disbrow (1983) interpreted many of the large Precambrian blocks as being faulted into place. Although contacts exist which argue in favor of each of the above hypotheses, evidence from current mapping suggests that most Precambrian rocks occur as xenoliths or roof pendants floating in porphyry (Figure 5A and B).

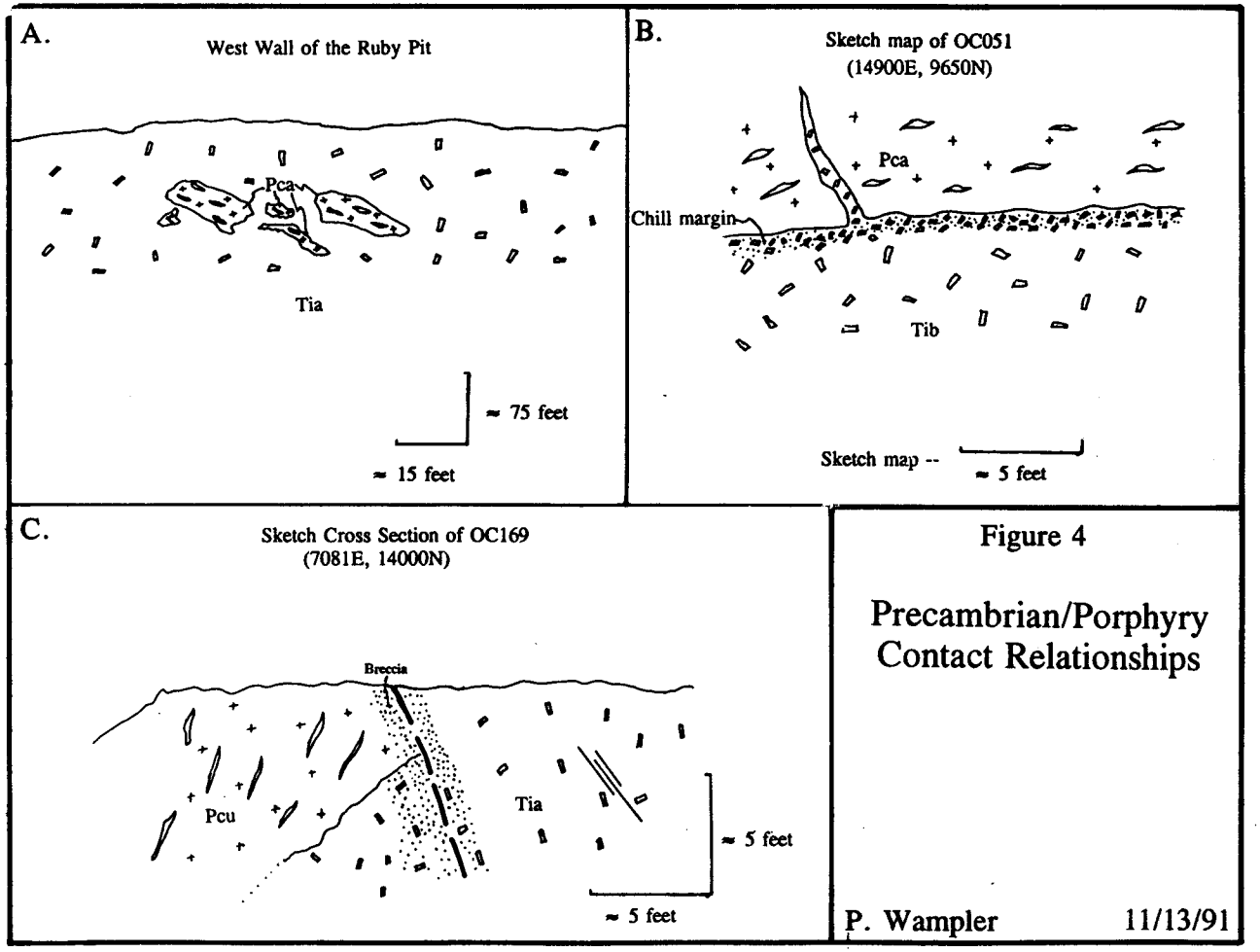

Figure 5. **Precambrian contact relationships. A. Precambrian blocks occurring as xenoliths. B. Igneous contact between Precambrian amphibolite and Beaver porphyry. C. A faulted contact between Antoine porphyry and Precambrian undifferentiated.**

Large blocks of Precambrian rock also occur as septa between different intrusive phases. The large Precambrian block west of Shell Butte and east of the Zortman Mine area is likely this type of septum, in this case, separating Antoine Butte porphyry from Shell Butte porphyry. Precambrian rocks separating different intrusive types or phases were found in several locations. Faulted contacts between intrusive rocks and Precambrian rocks are also common (see Figure 5C). In many cases, faulted contacts appear to have minimal offset, suggesting minor readjustment of a xenolith, rather than major fault displacement of a Precambrian block.

Tertiary Breccias

Several different lithologies and morphologies of breccia were encountered during mapping. The four types encountered included tectonic breccias; intrusive breccias, described above; mafic breccias; and potassically altered rock-flour matrix breccias.

Tectonic breccias are common throughout the map area. Tectonic breccias were distinguished from other breccia types by the presence of slickensides, angular clasts, and lack of matrix. Tectonic breccias occur along planar zones or faults and often are mappable for several meters to tens of meters along strike. The width of the brecciated zone typically ranges from a few centimeters to a few meters. Tectonic breccias commonly grade into what Kents (1964) referred to as "crackle breccias". In most cases, clasts are cemented together by iron oxides and/or thin coatings of drusy quartz.

Intrusive Breccia (Tibx)

Intrusive breccias (Tibx), occur as irregularly shaped bodies that commonly have a roughly elliptical shape. They are distinguished from other breccia types by their matrix-support and rounded to sub-rounded clasts in a matrix of rock flour of the same material as the clasts. Some occurrences have disseminated specular hematite in the rock-flour matrix. In thin section, the matrix most often consists of crystal fragments, but in some samples appears to have an igneous texture.

Mafic Breccia

At least one occurrence of "mafic breccia" was observed (PW169). It consists of both Precambrian amphibolite and sub-angular to sub-rounded clasts of porphyry containing 2 to 3 percent pyrite. The matrix is essentially unaltered pyroxene and amphibole indicating the breccia post-dates pyrite mineralization. It is possible that this breccia is a mafic dike rich in clasts and is actually a lamprophyre or diatreme similar to those described in the Missouri River Breaks to the south. It is also similar in many respects to a breccia body located west of the of the town of Zortman, near the town dump, which has been interpreted as a diatreme.

Dikes (Tid_3)

Several potassically altered, elongate, rock-flour-matrix breccias occur within the map area and were mapped as Tid_3. It is still unclear whether these features are truly breccias or strongly altered dikes with a fragmental texture. They are black

and very friable in hand sample with clasts of porphyry in an adularia(?)-flooded matrix. They consist of 10 to 20 percent, 0.3 to 1.5 mm diameter, angular fragments of both plagioclase and potassium feldspar in a matrix of very fine-grained rock flour, apparently flooded with adularia. They commonly have large amounts of pyrite, locally up to 15 percent. The relationship between potassically altered, rock-flour-matrix breccias and mineralization is unclear; however, the breccias are associated with anomalous gold values in both rock and soil samples from the area surrounding the mine. These breccia/dikes may represent structurally-controlled, pervasive, adularia alteration along gouge-rich shear zones during Stage I mineralization/alteration (see below), and may have a close temporal relationship to Tid_3 dikes.

Structural Geology

The structural geology surrounding the Zortman Mine is dominated by large shear zones which have strike lengths of hundreds of meters. Joints, joint sets, and master joints are common in the porphyritic intrusive rocks and may at least partially control mineralization. Regional tectonic controls may have provided the deep-seated fluid conduits which brought hydrothermal fluids to the surface.

Faults and Shear Zones

Several large shear zones have been mapped in the Zortman Mine and the surrounding area. The term "shear zone" is used to refer to a complex set of

parallel to sub-parallel vertical faults or fractures with no evidence of large scale displacement. Fault planes within many shear zones exhibit slickensides and are locally associated with tectonic breccias in the adjacent wallrock, as described above. Some areas described as shear zones may in fact be what Ramsay and Huber (1987) refer to as master joints, or regionally extensive joint sets. A good example of a set of master joints is the prominent lineament located in Alder Gulch (see Plate 1). Surfaces with slickensides were not observed in Alder Gulch, yet the lineament which the gulch follows is visible both in aerial photos and landsat imagery. The Ruby and Alabama shear zones, on the other hand, have abundant slickensides and, at least in the case of the Ruby shear zone, apparently offset small blocks of Precambrian amphibolite (see Plate 1). It is likely that a continuum exists between true faults with mappable separation and master joint sets which produce prominent lineaments but lack slickensides and evidence of displacement.

Often the lack of evidence for displacement is attributable to the fact that no stratigraphic markers are present to determine offset. Where Paleozoic strata are present, fault separation can often be documented. In the southeastern portion of the map, the presence of Paleozoic rocks with a well-known stratigraphy allowed interpretation of at least the sense of displacement for several faults.

The Ruby Gulch fault appears to offset the Shell Butte porphyry and the Mission Canyon Formation with a right-lateral sense of separation. The southern portion of the Shell Butte porphyry, as well as the contact between the Lodgepole Formation and the Mission Canyon Formation have an apparent right-lateral

separation of approximately 600 feet across the fault. In contrast, outcrops of Old Scraggy porphyry to the southeast do not appear to be offset by the Ruby Gulch fault. This creates a dilemma. How can the fault offset Shell Butte porphyry, which is inferred to be younger than the Old Scraggy porphyry, without creating similar offsets in the Old Scraggy porphyry? There are three plausible hypotheses to explain the observed field relationship (refer to Figure 6). One hypothesis is that the geometry of the Shell Butte porphyry is such that it dips in the same direction as the Mission Canyon Formation, whereas the Old Scraggy porphyry is orientated vertically. Thus, the fault displacement would be primarily down to southwest, and offset along the fault would have to have occurred post-Paleocene. A second hypothesis is that the Old Scraggy porphyry is actually younger than the Shell Butte porphyry and offset of Shell Butte porphyry and Mission Canyon Formation occurred prior to the emplacement of Old Scraggy porphyry. Displacement in this case could be either down to southwest, right-slip, or a combination of the two; and it would suggest that northwest-striking faults were active during the emplacement of Paleocene intrusions. The third hypothesis is that the Shell Butte porphyry is not really offset, and the apparent offset is merely a function of the geometry at the level of exposure of the Shell Butte porphyry. As in the second case, offset could be either down to southwest, right-slip, or a combination; but the timing of the faulting would have to be pre-Paleocene. This author favors the third hypothesis for the following reasons: 1) the shape of the Shell Butte porphyry elsewhere is stock-like and very irregularly shaped; 2) in at least one other area spatially displaced satellite

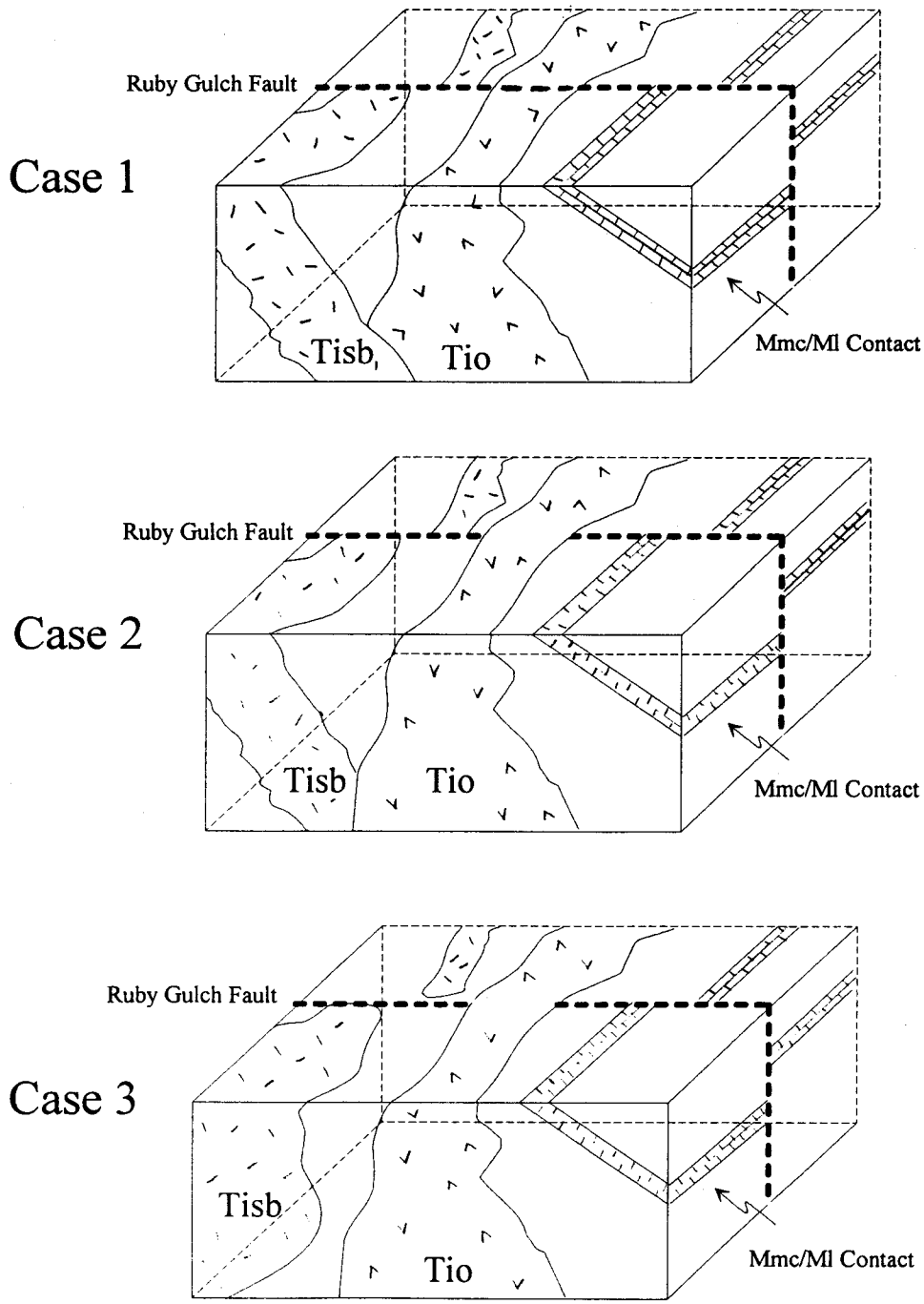

Figure 6. Ruby Gulch fault relationships. See text for description.

pods of Shell Butte porphyry are present (see Plate 1, 10700N, 11700E); and 3) the geometry of other Shell Butte contacts is typically vertical than gently dipping.

Folds

In addition to faulting, folding is also apparent in the Paleozoic rocks in the southeastern corner of the map. A syncline is apparent from outcrop patterns, and is less apparent in dip orientations. The syncline is cut by an arcuate, roughly north-south fault, which drops the west side down tens of feet relative to the east side. A minor component of left-lateral displacement is indicated by the offset of the fold axis. This may indicate that there is an intrusion to the southeast of the map area which is not yet exposed, perhaps the same intrusion which underlies Whitcomb Butte west of the town of Zortman. It is possible that the syncline outcrop pattern is partially the result of brittle deformation and is composed of several fault slices.

Joints

In an attempt to better understand the structural setting during emplacement and crystallization of the Paleocene intrusives, joint set strikes for selected intrusive units were collected and compiled in 15° increments on rose diagrams (see Figure 7). Joint and fracture data were collected during mapping and represent the most prominent joint set orientation for a given outcrop. Dip data are not compiled because a majority of the joint sets have dips greater than 80°.

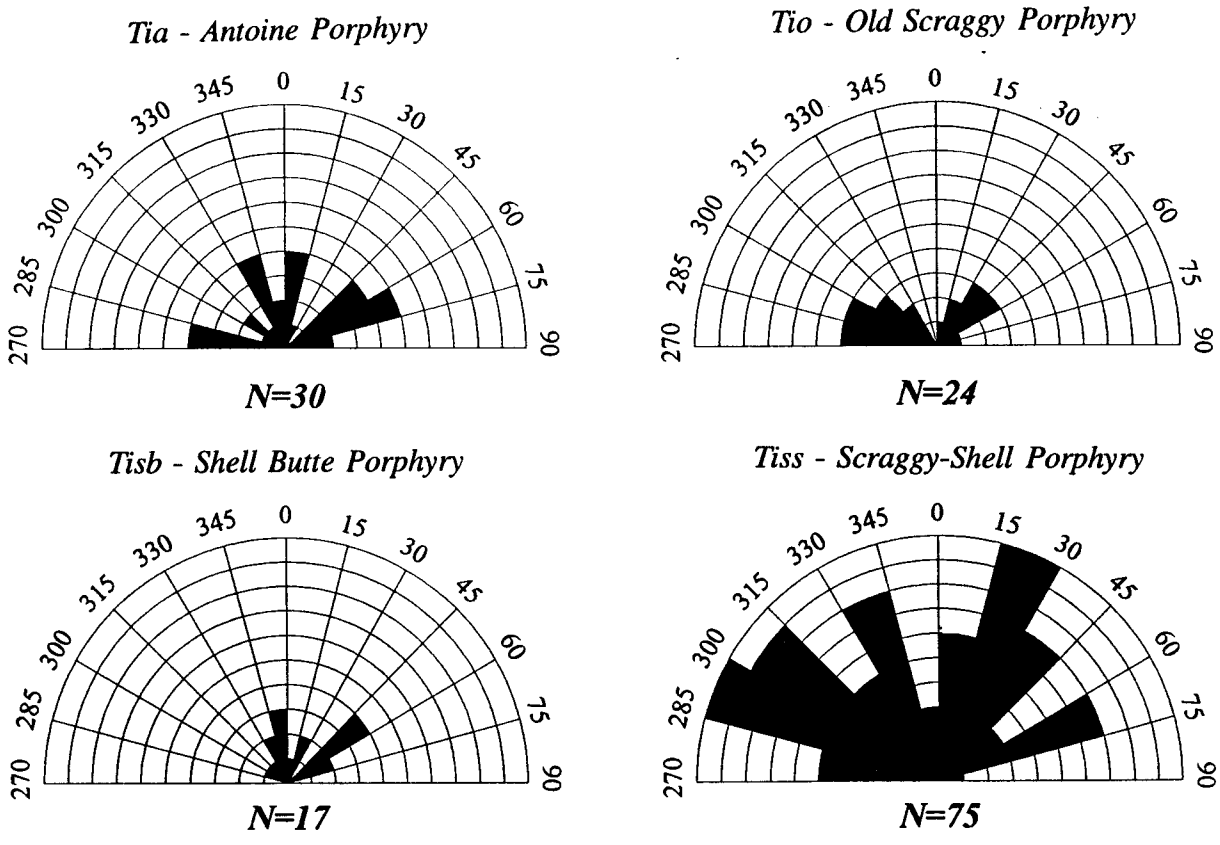

Figure 7. **Joint orientations. Prominent joint set orientation from four different porphyries (see text for description).**

Interpretation of joint data in intrusive rocks is made difficult by the fact that joints and fractures can result from several different mechanisms, including: 1) regional stresses present during the final stages of crystallization of the intrusion; 2) stresses produced by intrusion of nearby plutons before or after the magma is completely crystallized; and 3) tectonic stresses operating long after crystallization of the magma. Each porphyry for which data was compiled is summarized below.

The joints in the Antoine Butte porphyry exhibit three principal strikes: northeast, north-northwest to north-south, and east-west. All three of these strikes correspond to trends mapped for mineralized structures. The two main mineralized structures in the Zortman mine, the Ruby shear zone and Alabama shear zone, both occur in Antoine Butte porphyry (or its coarse-grained equivalent Tia(c)) and strike north-south to northwest-southeast. Several shear zones, likely composing one large shear zone, mapped in Antoine Butte porphyry south of Carter Butte, strike east-northeast. Soil and rock samples both indicate that this shear zone is also mineralized. Virtually all mineralized veins and shear zones on Shell Butte strike east-west. Tid_1, Tid_3, and bipyramidal quartz-bearing dikes all exhibit a distinct northeast alignment. Of these, Tid_3 and bipyramidal quartz-bearing dikes are altered and often mineralized, while Tid_1 is apparently post-mineralization. The Shell Butte porphyry is aligned north-northwest and may have been emplaced along a preexisting north-northwest shear zone or contact separating Antoine Butte porphyry from Precambrian wallrocks.

Joints and fractures in the Shell Butte porphyry exhibit strikes similar to those in the Antoine Butte porphyry, with the important exception of the lack of the east-west trend. This is somewhat surprising since most mineralization occurring on Shell Butte appears to be controlled by east-west-striking faults and veins. It is possible that joints and fractures oriented north-northwest and northeast represent stresses present during emplacement, and that the east-west mineralization on Shell Butte represents stresses that occurred after emplacement.

Joint orientations in the Scraggy-Shell porphyry exhibit less distinct trends. North-northeast, east-northeast, north-northwest, and west-northwest trends are the most common. Of these, the west-northwest trend is perhaps the most interesting since it is not apparent in Shell Butte or the Antoine Butte porphyries, nor is it a prominent orientation for any known mineralized faults or veins. Contrary to other indications, the Scraggy-Shell porphyry may be significantly younger the Shell Butte porphyry and younger than Stage I and Stage II mineralizing events (see Figure 2). This is supported by the distinct lack of significant alteration and mineralization in the Scraggy-Shell porphyry. Alternatively, the Scraggy-Shell porphyry may have simply been spatially, rather than temporally, isolated during mineralization.

The Old Scraggy porphyry exhibits prominent northeast and east-west to west-northwest joint strikes. Perhaps the most significant feature of the pattern is the lack of a prominent north-northwest striking joint set. If the Old Scraggy porphyry is indeed older, as has been suggested, why does it not reflect at least some of the north-northwest pattern prominent in both the Shell Butte and Antoine Butte

porphyries? The lack of a north-northwest pattern may indicate: 1) that the Old Scraggy porphyry was spatially isolated from the local tectonic stresses which presumably produced north-northwest joints in the Shell Butte porphyry and north-northwest joints and mineralized shear zones in the Antoine Butte porphyry; 2) the Old Scraggy porphyry is actually younger than both the Shell Butte and the Antoine Butte porphyries; or 3) insufficient data were collected to discern a north-northwest trend which was in fact present. Of the above three explanations this author favors the first, primarily based on the interpretation that the Old Scraggy is the oldest in the intrusive sequence.

Regional Tectonic Controls

The well-developed north-northwest-striking shear zones of the Zortman deposit have been noted by virtually every worker who has studied the area. Russell (1991) suggested a possible link between the northeast-striking Great Falls Tectonic Zone (GFTZ) described by O'Niell and Lopez (1985), and the northeast-striking structures controlling mineralization at the nearby Landusky Mine. The northeast-striking shear zone mapped on south Carter Butte, as well as Tid_1, Tid_3, and bipyramidal quartz-bearing dikes (Tibq) all exhibit a distinct northeast alignment which may bear some relation to the GFTZ. The north-northwest shear zones of the Zortman deposit may be tectonically unrelated structures which served as conduits for fluids flowing upward along the northeast-striking GFTZ. Alternatively, the north-northwest-striking shears may represent the north-northwest component of a

north-northwest/north-northeast conjugate fault set created by regional north-south compression. The northeast-striking structural trend may be evidence of a deep crustal weakness which allowed hydrothermal fluids and perhaps associated with alkaline magmas to reach the surface and provide the thermal energy to drive the Zortman hydrothermal system.

HYDROTHERMAL ALTERATION, MINERALIZATION, AND PARAGENESIS

Alteration at the Zortman Mine is probably best termed adularia-sericite-type alteration as described by Heald et al. (1987). Widespread potassium metasomatism and replacement of feldspars by adularia + sericite, and mafic minerals by sericite is common surrounding the mine area. The alteration assemblages and textures observed are very similar to those described at the Round Mountain epithermal gold deposit (Sanders and Einaudi, 1990). In contrast to Round Mountain, alteration at Zortman Mine probably involved several episodes of hydrothermal activity with significant time gaps between alteration events rather than one continuous hydrothermal event. The mineral assemblages associated with each event spatially overlap one another; and distinguishing between separate events is difficult due to the lack of cross-cutting vein relationships.

Alteration minerals which are readily identifiable in hand sample include chlorite, calcite, epidote, and pyrite associated with propylitic alteration; and quartz, fluorite, and calcite associated adularia alteration. Widespread weak sericite + pyrite, adularia, and carbonate alteration are more cryptic, and were delineated based on petrographic examination of approximately 400 thin sections (see Plate 3 for locations). Approximately 130 of these were collected by previous workers. Alteration types and their field characteristics are summarized in Table 3.

In the presentation that follows, the term "sericite" refers to a fine-grained white mica with moderate birefringence. X-ray diffraction (XRD) studies done by

Table 3. Summary of alteration types.

Type	Occurrence	Form	Added Minerals	Field Characteristics
Weak Sericite + Pyrite Alteration	Widespread, no obvious structural control	Pervasive and incipient replacement of primary feldspars and mafic minerals	Sericite/illite, euhedral cubes and anhedral blebs of pyrite ± quartz ± calcite, replacing groundmass	Difficult to distinguish in field, however, feldspars lose their hardness and often have a milky, pitted look.
Adularia Alteration				
Pervasive adularia + pyrite	Localized along mineralized shear zones central to adularia overgrowth veins	Complete replacement of primary feldspars by adularia	Adularia + quartz ± sericite/illite ± pyrite ± fluorite ± calcite	Often has the appearance of pervasive black silicification, however, alteration can also be cryptic and hard to identify in hand sample.
Fracture-controlled adularia ± jarosite overgrowth veins	Widespread and along shear zones and faults surrounding areas of pervasive adularia + pyrite alteration	Stockwork veinlets, adularia occurs as overgrowths on orthoclase and plagioclase and as replacement selvages, relict plag and K-spar are present	Adularia + quartz ± sericite ± jarosite ± hematite ± fluorite ± calcite(?)	Difficult to distinguish from stockwork quartz veins, generally requires thin section identification.
Propylitic Alteration	Localized, in younger dikes and Alder Gulch syenodiorite	Selective replacement; some chlorite veinlets, but rare	Chlorite + calcite + pyrite ± albite (?) ± quartz ± epidote ± sphene	Epidote and calcite are easily distinguished in hand sample. The porphyry has an overall greenish color.
Albitic	Localized along faults and shears	Replacement of Kspar and plagioclase by hydro-thermal feldspar (and as veinlet filling (?))	Albite feldspar ± chlorite	Cannot be distinguished in hand sample, requires thin section identification.
Carbonate Alteration	Widespread and peripheral to mineralized shear zones	Disseminated, patchy replacement of both groundmass and phenocrysts, and sparse veinlets	Calcite ± Dolomite(?)	Effervesces with dilute hydrochloric acid. Often has a bleached white appearance.

Wilson and Kyser (1989) indicate that at least some of the fine-grained white mica is more correctly termed illite, a potassium aluminum sheet silicate. XRD analyses were not done in conjunction with this study. The term potassium feldspar is used in cases where either the type of potassium feldspar was not determined or more than one type of potassium feldspar is being discussed. Most of the potassium feldspar identified in the porphyries was sanidine based on 2V determination. Adularia was identified by the presence of mottled extinction, crystal shape, and lack of incipient alteration.

Mineralization likely occurred during at least two stages, divisible on the basis of the age of porphyry intrusion affected. Low-grade disseminated gold/silver mineralization likely occurred during widespread weak sericite + pyrite alteration. This mineralizing event shall be referred to as Stage I mineralization. Higher grade, shear-zone-controlled mineralization occurred during adularia alteration. This mineralizing event shall be referred to as Stage II mineralization. Stage II mineralization is further divided into early and main phases. Pervasive adularia ± sericite ± pyrite ± marcasite ± fluorite ± calcite (?) alteration was associated with early Stage II mineralization, and adularia ± sericite ± jarosite ± fluorite ± calcite alteration, occurring primarily as overgrowth veinlets, was associated with main Stage II mineralization. The distribution of gold in grab samples, soil samples, and exploration drilling samples indicates a strong correlation between gold mineralization and pervasive adularia alteration and adularia overgrowth veining of Stage II mineralization.

Widespread Weak Sericite + Pyrite Alteration

Weak sericite + pyrite alteration appears to be a widespread, early alteration event designated Stage I alteration. However, no cross-cutting relationships were observed which fix the timing of the alteration relative to other alteration types. This alteration type occurs over much of the area mapped and is outlined on Plate 2. It should be noted that the area outlined on Plate 2 shows the generalized outer limit of weak sericite + pyrite alteration; within this limit weak sericite + pyrite is widespread, but is absent locally. Weak sericite + pyrite alteration does not significantly affect porphyries younger than the Antoine Butte porphyry. Since younger porphyries do exhibit other alteration types such as propylitic and adularia alteration, this distribution suggests that there were at least two temporally distinct alteration events: Stage I mineralization/alteration which affected the Antoine Butte porphyry, and younger Stage II mineralization/alteration that affected both the Antoine Butte porphyry and post-Antoine Butte intrusions. The lack of primary mafic minerals in the Shell Butte porphyry make it difficult to quantify the amount of weak sericite + pyrite alteration in that porphyry. Plagioclase in the Shell Butte porphyry is not significantly altered to sericite except near veins on north Shell Butte.

Weak sericite + pyrite alteration is characterized by partial replacement of primary sanidine and plagioclase feldspars by sericite ± quartz ± pyrite ±

adularia(?) ± fluorite(?) ± calcite ± quartz(?), and replacement of mafic minerals by sericite ± pyrite (see Figure 8). Alteration of feldspars to sericite ranges from trace amounts of incipient alteration to almost complete replacement, and most commonly ranges from 10 to 15 volume percent replacement. Plagioclase feldspars are invariably altered to a greater extent than sanidines in a given thin section. Mafic minerals are commonly completely altered to sericite ± iron-titanium oxides. Locally, pyroxene and hornblende are replaced by green clay (smectite). One to 3 volume percent pyrite is added as blebs and euhedral cubes. Widespread weak sericite + pyrite alteration is the most difficult alteration type to delineate and map in the field due to the fine-grained nature of the alteration and the later partial replacement of primary feldspars by secondary clays, presumably derived from surface weathering. Widespread quartz veinlet stockworking occurs in sericite + pyrite altered rocks and is likely cogenetic. The quartz veinlets consist of 0.5 to 1.0 mm-wide grey quartz veinlets which locally grade into crackle breccia with minor drusy, euhedral quartz lining cavities. Grey quartz veinlets rarely have any associated minerals and have no discernable selvages. Distinguishing these veinlets from later adularia veinlets in hand sample can be very difficult. Quartz veinlet stockworks are most common in the Antoine Butte porphyry.

Fluorite occurring as a feldspar replacement, in which fluorite preferentially replaces both sanidine and plagioclase feldspar phenocrysts in an irregular, blebby fashion (see Figure 9) is spatially associated with both the early weak sericite + pyrite alteration and the later adularia alteration.

A. Cross-Polarized Light

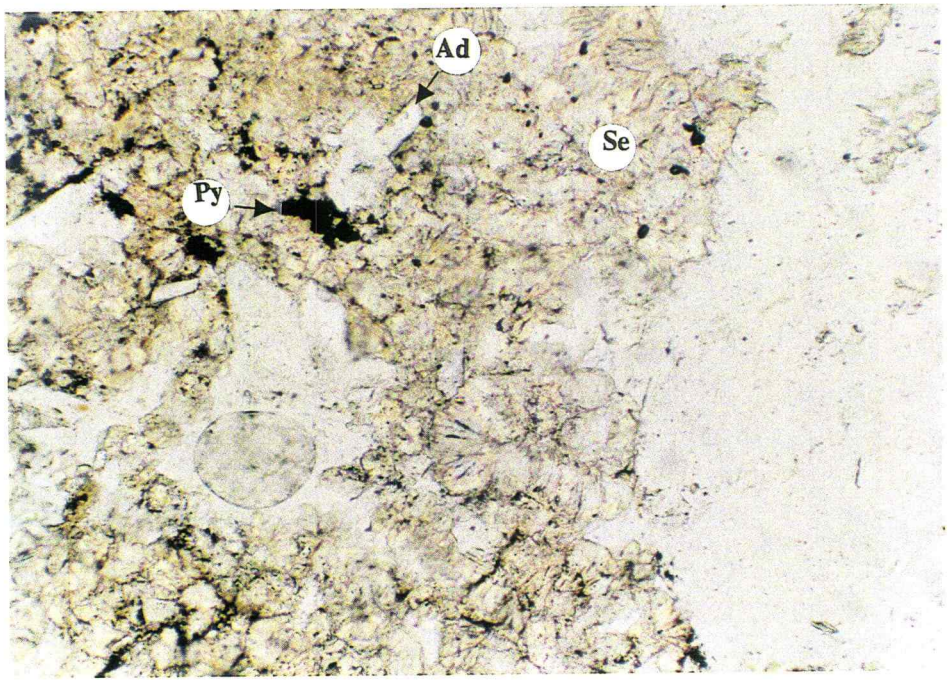

B. Plane-Polarized Light

Figure 8. Pervasive sericitic + pyrite alteration ± adularia(?). Note pale brown radiating sericite (Se); opaque pyrite blebs (Py); and clear adularia(?) (Ad). Magnification 100x.

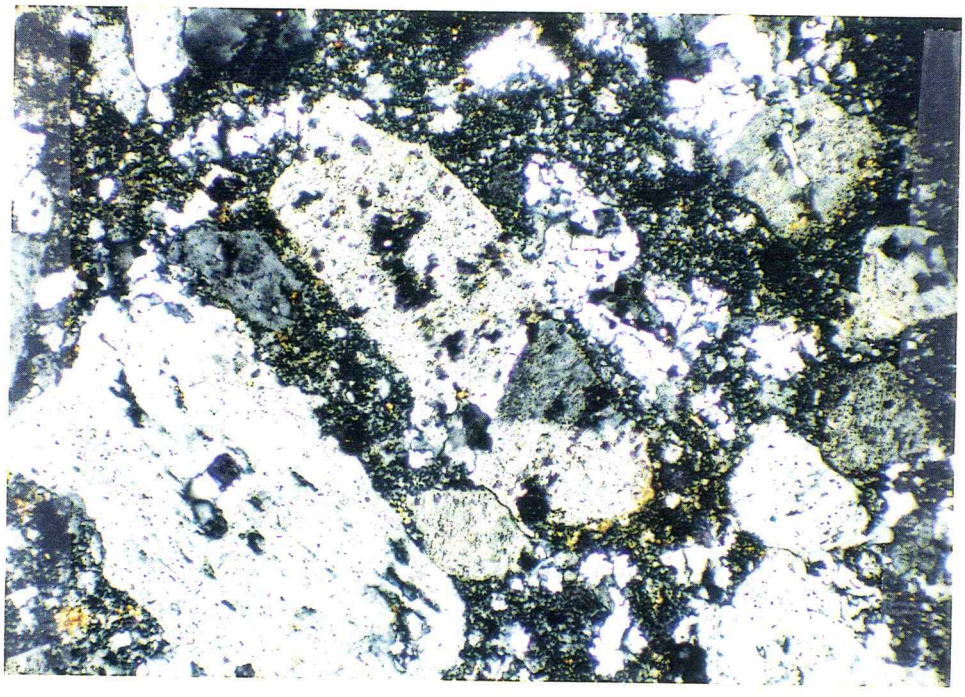

A. Cross-Polarized Light

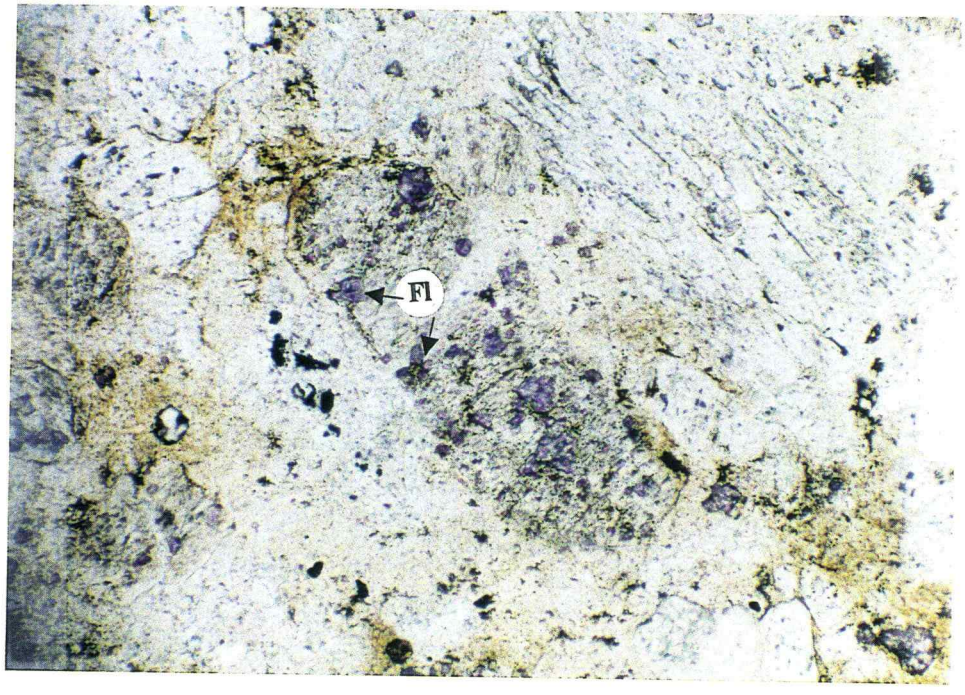

B. Plane-Polarized Light

Figure 9. Partial replacement of feldspar phenocrysts and groundmass by purple fluorite (Fl) in Antoine Butte porphyry. Magnification 100x.

Weak sericite + pyrite alteration at the Zortman deposit is similar to the widespread phyllic/argillic halo described by Buchanan (1979) which surrounds the Las Torres Mine near Guanajuato, Mexico. It is also similar, although much weaker in intensity, to sericitic alteration which is described around many porphyry ore deposits, but the latter typically lacks calcium minerals such as calcite and fluorite. The widespread occurrence and apparent lack of structural control for widespread weak sericite + pyrite alteration suggest that the alteration was related to a large-scale hydrofracturing event rather than localized hydrothermal alteration surrounding fluid pathways. Interpretation of the paragenesis of the widespread weak sericite + pyrite alteration is further complicated by the presence of superimposed Stage II adularia-rich alteration, which is clearly structurally controlled. It is unclear how much gold mineralization, if any, was associated with the sericite + pyrite event. Anomalous gold values (< 0.005 ounces of gold per ton) which occur over much of the area affected by widespread weak sericite + pyrite alteration would suggest that at least some gold was introduced at this time. Remobilization of this earlier low-grade gold mineralization during later epithermal mineralization may have been important in the formation of shear-zone-controlled economic mineralization. The spatially extensive low-grade gold event and the associated weak sericite + pyrite alteration, as mentioned above, constitutes Stage I mineralization.

Adularia Alteration

Two types of adularia-rich alteration, constituting stage II alteration, are prevalent at Zortman, and both are enclosed within the broad zone of weak sericite + pyrite alteration. Pervasive adularia + pyrite alteration is restricted to narrow zones (<200 meters (650 feet) wide) along major shears, and is entirely enclosed by a zone of weaker alteration characterized by adularia + jarosite overgrowth veinlets. Several areas of pervasive adularia alteration were identified including: a roughly 180-meter (600-foot) wide by 430-meter (1,400-foot) long zone in the O.K. Pit in the Zortman Mine, a zone roughly 100 meters (330 feet) in diameter on southeast Carter Butte, and several smaller linear zones on north Antoine Butte. In all of these areas, pervasive adularia alteration is associated with, and central to, a larger area of adularia ± jarosite overgrowth veining.

Pervasive Adularia + Pyrite Alteration

In order to better constrain adularia alteration, a detailed study was performed on a well-exposed bench in the O.K. Pit. Mapping was done at a 1-inch = 20-foot scale along a 550-foot (168-meter) long bench which traverses the Ruby shear zone. Particular attention was paid to alteration, vein relationships, and subtle lithology changes. Rock samples were taken both at regular intervals and in areas of particular geologic interest. Whole rock geochemical analyses for the O.K. Pit samples and for representative "unaltered" samples are summarized in Appendix A.

The term "unaltered" is used to refer to the least altered example available for a given porphyry.

The mapping defined a large shear zone and broad area of cryptic pervasive adularia + pyrite ± marcasite alteration approximately 180 meters (600 feet) wide enclosing a 30-meter (100-foot) wide central shear zone (see Figure 10). A dike of Tid_2 emplaced along the shear zone and offset by later faulting is also altered. A zone of pervasive black adularia + pyrite alteration termed "cataclasite" occurred east of the central shear zone. The term cataclasite is used to refer to a rock which has a texture similar to a porphyry dike but the phenocrysts are elongated and contorted parallel to the strike of the bounding walls. The last sample taken on the western end of the bench had essentially the same whole rock geochemical composition as that of "unaltered" Antoine Butte porphyry. Sampling on the eastern end of the bench did not extend outside the altered area based on geochemical analyses. Interestingly, in samples from the altered zone, both the weight percent of Al_2O_3 and the weight percent of SiO_2 remained essentially the same as that of "unaltered" Antoine Butte porphyry across the altered zone, whereas Na_2O was strongly depleted and K_2O was strongly enriched (see Figure 10). Wilson and Kyser (1989) concluded, based on samples from both the Zortman and Landusky mines, that the variation of Na_2O and K_2O in the rocks could be ascribed to a simple magmatic mixing model. However, data from this study clearly indicate that the potassium/sodium ratios in samples from the O.K. Pit have been significantly perturbed by potassium metasomatism (see Figure 11). Metasomatism may be

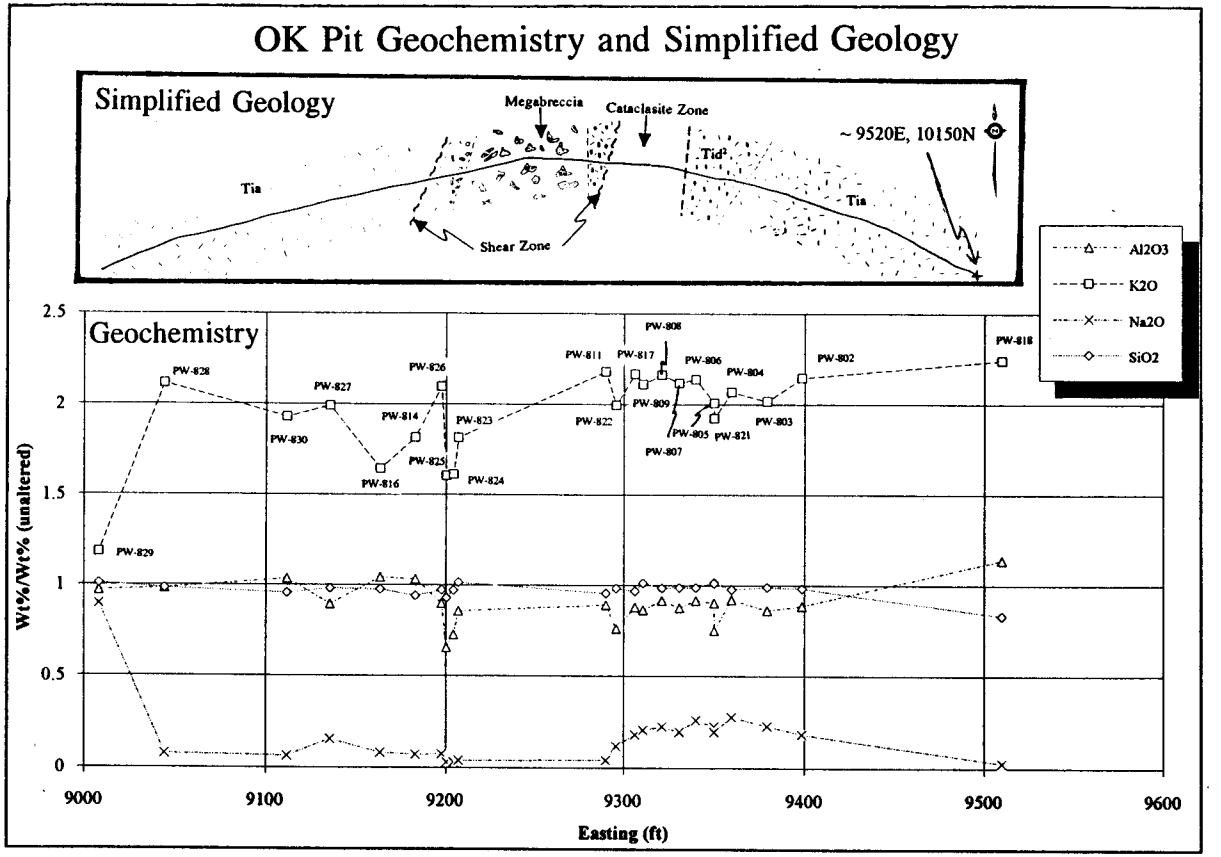

Figure 10. **O.K. Pit geochemistry and simplified geology. Y-axis is weight percent oxide in a bench face sample divided by weight percent oxide in a representative "unaltered" sample of Antoine Butte porphyry. See Appendix A for whole rock geochemical data. The eastings on the inset geology coincide with those on the X-axis. Tia = Antoine Butte porphyry; Tid_2 = diking phase (see text for description). The "unaltered" sample is PW123, SiO_2 = 68.91 weight percent; Al_2O_3 = 17.32 weight percent; K_2O = 5.71 weight percent; and Na_2O = 4.99 weight percent.**

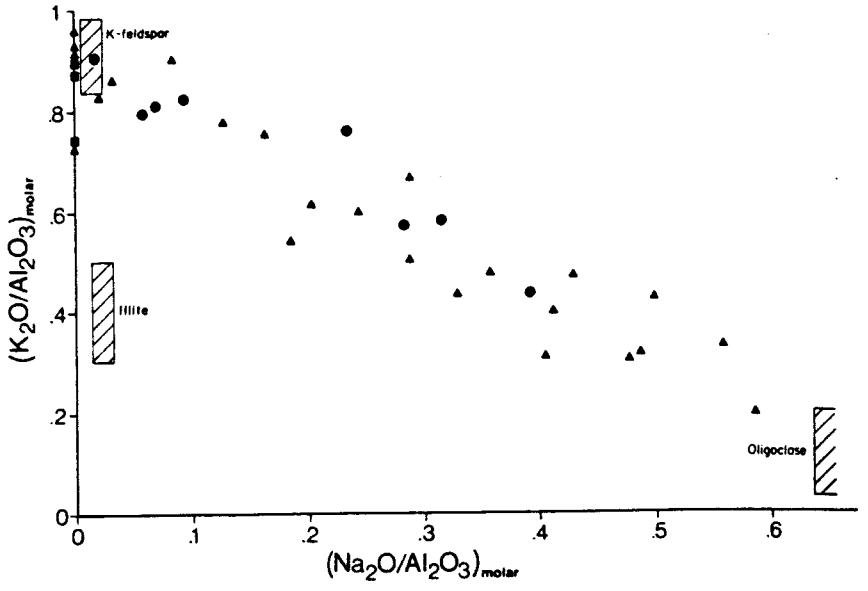

A

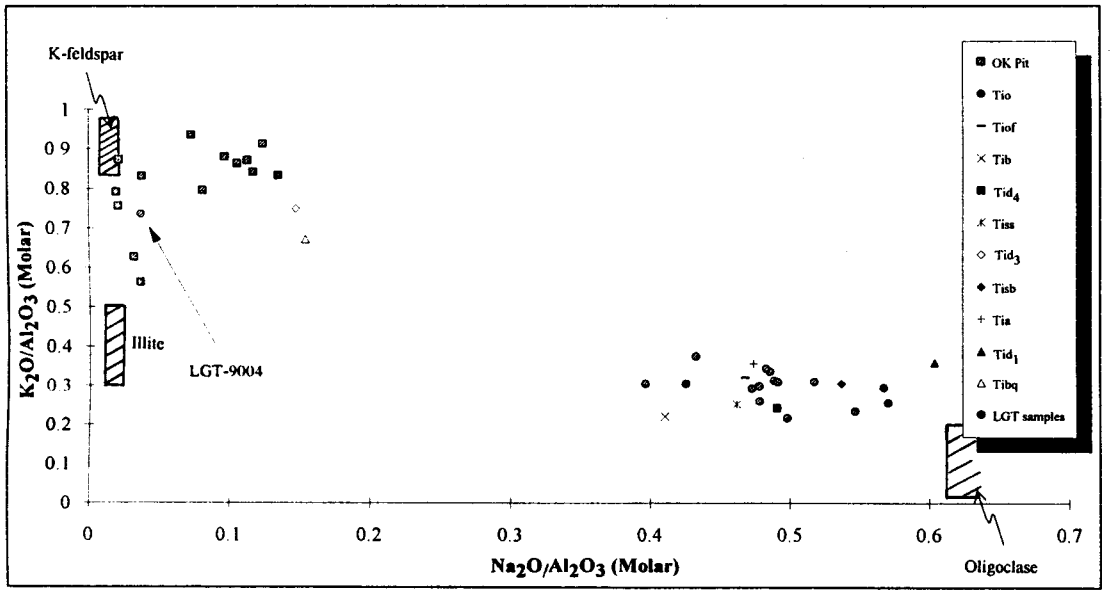

B

Figure 11. **Comparison of geochemical data from Wilson and Kyser (1989) and this study. Figure 11A is from Wilson and Kyser (1989). Note the distinct gap in the linear trend in the data from this study which requires a geochemical model other than magmatic mixing. Hydrothermal replacement of oligoclase by >90 percent K-spar effectively models alkali compositions. In 11B, O.K. Pit samples are K-altered as are Tid_3 and Tibq. All other samples shown are the least altered samples available. LGT samples were taken by Zortman Mining personnel.**

simply modelled by alkali exchange between the hydrothermal fluid and feldspars, causing complete replacement of sodium plagioclase by K-feldspar, and is governed by the reaction $K^+ + NaAlSi_3O_8 \rightleftarrows Na^+ + KAlSi_3O_8$. Gold values from 10 foot composite rock chip samples taken along the bench ranged from <0.02 ounces per ton to 0.030 ounces per ton, with the highest values occurring in the shear zones. The average of all samples taken was 0.007 ounces of gold per ton, quite low for the Zortman deposit.

Pervasive adularia alteration is characterized by complete (>90 volume percent) replacement of primary plagioclase and potassium feldspar phenocrysts by adularia, 2 to 10 volume percent pyrite addition, and apparently no change in SiO_2 content (see Figure 10). Mafic minerals are typically either completely destroyed, or are completely altered to sericite. Increasing degrees of alteration observable in thin section and whole rock geochemical compositions are often not apparent in hand sample, where igneous textures are often well-preserved. One to two volume percent sericite addition to the groundmass and feldspar phenocrysts is also apparently associated with the pervasive adularia + pyrite alteration event. Pervasive adularia alteration is apparent outside the mine area in Tid_3 dikes. In the case of Tid_3 dikes, it is spatially associated with replacement of feldspar phenocrysts by fluorite on north Antoine Butte.

Semi-quantitative electron microprobe analyses of groundmass feldspars in altered and "unaltered" porphyritic quartz monzonite samples confirm that plagioclase and magmatic potassium feldspar in the porphyry groundmass were

replaced by adularia ± sericite. The average of all feldspar analyses in the altered porphyry groundmass was $Ab_{4.0}Or_{95.9}$, whereas the average of all "unaltered" groundmass feldspars compositions was $Ab_{34.9}Or_{64.7}$. SiO_2 content was comparable for "unaltered" (average 66.10 percent) and altered (average 64.88 percent) porphyries, suggesting that overall SiO_2 content was not significantly changed during alteration. Table 4 summarizes groundmass feldspar analyses. Analyses of groundmass feldspar compositions showed a distinct difference in the composition of altered versus "unaltered" groundmass. Figure 12A is a plot of K_2O versus $K_2O/(Na_2O+K_2O)$ for altered and "unaltered" groundmass analyses. Figure 12B plots K_2O versus $K_2O/(Na_2O+K_2O)$ for typical feldspar types from Deer, Howie, and Zussman (1963). The "unaltered" analyses fall in three main areas on the graph (refer to Figure 12). One analysis falls in the lower left corner, close to the typical albite in Figure 12B. This analysis represents magmatic plagioclase feldspar of albite to oligoclase composition. One analysis had intermediate $K_2O/(Na_2O+K_2O)$ values. This is the result of fluorescing intergrown plagioclase and orthoclase feldspar. The majority of the unaltered analyses have moderately high $K_2O/(Na_2O+K_2O)$ values. This is consistent with typical magmatic orthoclase and/or sanidine (see Figure 12B). Analyses from the altered groundmass show a distinctly different trend and location on the graph. All the altered groundmass analyses fall either near the composition of typical adularia, or along a linear trend toward decreasing K_2O. This is consistent with the interpretation that magmatic potassium feldspar has been extensively replaced by adularia in the groundmass of the altered

Table 4. Summary of porphyry groundmass analyses.

Altered/Unaltered	Sample No.	Na_2O	MgO	Al_2O_3	SiO_2	K_2O	CaO	Fe_2O_3	BaO	Total	Ab	Or	An	Fm	$K_2O/(K_2O+Na_2O)$
Altered	PW809	0.515	0.000	18.68	63.35	15.68	0.000	0.426	0.045	98.70	4.756	95.24	0.001	0.999	0.97
Altered	PW809	0.574	0.039	16.08	67.2	13.44	0.015	0.497	0.011	97.86	6.091	93.82	0.09	0.866	0.96
Altered	PW809	0.515	0.000	18.68	63.35	15.68	0.000	0.426	0.045	98.70	4.756	95.24	0.001	0.999	0.97
Altered	PW809	0.574	0.039	16.08	67.2	13.44	0.015	0.497	0.011	97.86	6.091	93.82	0.09	0.866	0.96
Altered	PW802	0.270	0.016	18.41	64.36	15.89	0.000	0.095	0.056	99.10	2.518	97.48	0.747	0.000	0.98
Altered	PW802	0.248	0.003	18.46	64.54	15.95	0.000	0.099	0.005	99.31	2.311	97.69	0.000	0.947	0.98
Altered	PW802	0.348	0.004	18.65	64.56	16.06	0.000	0.334	0.050	100.01	3.187	96.81	0.000	0.98	0.98
Altered	PW802	0.288	0.016	18.35	64.46	15.91	0.000	0.161	0.042	99.23	2.677	97.32	0.000	0.84	0.98
Average		0.417	0.015	17.92	64.88	15.258	0.004	0.317	0.033	98.92	4.048	95.93	0.116	0.812	0.97
Standard Deviation		0.141	0.016	1.146	1.519	1.127	0.007	0.173	0.020	N/A	1.573	1.61	0.258	0.334	0.96
"Unaltered"	PW123	2.431	0.000	18.97	64.68	13.07	0.09	0.144	0.067	99.45	21.94	77.61	0.45	1.000	0.84
"Unaltered"	PW123	3.815	0.000	18.76	66.63	10.59	0.084	0.047	0.059	99.99	35.24	64.33	0.426	1.000	0.74
"Unaltered"	PW123	0.526	0.000	18.73	64.43	15.48	0.002	0.101	0.057	99.33	4.909	95.08	0.009	0.991	0.97
"Unaltered"	PW077	1.007	0.013	16.08	68.39	12.38	0.028	0.786	0.082	98.77	10.99	88.85	0.167	0.968	0.92
"Unaltered"	PW077	6.339	0.007	17.1	70.06	5.262	0.013	0.255	0.026	99.06	64.63	35.3	0.072	0.95	0.45
"Unaltered"	PW077	4.167	0.000	19.1	65.57	10.32	0.027	0.252	0.182	99.62	37.98	61.88	0.136	1.000	0.71
"Unaltered"	PW077	8.502	0.023	17.08	67.77	1.828	0.037	3.791	0.048	99.08	87.42	12.37	0.211	0.988	0.18
"Unaltered"	PW123	3.802	0.011	19.13	64.76	10.19	0.182	0.125	0.089	98.29	35.84	63.22	0.946	0.852	0.73
"Unaltered"	PW123	2.618	0.029	19.04	64.04	12.65	0.175	0.08	0.126	98.76	23.72	75.41	0.876	0.581	0.83
"Unaltered"	PW123	2.809	0.008	19.01	64.69	11.68	0.148	0.099	0.113	98.56	26.57	72.66	0.772	0.862	0.81
Average		3.602	0.010	18.30	66.10	10.345	0.079	0.568	0.085	99.14	34.92	64.67	0.407	0.919	0.69
Standard Deviation		2.382	0.010	1.11	2.03	3.993	0.068	1.153	0.045	N/A	24.69	24.64	0.347	0.131	0.68

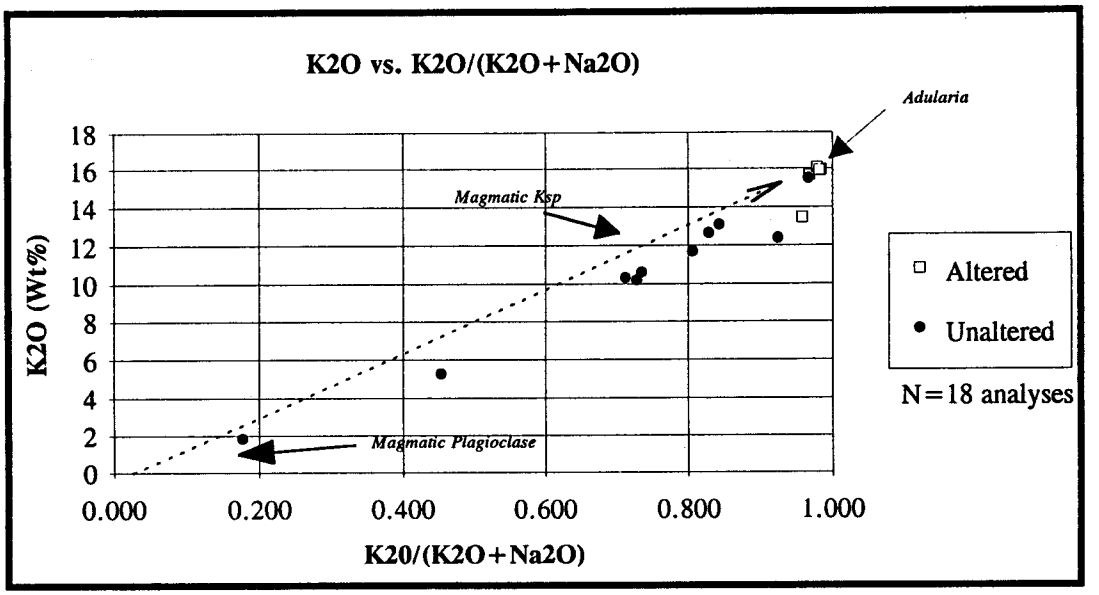

A

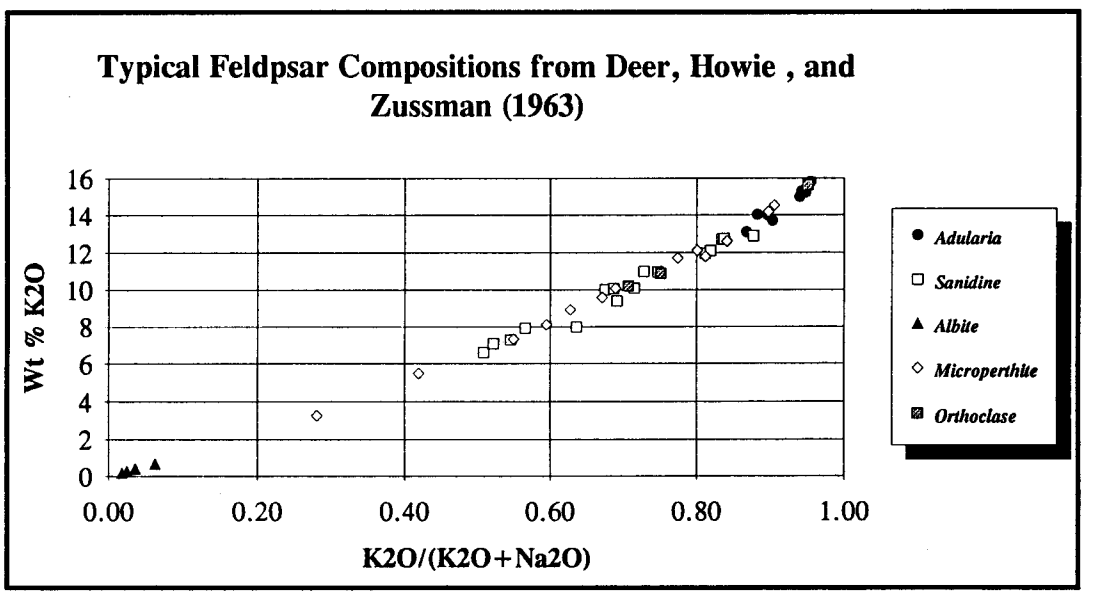

B

Figure 12. **Microprobe analyses from the Zortman Mine area. A. Semi-quantitative microprobe analyses of groundmass from adularia altered and "unaltered" samples. Data are summarized in Table 4. B. Typical feldspar compositions from Deer, Howie, and Zussman (1963).**

samples. The analysis with lower a K_2O values is a composite analysis with quartz, the quartz effectively lowering the measured values of K_2O and Na_2O.

Veinlets, although not megascopically visible, in many cases are apparent in thin section (see Figure 13). They commonly exhibit irregular, indistinct boundaries with the wallrock and have no selvages. Both open-space-filling and replacement type veinlets were observed. They are composed of quartz and adularia and, in rare occurrences, appear to destroy earlier weak sericite + pyrite alteration. Adularia veinlets associated with the adularia + pyrite event are more difficult to identify and distinguish than adularia veinlets associated with adularia + jarosite alteration. It is difficult to determine the timing of the pervasive adularia + pyrite alteration event relative to other alteration events; however, one cross-cutting relationship indicates that pervasive adularia + pyrite veinlets predate fracture-controlled adularia + jarosite overgrowth veinlets, which suggests that the two events may be temporally distinct. Alternatively, they could be contemporaneous zones with the inner zones encroaching with time on outer zones as fluid fronts advance or collapse.

Adularia + Jarosite Overgrowth Veinlet Alteration

Fracture-controlled adularia + jarosite overgrowth veinlets are more widespread than pervasive adularia + pyrite alteration, and also appear to be localized along the same mineralized shear zones. This alteration type comprises roughly 10 percent of the area mapped and commonly surrounds areas of pervasive adularia + pyrite alteration. As mentioned above, it is unclear whether adularia +

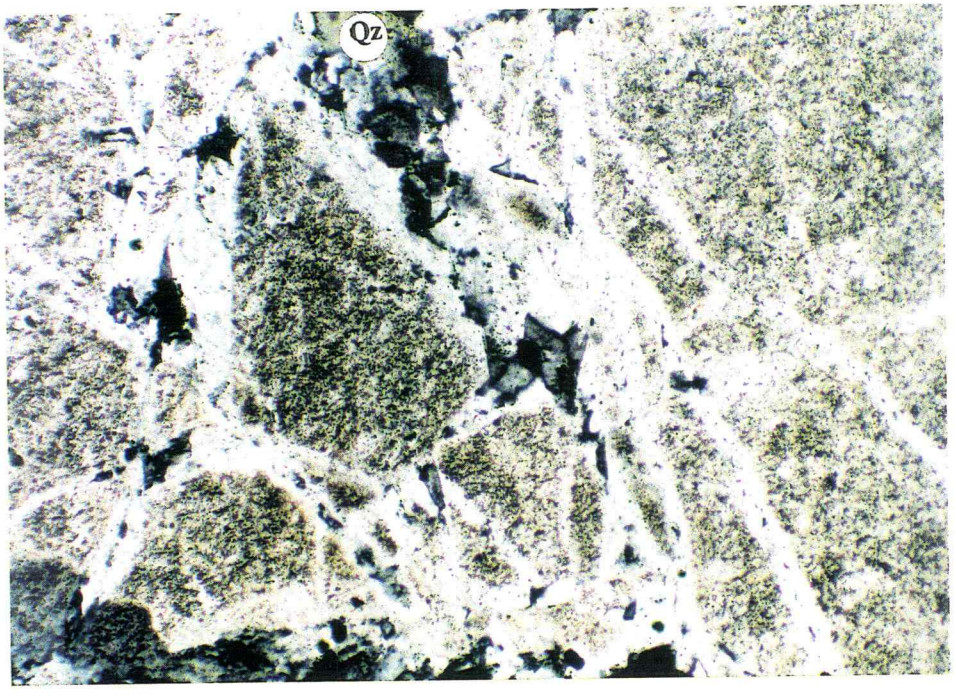

A. Cross-Polarized Light

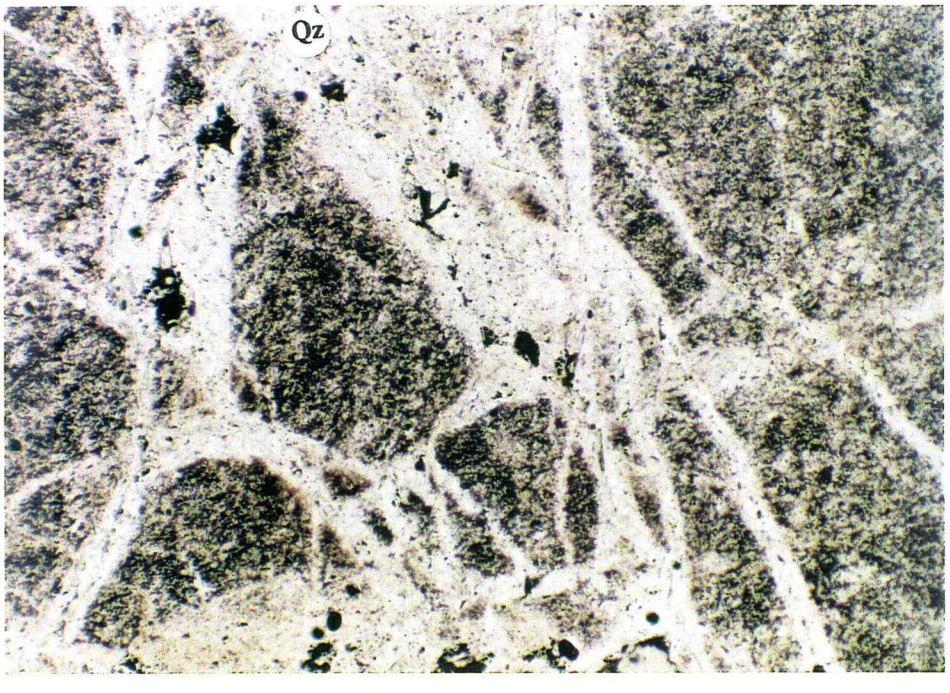

B. Plane-Polarized Light

Figure 13. Pervasive adularia + pyrite alteration. Quartz (Qz) occupies the vein core. Clear veins are adularia + quartz. Cloudy areas are incipiently clay-altered feldspar. Pyrite is not visible in photo. Magnification 100x.

jarosite veinlets were emplaced contemporaneously with pervasive adularia + pyrite alteration or as a separate alteration event utilizing the same fluid pathways. Adularia + jarosite alteration was not observed in intrusions younger than the Shell Butte porphyry indicating the alteration may have occurred before the emplacement of the younger intrusions.

This alteration type is characterized by stockwork and veinlet adularia. Both fracture-filling adularia crystals growing on plagioclase and potassium feldspars, and adularia replacing plagioclase and potassium feldspars in selvages surrounding veinlets are present. Other minerals which occur within the adularia overgrowth veinlets include quartz, jarosite, sericite, hematite, and fluorite.

Both open-space- and replacement-type veinlets were observed in thin section. Veinlets tend to be dominated by quartz in the groundmass, and often contain adularia only where they pass through potassium or plagioclase feldspar phenocrysts. Both veinlet and replacement adularia exhibit a characteristic mottled extinction and lack of clay or sericite alteration typical of relict igneous feldspar (see Figure 14). Adularia often occurs as overgrowths on potassium feldspar, and less often as overgrowths on plagioclase feldspar (see Figure 15). Euhedral adularia crystals commonly line the veinlet walls and project into veinlets. The projections are intimately associated with jarosite and less often with hematite and goethite (see Figures 15 and 16). Individual crystals of jarosite are often visible (>5 μm) and may be of hypogene origin (see Jarosite - Hypogene versus Supergene section below). One cross-cutting relationship was observed in which an adularia + jarosite

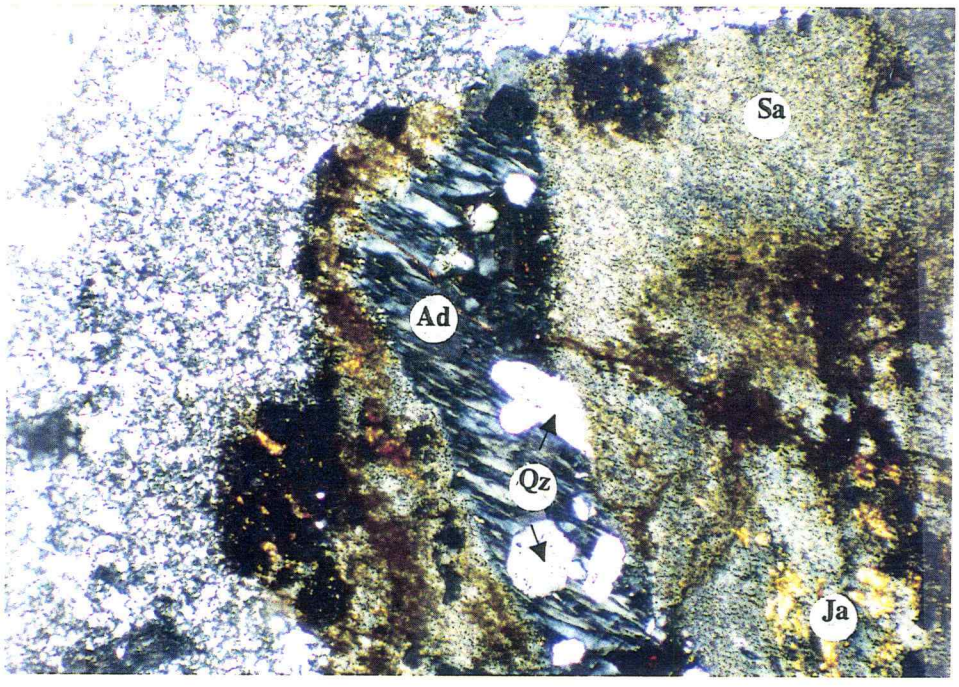

A. Cross-Polarized Light

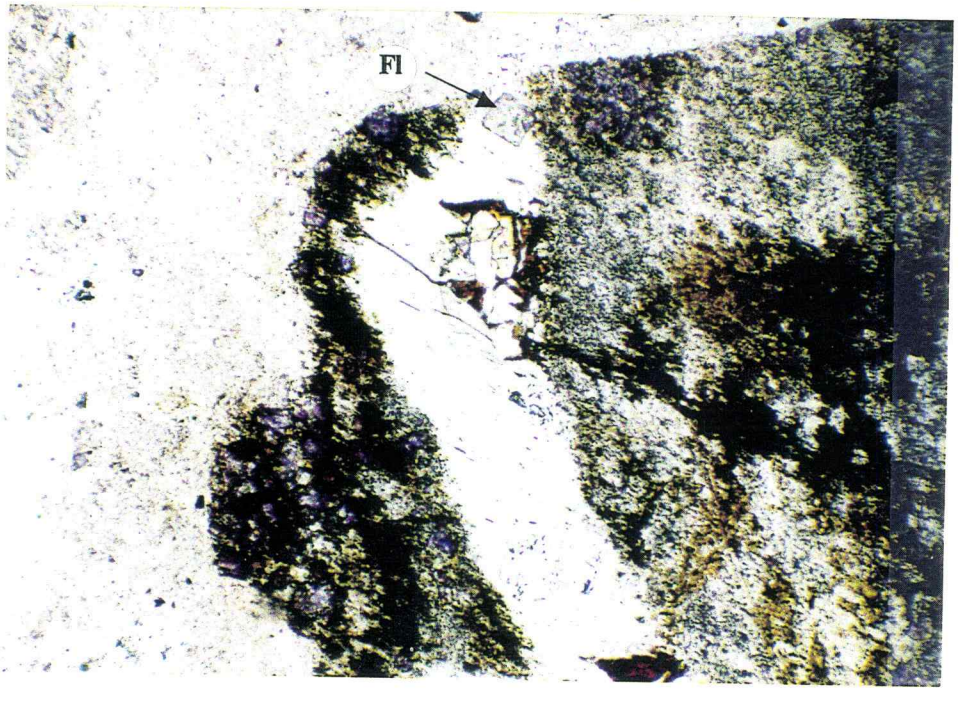

B. Plane-Polarized Light

Figure 14. Adularia vein showing characteristic mottled extinction and lack of "clouding". Note purple fluorite (Fl), euhedral quartz (Qz), sanidine (Sa) phenocrysts dusted with jarosite (Ja), and clay. This replacement vein is replacing the primary feldspar with adularia (Ad) + quartz + fluorite. Magnification 100x.

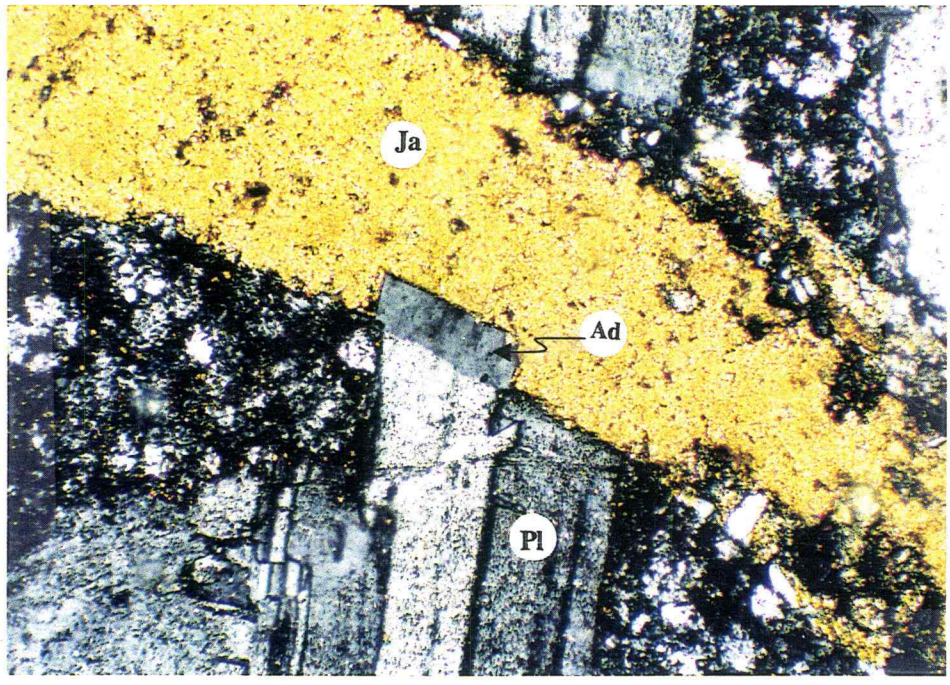

A. Cross-Polarized Light

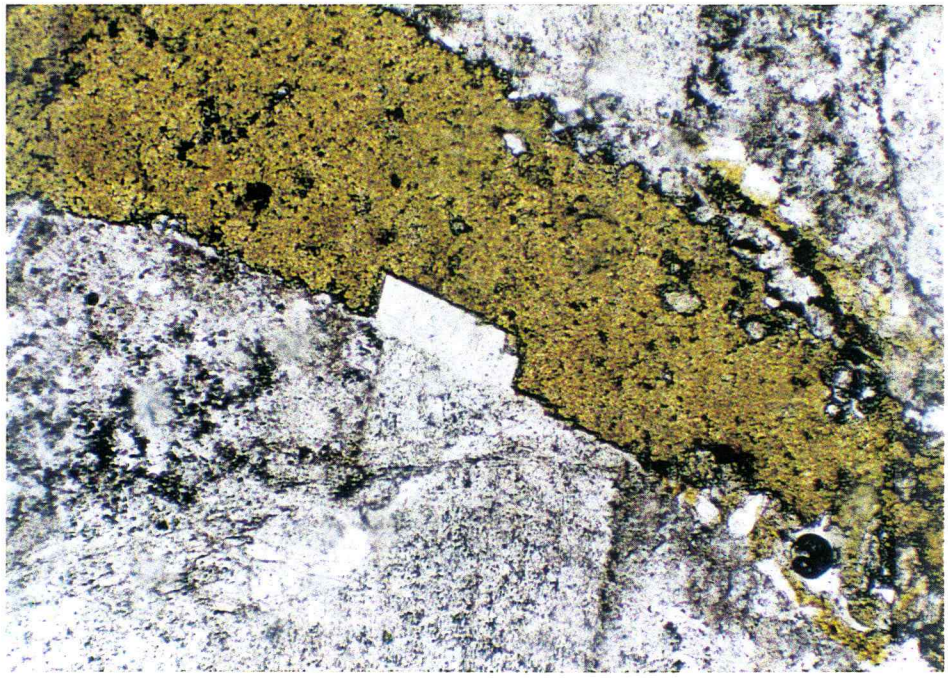

B. Plane-Polarized Light

Figure 15. Jarosite (Ja) vein traversing twinned plagioclase (Pl) phenocryst. The adularia (Ad) rhombohedron occurs as an overgrowth on the plagioclase phenocryst and is not affected by fine-grained clay alteration. Note the relatively sharp vein boundary characteristic of open-space veins. Magnification 100x.

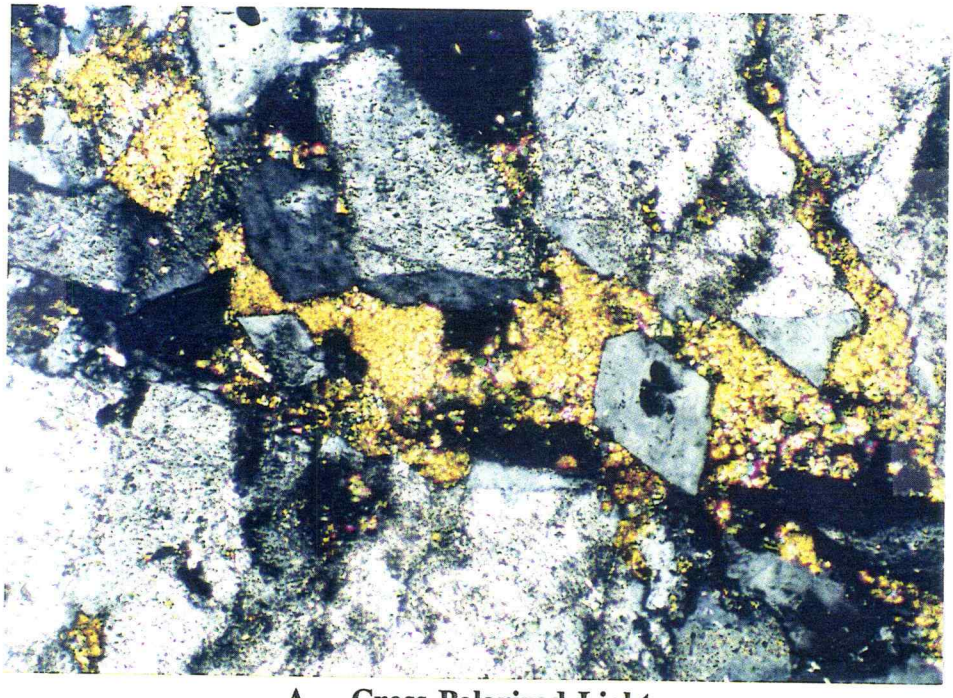

A. Cross-Polarized Light

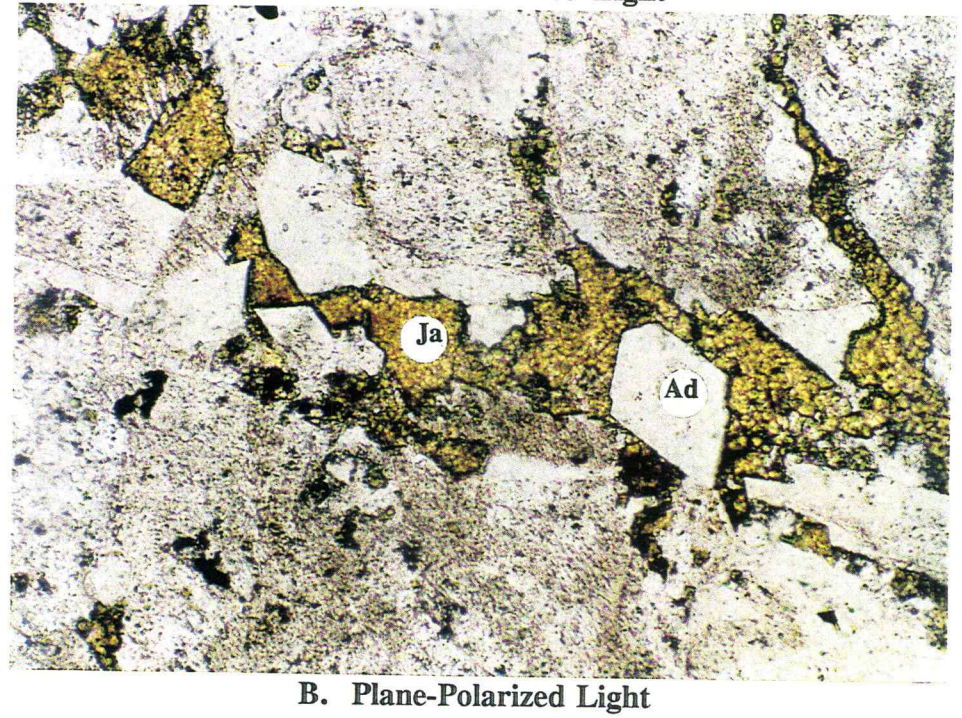

B. Plane-Polarized Light

Figure 16. Intimate intergrowth of adularia and jarosite (>5 μm). Jarosite (yellow; Ja) forms as fracture filling and encloses two rhombohedrons of non-cloudy adularia (Ad) center-right and center left); note clear adularia overgrowths on mottled igneous feldspars occurring as vein selvages. Magnification 100x.

overgrowth veinlet clearly offsets an adularia + pyrite veinlet, the latter presumably associated with the pervasive adularia event described above (see Figure 17). It is not possible to determine, however, whether the adularia + jarosite stable-event is a separate alteration event or merely the waning stage of the alteration event that produced pervasive adularia + pyrite alteration.

East-west-striking, open-space-filling quartz veins, occurring predominantly on Shell Butte, are spatially associated with adularia overgrowth veining. Shell Butte quartz veins range from 2 to 20 cm in width and are characterized by large, 2 to 3 cm in length, quartz crystals with terminations which project into vein centers. These veins are locally associated with adularia, hematite, jarosite, and gold (Figure 18). The spatial association of these veins with adularia alteration suggest that they are contemporaneous; however, no cross-cutting relationships were observed. Many of the veins exhibit several discrete layers of quartz crystals, suggesting cyclic deposition. This, combined with the observation of both fluid- and vapor-rich fluid inclusions during this study and by Reynolds (1991) suggest a throttling or boiling environment.

Another type of silica deposition associated with adularia alteration is pervasive, cryptocrystalline silicification which imparts a grey color to hand samples of Antoine Butte porphyry. Thin sections of this cryptic silicification revealed that in at least some cases the mineral added was actually adularia rather than silica. Much of the area tentatively identified in the field as containing cryptocrystalline silicification may in fact contain widespread adularia alteration rather than

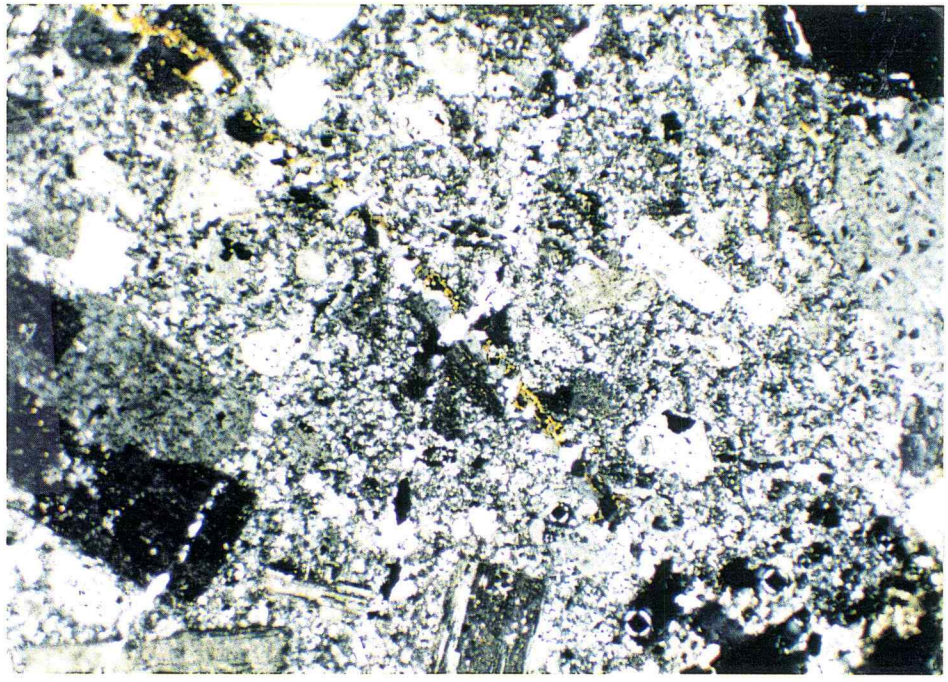

A. Cross-Polarized Light

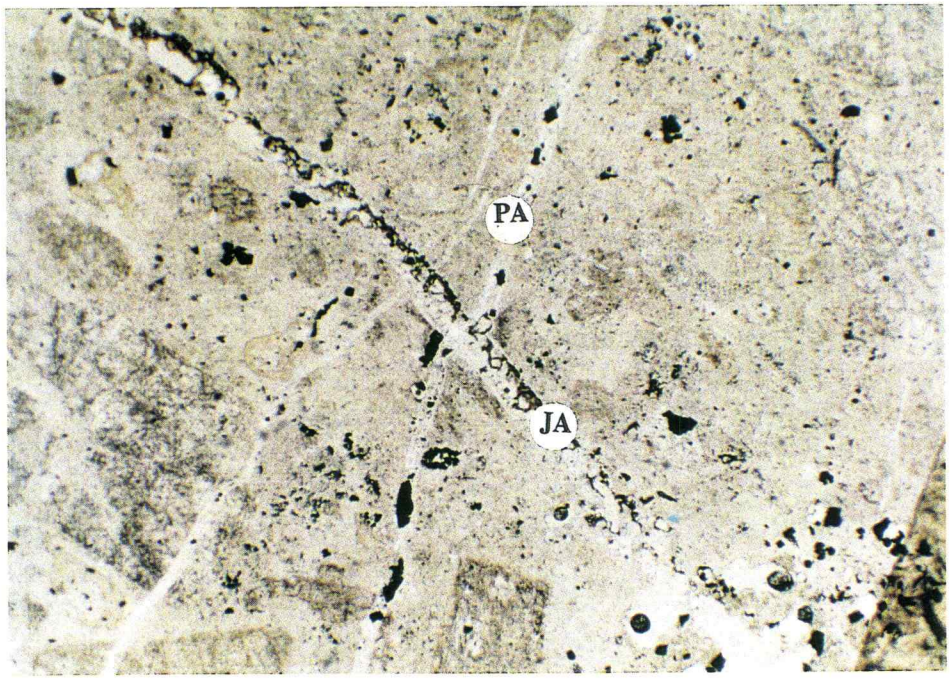

B. Plane-Polarized Light

Figure 17. Jarosite (yellow) + adularia (clear) vein (JA) traversing from the upper left to the lower right off-setting near center a pyrite (black, opaque) + adularia-stable vein (PA). Magnification 25x.

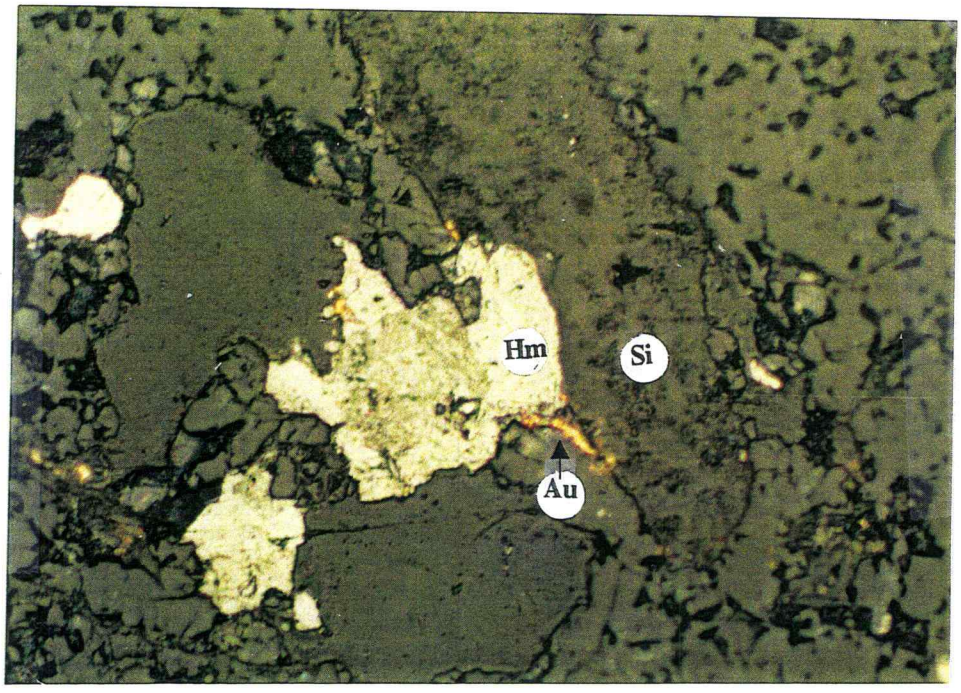

A. Plane-Polarized Reflected Light. Magnification 200x.

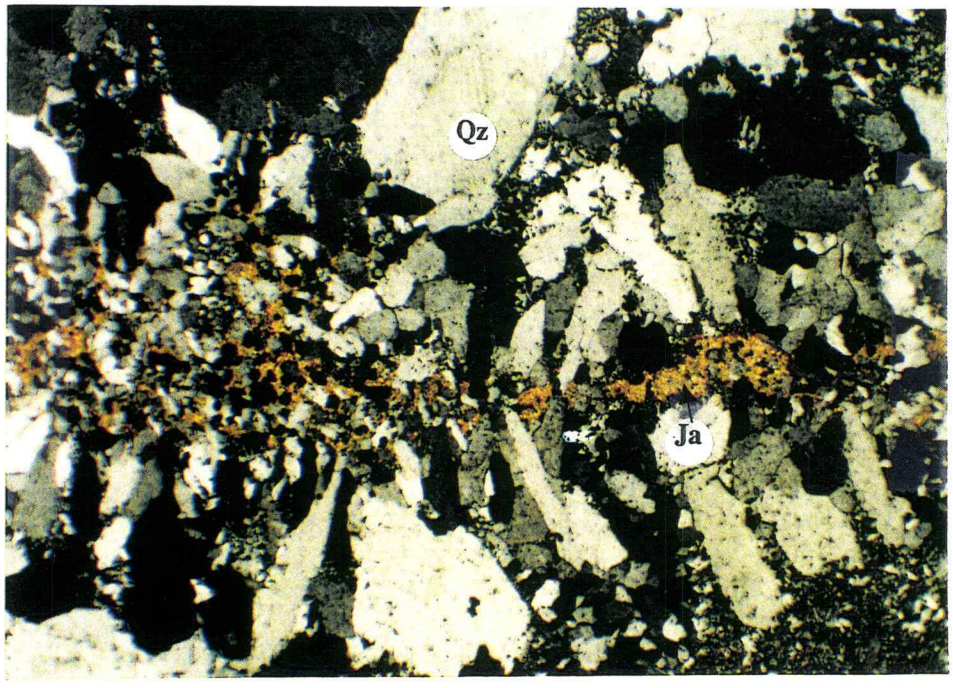

B. Cross-Polarized Light. Magnification 25x.

Figure 18. Shell Butte quartz vein with jarosite, hematite, and gold. A. Note light grey hematite (Hm), yellow gold (Au), and dark grey silicates (Si). B. Note cockscomb quartz (Qz), yellow jarosite (Ja). Gold, not visible, occurs in the jarosite.

silicification. If this is the case, then a much of larger area of northeast and northwest Antoine Butte was affected by adularia alteration than is indicated on Plate 2.

Both "wispy" fluorite, occurring disseminated throughout the groundmass, and vein or breccia-hosted fluorite are likely associated with adularia overgrowth veining. Adularia was observed in the high walls of the Alabama Pit where purple fluorite occurs as thick veins, veinlets, and the breccia matrix. Locally, fluorite is intergrown with adularia and jarosite (see Figure 19), suggesting that at least some fluorite was deposited during adularia deposition.

The origin of the jarosite + adularia overgrowth veinlets remains unclear. Were they formed at the same time as adularia + pyrite-stable alteration, as hot hydrothermal waters cooled and mixed with oxidizing meteoric water? Or, do jarosite + adularia overgrowth veinlets simply represent less intense adularia + pyrite veinlets that have undergone supergene alteration (see discussion below)?

Propylitic Alteration

Propylitic alteration was identified in only a few zones within the area mapped, and is most pronounced in areas where mafic minerals were present prior to alteration. Propylitic alteration is localized along mineralized structures, in Tid_2 dikes, and in pods of Precambrian amphibolite; it is ubiquitous in all mapped occurrences of the Alder Gulch syenodiorite (Tias). Propylitic alteration appears to

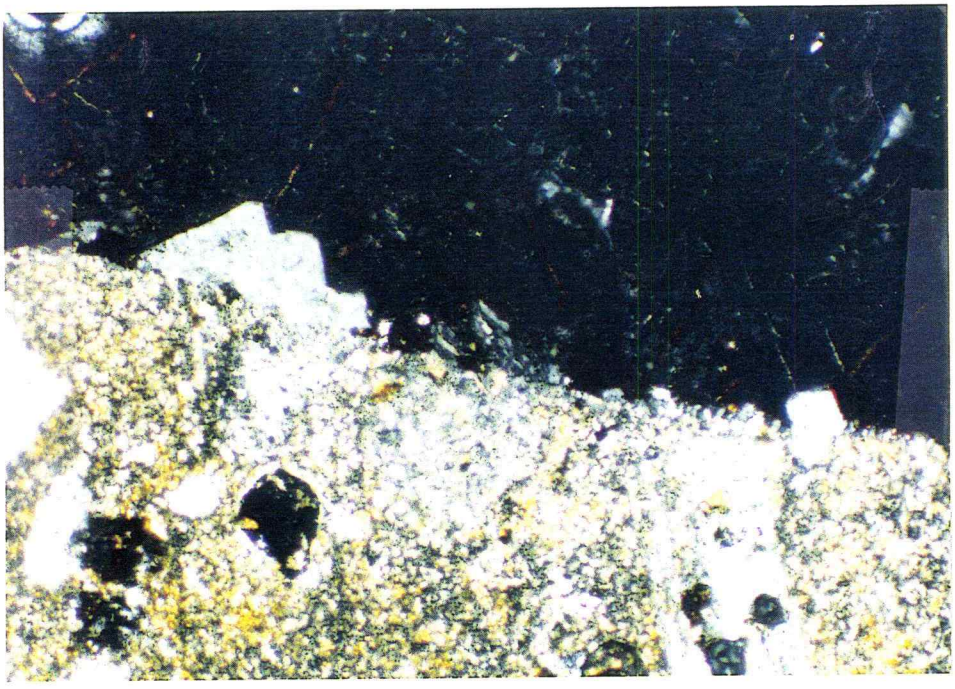

A. Cross-Polarized Light

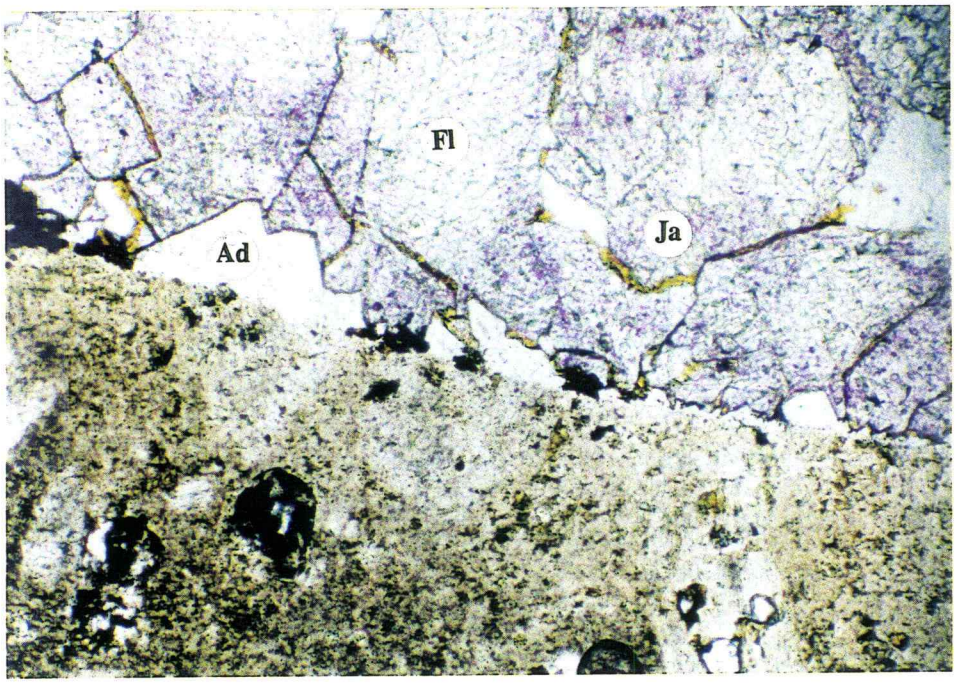

B. Plane-Polarized Light

Figure 19. Adularia (Ad) crystals lining a purple fluorite (Fl) vein. Note honey yellow colored jarosite (Ja) coating along partings in fluorite. Magnification 100x.

have occurred late in the hydrothermal alteration sequence, since it is restricted to units which are inferred to have been emplaced late in the intrusive sequence.

Potassium and plagioclase feldspars are relatively stable during propylitic alteration. The one notable exception is within one northeast-striking zone in which primary sanidine phenocrysts are altered to what appears to be hydrothermal albite. No unaltered outcrops of Alder Gulch syenodiorite were observed, making determination of primary mineral assemblages difficult. It is likely that primary mafic minerals were biotite, amphibole, and pyroxene, which were hydrothermally replaced by chlorite + calcite + pyrite ± epidote, while plagioclase and potassium feldspar were replaced by albite(?) ± quartz ± epidote ± sphene (see Figure 20). Pyrite and specular hematite are added in amounts ranging from 2 to 5 volume percent and 1 to 2 volume percent, respectively.

Propylitic alteration is distributed only in Tid_4, Tias, and locally in Precambrian lithologies, which suggests that propylitic alteration is younger than overgrowth and pervasive adularia alteration. Propylitic alteration is thought to be associated with late Stage II mineralization, or perhaps a temporally distinct event which occurred after Stage II mineralization. Propylitic alteration was not observed in the Antoine Butte porphyry, indicating that either propylitic alteration was restricted to narrow shear zones leaving the Antoine Butte porphyry largely unaffected. Or, alternatively, mafic igneous minerals may have been destroyed during earlier weak sericite + pyrite alteration in the Antoine Butte porphyry, thus there was insufficient iron and magnesium left to produce the characteristic

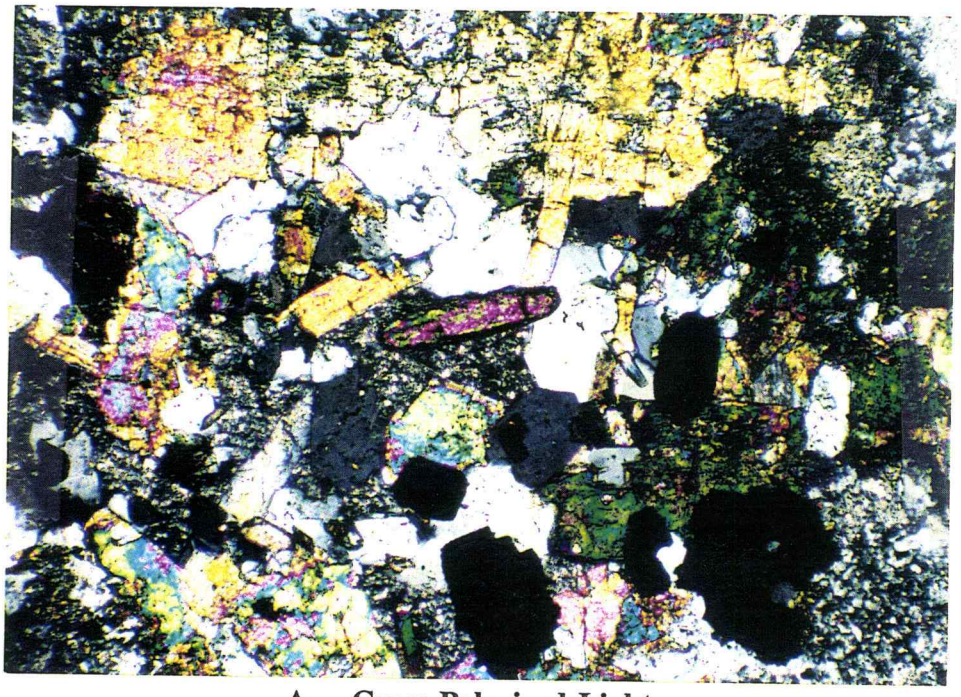

A. Cross-Polarized Light

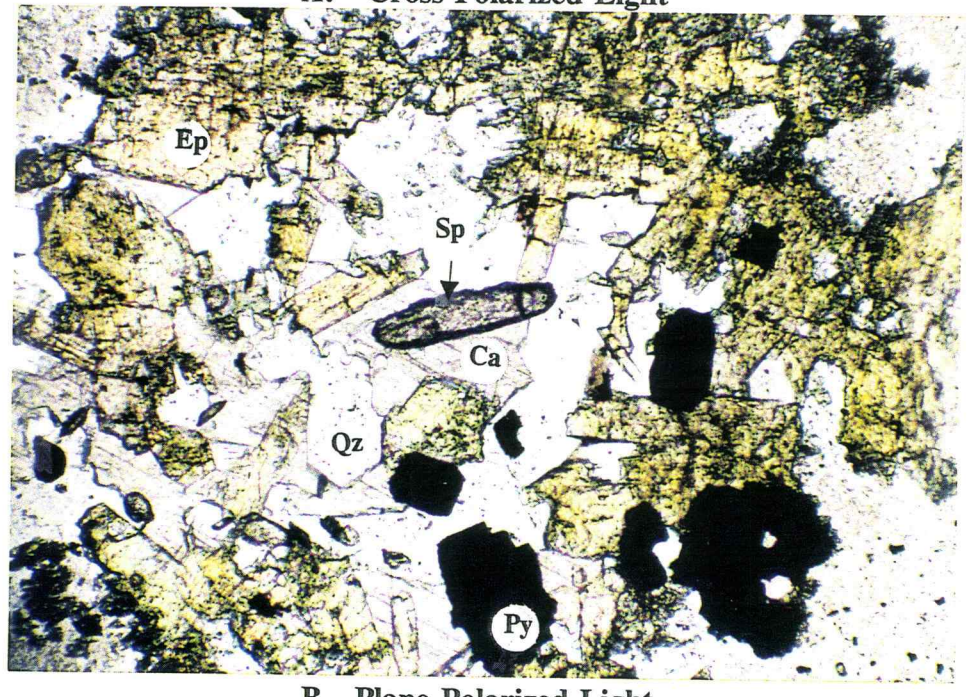

B. Plane-Polarized Light

Figure 20. Propylitic alteration in sample PW202, Alder Gulch syenodiorite. Note opaque pyrite (Py), green and yellow pleochroic epidote (Ep) replacing plagioclase, clear euhedral to subhedral quartz (Qz), and calcite (Ca). The high relief mineral in the center of the photo is sphene (Sp). Magnification 100x.

ferromagnesian minerals of the propylitic assemblage. The presence of well-defined shear zones within the Antoine Butte porphyry with no significant propylitic alteration, and the presence of propylitic alteration in younger dikes on Antoine Butte argue for the latter. It is possible that propylitic alteration occurred after Stage II mineralization, perhaps caused by hydrothermal fluids and heat generated by an underlying alkalic intrusive represented only by trachytic dikes (Tid_1) at the current level of exposure.

Albitic Alteration

Albitic alteration is presumed to be contemporaneous with the propylitic alteration due to the similarity in its spatial distribution. It occurs in the Shell Butte porphyry, in Precambrian amphibolite, and possibly in the Old Scraggy fine-grained porphyry. Secondary albite was distinguished from primary plagioclase by its presence in phenocrysts which clearly had a potassium feldspar precursor, and the presence of fine patchwork twinning, typical of hydrothermal albite (Carten, 1986). Albitic alteration is most easily distinguished in Precambrian lithologies where plagioclase feldspar (albite) is stable while microcline is almost completely altered to hydrothermal albite (see Figure 21). Amphibole is commonly stable, but may be altered to chlorite $\pm$ pyrite $\pm$ magnetite along cleavages and fractures (see Figure 21). It is difficult to tell whether the distribution of albitic alteration represents lateral zonation along mineralized structures or a unique event occupying the same

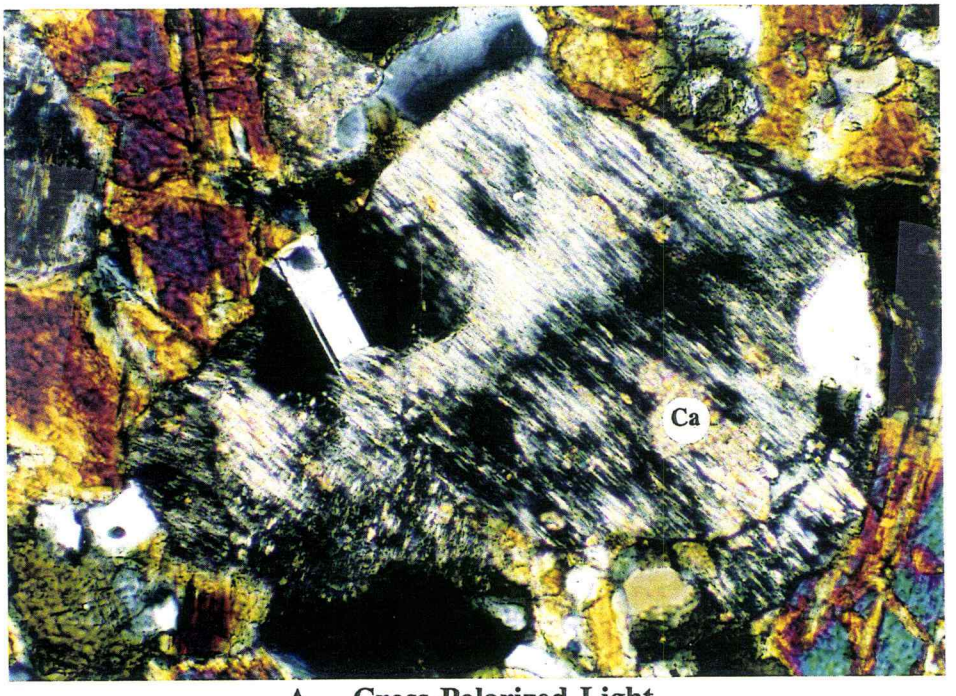

A. Cross-Polarized Light

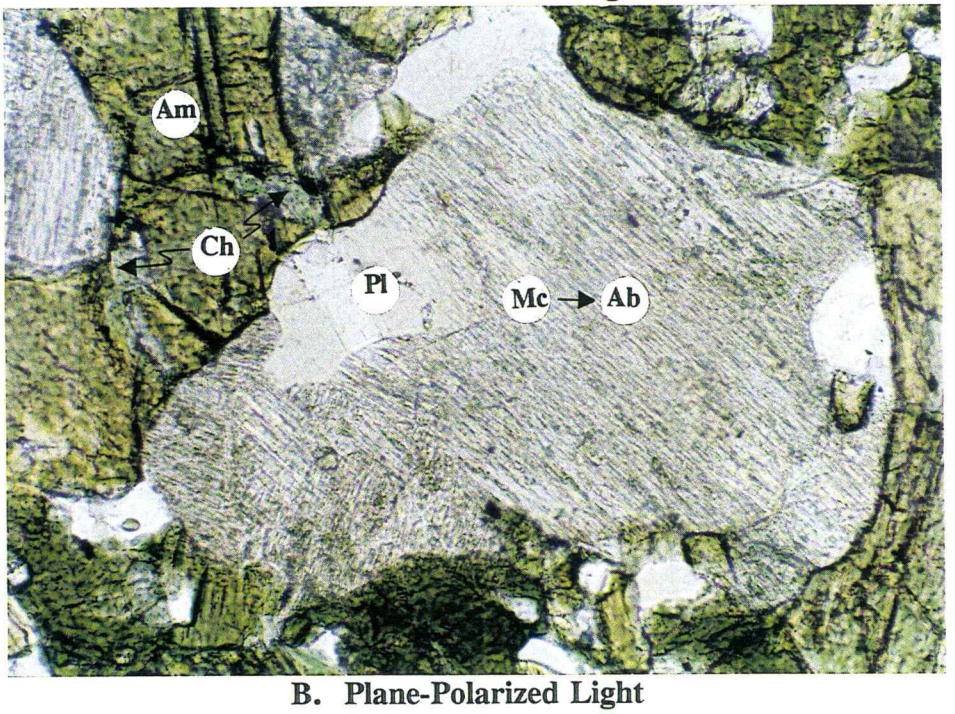

B. Plane-Polarized Light

Figure 21. Albitically altered Precambrian amphibolite. The microcline (Mc) crystal is almost completely altered to a lamellae of albite (Ab) + calcite (Ca), while plagioclase (Pl) remains unaltered. Amphibole (Am) is green to dark green and locally altered to chlorite (Ch) along fractures.

shear zone as propylitic alteration. Propylitic and albitic alteration are spatially associated with anomalous gold and base metal values in soil and rock samples.

Carbonate Alteration

Carbonate alteration occurs peripheral to widespread weak sericite + pyrite alteration, and both north and south of the Ruby shear zone (see Plate 2). The timing of carbonate alteration is problematic. There are no cross-cutting relationships with which to determine the relative age of the alteration; and the spatial distribution could be interpreted as being related to the widespread weak sericite + pyrite, or later structurally controlled adularia alteration, or perhaps propylitic alteration.

Carbonate alteration is characterized by partial to complete replacement of plagioclase, potassium feldspar, and groundmass by carbonate (see Figure 22). Both calcite and dolomite are locally present. Alteration of plagioclase phenocrysts ranges from purely fracture-controlled carbonate addition to replacement ranging from 5 to almost 100 percent in rare occurrences, and averages 10 to 30 percent. Sanidines are usually less altered than the plagioclase phenocrysts for a given sample. Alteration of the groundmass typically ranges from 10 to 30 volume percent. Mafic minerals, when present, are completely altered to calcite + iron-titanium oxides $\pm$ clay.

It is unclear whether carbonate alteration represents: 1) distal chemical zonation created during the widespread weak sericite + pyrite alteration event which

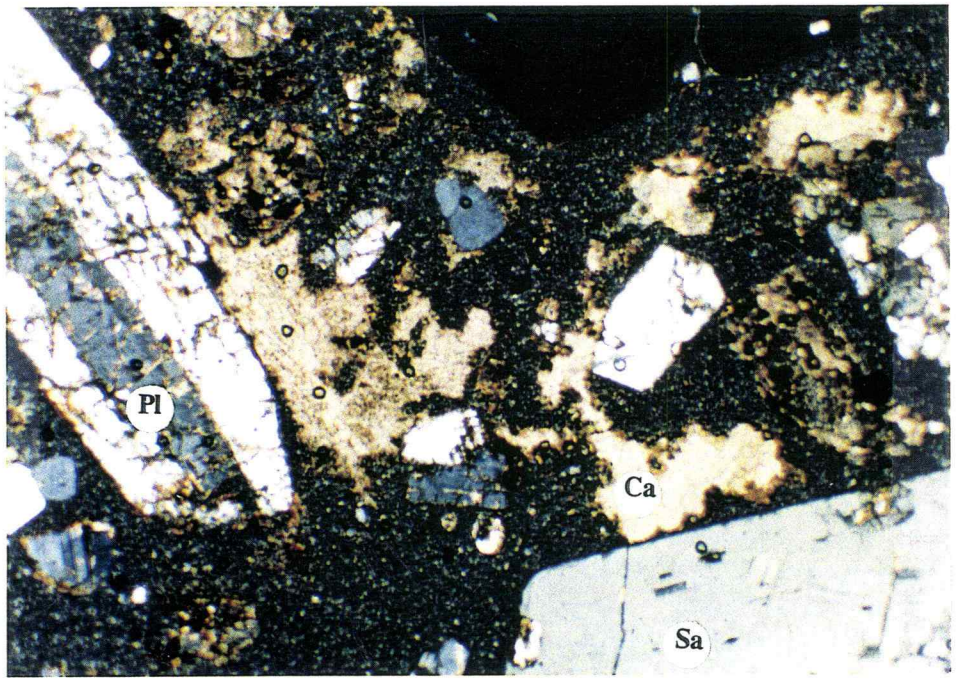

Figure 22. **Carbonatic alteration. Calcite (pale brown; Ca) occurs along fractures in plagioclase (Pl) and as irregular blebs in the porphyry groundmass. Sanidine (Sa), lower right, exhibits very little carbonatic alteration. Magnification 100x, cross-polarized light.**

also commonly introduced carbonate; or 2) carbonate alteration directly associated with shear-zone-controlled adularia alteration in which carbonate is less abundant. The distribution of carbonate alteration is most consistent with the second interpretation, since carbonate alteration predominantly occurs along the extensions of mineralized shear zones, rather than as a halo surrounding the entire area affected by widespread weak sericite + pyrite alteration. However, the large zone of carbonate alteration located east of Shell Butte argues for the first interpretation, since large shear zones are not known to be present there. It is possible that both spatially extensive carbonate alteration and shear-zone-controlled carbonate alteration are present.

In either case, the carbonate is likely the result of precipitation upon heating of carbonate-rich meteoric waters as they mixed with hot hydrothermal waters. Mixing could have occurred over a large area which was later overprinted by younger alteration, or, alternatively, mixing may have occurred as upwelling hydrothermal waters, restricted to shear-zones, mixed with meteoric waters.

Jarosite - Hypogene versus Supergene

The debate over whether iron-sulfate and oxide minerals are supergene or hypogene is a common and often heated one for many epithermal deposits (e.g., Jensen, 1971; Stoffregen, 1986; Scott, 1990). In many, and perhaps most, cases the evidence clearly indicates that iron-sulfates and oxides are of supergene origin. Common arguments in favor of a supergene origin for oxides and sulfates can be

summarized as follows: 1) the amount of oxidation varies proportionately with the amount of adjacent unoxidized sulfides; 2) oxides are distributed in an elevation-controlled blanket of relatively equal thickness over a sulfide deposit; 3) hydrogen and oxygen isotopic ratios indicate iron-oxide minerals were formed by 25°C meteoric water; and 4) K-Ar age dates on alunite and jarosite are significantly younger than K-Ar dates on hypogene alteration minerals.

There is significant evidence in support of a hypogene origin for at least a portion of the iron sulfates and oxides at the Zortman Mine. The arguments in favor of a hypogene origin are as follows: 1) jarosite is observed both completely enclosing and enclosed by hydrothermal adularia in overgrowth veinlets; 2) the depth of oxidation is extremely variable in and surrounding the Zortman Mine; 3) jarosite is commonly microcrystalline ($>5\mu$m; see Figure 16); and 4) adularia + jarosite veinlets offset adularia + pyrite veinlets.

As was seen in several of the preceding figures (see Figures 15 and 16), jarosite and adularia are intimately associated in veinlet-fillings. Several examples were observed where adularia was completely surrounded by jarosite. The argument can be made that the jarosite is a supergene weathering product which has simply precipitated upon previously deposited adularia. In the two dimensions provided by a thin section, there is no way to adequately demonstrate that this is not the case. However, the number of examples of adularia which are bounded completely by jarosite, and a few examples of adularia enclosing jarosite argue against the interpretation that jarosite is simply precipitating around the adularia.

The depth of oxidation is highly variable surrounding and within the Zortman Mine. Although such variability can be explained by increased permeability along fracture zones which allow meteoric water to percolate to depth; an alternative explanation is that hot, oxidizing waters welled upward along the fractured shear zones due to increased permeability creating the highly irregular oxidation depths observed. The only way to demonstrate that this is the case would be to find examples where oxidation does not extend to the present surface but occurs at depth. Since most of the exploratory drilling was done at angles ranging from 45 to 60 degrees, a vertical section through an oxidized zone is not available.

The microcrystalline nature of jarosites combined with the numerous examples of jarosite and adularia intergrowths in which there is a complete lack of alteration in the adularia, support a hypogene origin for jarosite. Examples were not observed in which adularia was in contact with jarosite was clay- or sericite-altered. Since lack of clay alteration, and to a lesser extent mottled extinction and crystal shape, were the only useful criteria for identifying hydrothermal adularia in thin section, this argument remains unconvincing without an independent means of identifying hydrothermal adularia.

It is clear that weathering pyrite and marcasite would produce very low pH, sulfuric acid-rich, solutions. For jarosite to be deposited at 25°C, as a supergene weathering product, the pH of the solution must be at most 1.2 (Stoffregen, 1986). It seems likely that adularia subjected to waters with a pH of 1.2 for any length of time would show some sign of hydrolysis and clay alteration. Keller (1957)

summarizes the effect of oxidizing sulfides as follows, "Strong mineral acids such as hydrosulfurous, sulfurous, and sulfuric acid which originate from oxidizing marcasite, pyrite, and other sulfide minerals effectively implement hydrolysis, although they are probably local in occurrence." Busenberg and Clemency (1976) studied the dissolution kinetics of orthoclase, microcline, and plagioclase feldspars at 25°C and found that crushed orthoclase feldspars placed in a 3.92 pH solution for 20 days released 4 X 10^4 moles of cations. This amount of hydrolysis would undoubtably be visible as a clouding of feldspars with clay. It must be noted that the kinetics of reaction for adularia are not well known and may differ significantly from that of orthoclase, sanidine, or plagioclase. An alternative explanation to the lack of clay alteration in adularia is that jarosite and adularia co-precipitated from a potassium-rich solution at relatively high temperatures and high pH (see Figure 23). As the activity of the potassium ion in the hydrothermal fluid increases above approximately 0.001, the jarosite + K-feldspar assemblage becomes stable at high temperatures. Therefore it is possible to precipitate K-feldspar + jarosite at relatively high temperatures (100 to 250°C) from a solution with a neutral to slightly alkaline pH between 7 and 9.5.

As seen in Figure 17, adularia + jarosite veinlets locally offset adularia + pyrite veinlets. The jarosite present immediately adjacent to unoxidized pyrite and the observed offset suggest active hydrothermal emplacement rather than passive supergene weathering.

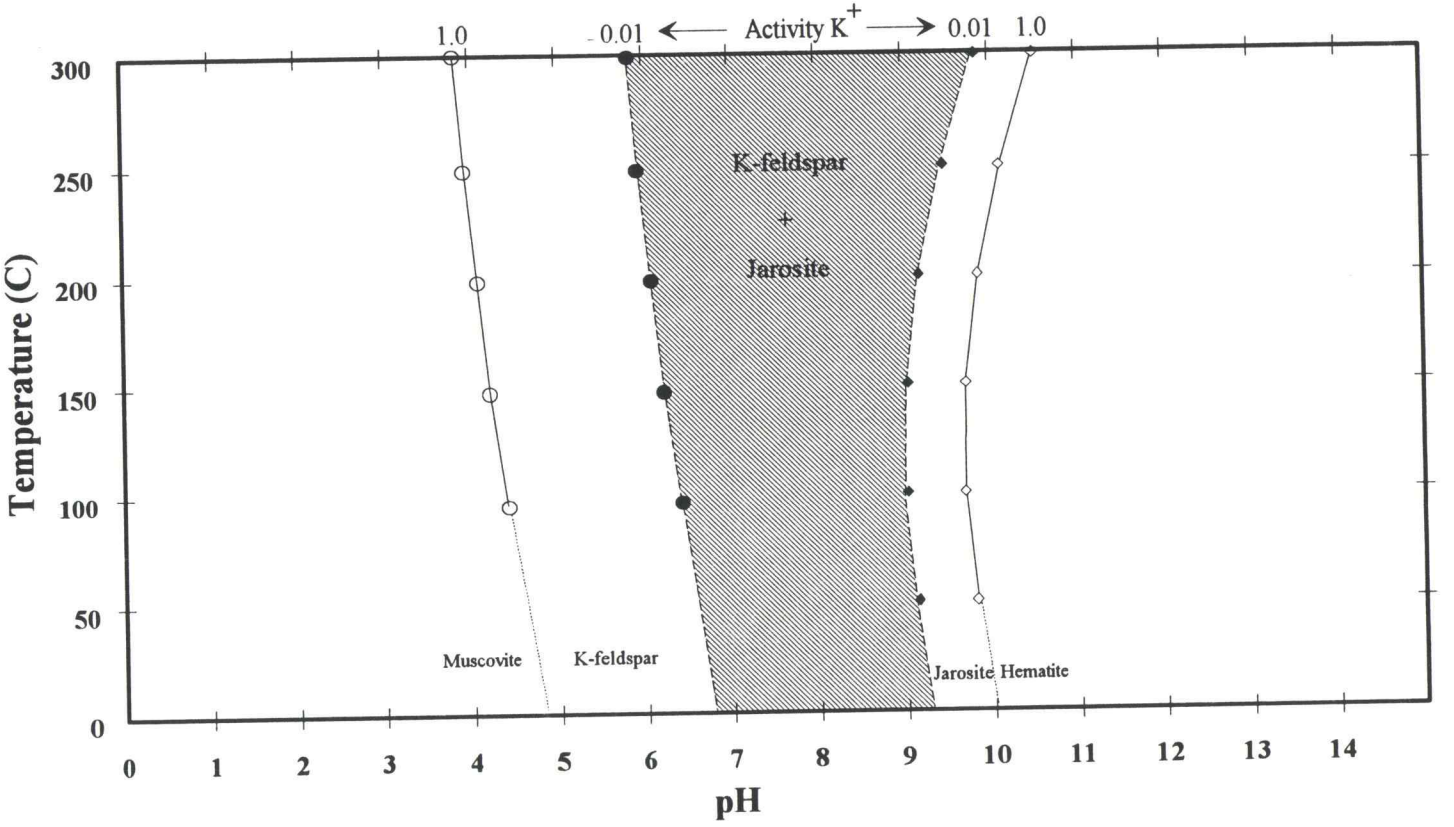

Figure 23. **Jarosite + K-feldspar stability diagram. Total sulfur used to calculate jarosite/hematite stability was $\Sigma S = 0.003$ as SO_4^{2-}. Note that as potassium increases in solution, the assemblage becomes increasingly stable at high temperature and pH's. Thermodynamic data for jarosite are from Wolery (1990). Hematite is from the soltherm database compiled by Reed (1989). K-feldspar and muscovite data are from a plot of Barnes (1979, Figure 8.2).**

A similar assemblage of jarosite + illite + potassium feldspar alteration was described near the Kennecott copper mines near Wrangell, Alaska (MacKevett and Radtke, 1966). MacKevett and Radtke describe the assemblage as follows, "Hydrothermal alteration at the Kennecott mines consists of an extensive dolomitic phase and a subsequent, more restricted, jarosite-illite-potassium phase ..." No evidence is sited to explain how they concluded that the assemblage was of hydrothermal origin; however, it is interesting that a hydrothermal origin was presumed.

Supergene Alteration

Supergene processes are widespread surrounding the Zortman Mine and are apparently related to the oxidation of widespread disseminated pyrite; and result in the formation of clay minerals and iron- and manganese-oxides. Supergene alteration, in the form of iron and manganese oxides is extensive near the crest of Antoine Butte, presumably due to higher fracture density. Potassium, and to a greater extent, plagioclase feldspars are often dusted with clays giving them a clouded appearance. The depth of oxidation of hydrothermal pyrite, based on reverse circulation drilling logs, is highly variable, ranging from no oxidation at the surface to oxidation depths in excess of 100 meters (328 feet). Red (hematite), brown (goethite), and yellow (jarosite) iron oxides were observed in a number of exploration drill holes and on the surface. The red iron-oxides are often accompanied by fine-grained silica which floods the groundmass of the Antoine Butte

porphyry, giving it an almost jasperoidal appearance. The crustiform and mammillary texture and occurrence of goethite and earthy hematite in close association with weathering pyrite suggest a supergene origin for the oxides in most cases. However, it is possible that some of the hematite and jarosite observed is a hypogene alteration product, as discussed above. Detailed drill logs and cross sections prepared from the drill holes on Antoine Butte revealed hematite and jarosite to depths in excess of 100 meters in some areas. Wampler (1990) interpreted this deep oxidation to be the result of increased oxidation associated with areas of increased fracture density. The abundance of jarosite associated with adularia + jarosite alteration, the highly variable depth of oxidation, and the microcrystalline texture of some of the jarosite observed in thin section, lend support to the hypothesis that at least some oxidized zones may represent hypogene alteration caused by oxidizing hypogene waters rather than areas in which cold supergene waters percolated downward.

Mineralization

Ore mineralogy at the Zortman deposit consists of native gold associated with pyrite, electrum, and gold tellurides (Enders and Rogers, 1983). Silver/gold ratios, although relatively constant within the Zortman Mine area, vary considerably on the larger scale. Most notably, the silver/gold ratios from the Shell Butte area are typically one to two orders of magnitude greater than those from the mine area. Graphs of silver versus gold assays from drilling samples show a distinct bimodality

to silver/gold ratios, with the Shell Butte having silver/gold ratios of approximately 160 and Antoine Butte approximately 5 (see Figure 24A). The bimodal nature of the distribution suggests that there were two chemically distinct mineralizing fluids or events. The low silver/gold ratios, present on both Antoine and Shell Buttes, may represent typical silver/gold ratio values for Stage II mineralization and associated adularia alteration, whereas high silver/gold ratios, present only on Shell Butte, may be the result of boiling that occurred only in the vicinity of Shell Butte.

Plots of gold and silver abundance versus elevation from drill holes also show distinct differences between the Shell Butte and Antoine Butte mineralization. Near the surface on Antoine Butte, there is a marked increase in gold grades which drops off rapidly with depth, possibly related to supergene gold enrichment (see Figure 24B). In contrast, on Shell Butte gold grades are typically low (<0.02 ounces per ton) except in a well defined interval between 5,300 and 5,000 feet in elevation (see Figure 24C). This interval may represent a boiling horizon within which gold is preferentially deposited. Alternatively, the interval may represent supergene depletion of gold near the surface and enrichment at depth. The abrupt boundaries of the interval, combined with fluid inclusion, metal ratio, and vein morphology evidence support the hypothesis that the gold/silver-rich zones on Shell Butte resulted from boiling rather than supergene enrichment. The implication is that gold mineralization on Shell Butte, although seemingly controlled by vertical veins near the surface, may actually be localized within a physicochemically controlled horizon.

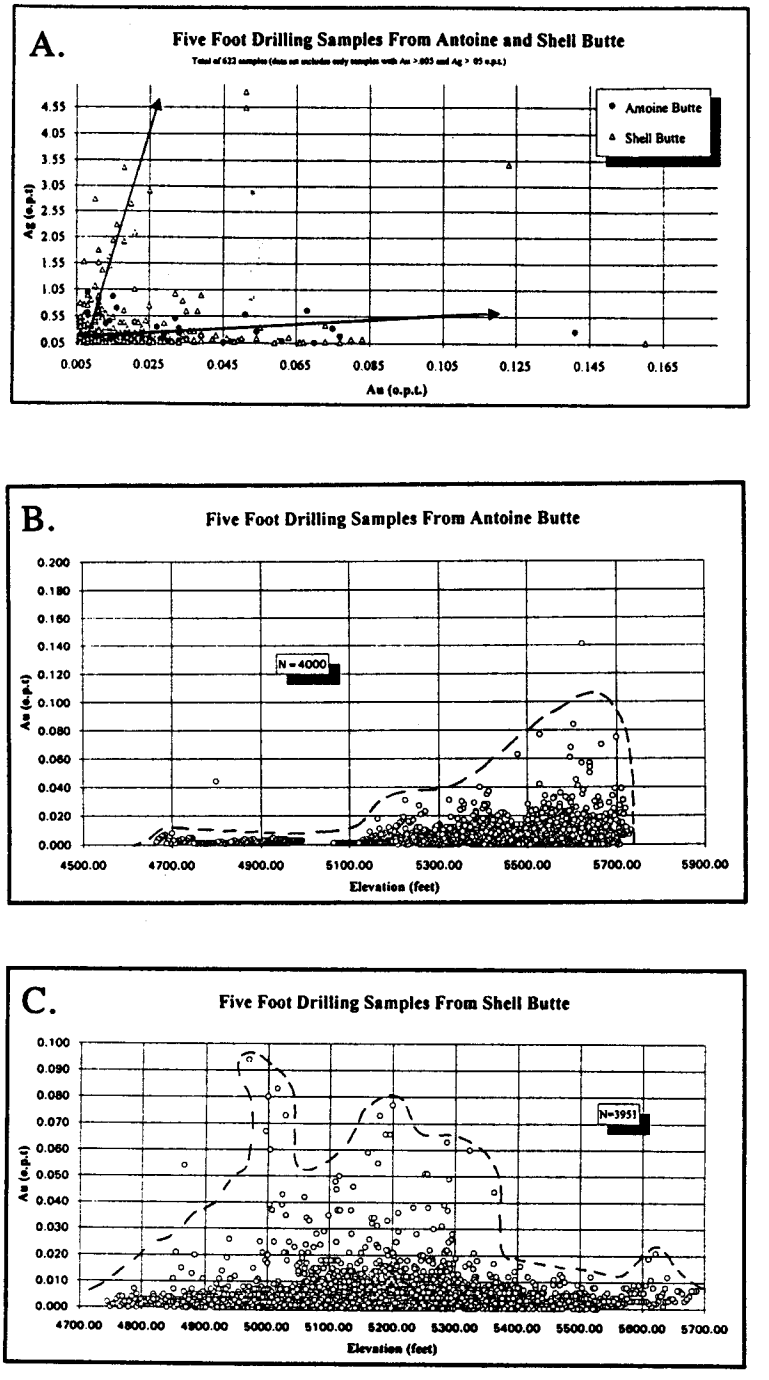

Figure 24. **Summary of gold and silver in drilling results from Shell and Antoine buttes. A. Silver versus gold for drilling samples on Antoine and Shell buttes. B. Gold versus elevation for drilling samples from Antoine Butte. C. Gold versus elevation for drilling sample from Shell Butte.**

Discussion

In the discussion which follows, several assumptions have been made to allow an interpretation of the genetic history of the Zortman deposit. It is assumed that a lack of alteration in a given porphyry, which according to age relationships should be altered, represents a time gap in the alteration sequence rather than a spatial separation of that unit from hydrothermal fluids. If relative age relationships are constrained by good cross-cutting relationships, this is a very good assumption. However, significant uncertainties in the age relationships between different intrusions remain, making interpretation difficult.

Another important source of uncertainty lies in the source for hydrothermal fluids which caused hydrothermal alteration and mineralization. Wilson and Kyser (1989) concluded, based on isotopic data, that the bulk of mineralizing fluids were likely meteoric water that had reacted with country rocks, largely Precambrian amphibolites and gneisses. The large amounts of potassium and lesser hydrogen metasomatism outlined in this study suggest a magmatic fluid component.

The genetic sequence outlined below includes only those intrusions which crop out within the mapped area.

Progression of Alteration, Intrusive Emplacement, and Mineralization

Intrusive activity commenced approximately 57 to 62 million years ago with the emplacement of the Old Scraggy and Old Scraggy fine-grained porphyries south

and east of the mine area. The Beaver porphyry was emplaced after the Scraggy porphyries, mainly north and east of the mine area, and may have been contemporaneous with the emplacement of the Antoine Butte porphyry and the coarse phase of the Antoine Butte porphyry. Either during, or shortly after, intrusion of the Antoine porphyry, Stage I mineralization and associated weak sericite + pyrite alteration and low-grade (< 0.005 ounces per ton) disseminated gold deposition affected the Antoine porphyry (see Figure 25A). Mapping done by Zortman Mining Inc. personnel on Beaver Mountain, located northeast of the mine area, revealed widespread alteration and mineralization in the Beaver porphyry similar to that found in the Antoine Butte porphyry (Unpublished Zortman Mining Inc. Data, 1989).

The Shell Butte and Scraggy-Shell porphyries were emplaced after the Antoine Butte porphyry and presumably after Stage I alteration and mineralization had waned, based on the observation that neither porphyry is affected by widespread weak sericite + pyrite alteration. Although it is unclear when the major north-northwest-striking shear zones were formed, it is likely that they were either formed or reactivated at this time (see Figure 25B).

Emplacement of the Shell Butte porphyry was either contemporaneous with, or followed shortly after, the first episode of dike emplacement, manifested by the emplacement of north-northwesterly striking Tid_2 dikes, some along north-northwest striking shear zones; and northeast-striking Tid_3, and Tibq dikes (see Figure 25C).

Stage II mineralization and pervasive adularia + pyrite ± fluorite alteration is localized along large shear zones striking NNW and NE. The majority of the

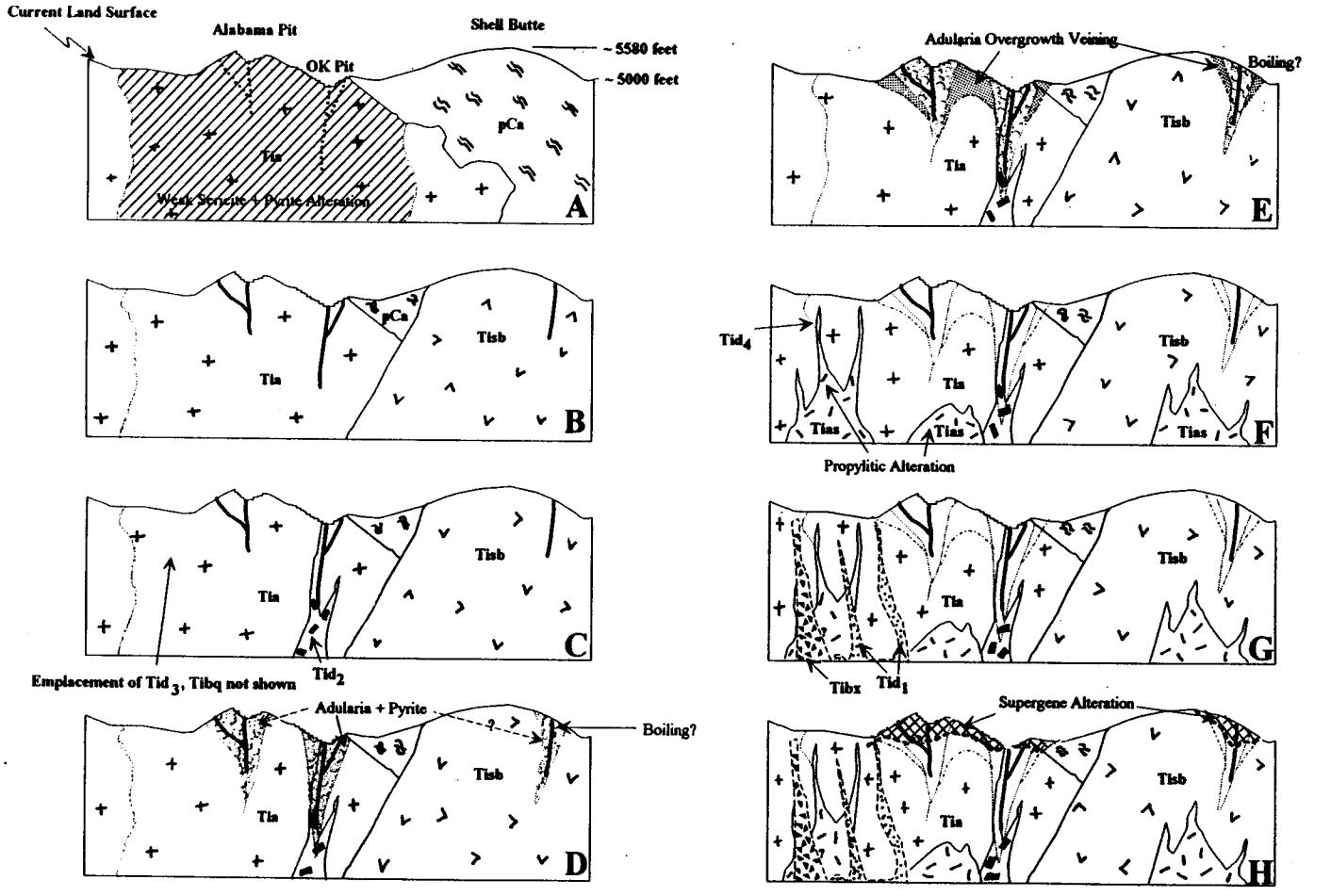

Figure 25. **Cross-sectional view, looking north, schematically illustrating the progression of alteration, intrusive emplacement, and mineralization of the Zortman epithermal deposit. See text for explanation.**

economic mineralization within the Zortman mine likely occurred at this time. Deposition of some gold occurred after the emplacement of Tid_2, Tid_3, and Tibq dikes on Antoine Butte. Textural evidence from the Shell Butte porphyry indicates that boiling and/or throttling may have occurred at this time or during late Stage II mineralization to deposit significant amounts of high grade gold within a physicochemically controlled interval between 5,300 and 5,000 feet in elevation (see Figure 25D).

Main Stage II mineralization, presumably caused by mixing of hot hydrothermal fluids with cold oxidized meteoric fluids, resulted in the formation of extensive areas of adularia overgrowth veinlets + jarosite + hematite + goethite + fluorite $\pm$ calcite deposition, and continued deposition of gold (see Figure 25E). The adularia + jarosite alteration was more extensive than adularia + pyrite alteration but was localized along the same structures.

Cessation of the main Stage II mineralization was followed by another period of dike emplacement, which includes generally north-northwest-striking Tid_4 dikes west of the mine area and stocks of equigranular Alder Gulch syenodiorite near Alder Gulch (see Figure 25F). Propylitic alteration occurred at this time but was essentially restricted to dikes of Tid_4, Alder Gulch syenodiorite, and mafic-rich Precambrian lithologies. Propylitic alteration was either related to dike emplacement or with the emplacement of alkaline intrusions at depth (see Figure 25F).

The last recorded period of intrusive activity included northeast-striking, alkalic Tid_1 dikes, perhaps associated with emplacement of larger alkalic intrusions at

depth; and intrusion of randomly oriented intrusive breccia (Tibx) pods west of the mine area. The timing of emplacement of a mafic diatreme near the town of Zortman may coincide with the emplacement of Tibx pods (see Figure 25G).

The last event in the genetic sequence was supergene oxidation of pyrite and the formation of goethite, hematite, and jarosite during uplift, erosion, and weathering. Clay alteration of plagioclase and, to a lesser extent, of potassium feldspars occurred throughout the area affected by pyrite oxidation. Based on the distribution of gold grades in drilling from Antoine Butte, there may have been some enrichment of the gold grades near the surface due to remobilization of gold (see Figure 25H).

Comparison with the Round Mountain Epithermal Deposit

As mentioned previously, perhaps the best analogue for the alteration and mineralization at the Zortman epithermal deposit (Zortman) is the alteration and mineralization at the Round Mountain epithermal deposit (Round Mountain) described in detail by Sanders and Einaudi (1990). The following paragraphs summarize the similarities and differences between the two deposits.

Both Round Mountain and Zortman contain several spatially overprinted mineral assemblages, dominated by adularia overgrowth veinlets and potassium metasomatism associated with gold deposition. Propylitic alteration is a separate, younger, hydrothermal event at Zortman, whereas propylitic alteration was early and synchronous with adularia overgrowth veinlet development and gold deposition

forming an outer alteration zone at Round Mountain. An advanced argillic assemblage of kaolinite or pyrophyllite was not identified at either Zortman or Round Mountain, indicating that the pH of hydrothermal fluids was relatively high. Alunite was identified at Round Mountain, where it formed late and at high levels, perhaps as a result of both hypogene and supergene alteration. Alunite was not identified at Zortman; however, jarosite, the Fe^{3+} analogue of alunite, is abundant and at least some jarosite may be of hypogene origin. Fluorite is abundant at Zortman, perhaps due to the relatively abundant alkalic igneous host rocks, whereas fluorite is not reported at the Round Mountain deposit.

Both deposits have cockscomb, open-space, quartz veins and indirect evidence that hydrothermal fluids boiled. At Round Mountain, mixing of magmatic and meteoric fluids is the postulated method of gold deposition rather than boiling. At Zortman a boiling mechanism for gold deposition is supported in only one area, Shell Butte, whereas in all other areas evidence for boiling is absent. The Zortman model, as presented above, requires that KCl, HCl, H_2S be derived from magmatic fluids which then mix with more dominant meteoric fluids as documented by Wilson and Kyser (1989). Mixing of the two fluids is a viable mechanism to cause gold + pyrite deposition and adularia + sericite type epithermal alteration (Reed, 1985).

Alkalic post-mineralization dikes were identified at Zortman, whereas no post-mineralization dikes were identified for Round Mountain. Alkalic intrusions at depth may have provided both heat and alkaline-rich magmatic fluids to drive late propylitic alteration at the Zortman deposit. The heat source for the stage II

hydrothermal fluid at Zortman is likely the porphyritic monzonites and syenites in which mineralization is hosted, whereas at Round Mountain the source of fluids is inferred to be a rhyolite caldera adjacent to the mine area. The host for mineralization at Round Mountain is a rhyolite tuff; at Zortman it is monzonite and syenite porphyries and minor amounts of Precambrian amphibolite and gneiss. Geochemically the rocks are very similar with respect to silica, aluminum, and total alkalies.

Implications for Exploration

Several observations made during the course of this study have implications for exploration and discovery of hydrothermal gold, silver, and base-metal ore deposits within the Zortman mining district and other similar adularia + sericite type hydrothermal systems. They are summarized as follows:

1) The close correlation between pervasive adularia + pyrite alteration, more regionally extensive adularia overgrowth veinlets, and gold mineralization provides a useful tool in delineating areas of undiscovered gold mineralization. Adularia alteration typically encloses gold mineralization and provides a larger target than gold mineralization alone. A rock sampling survey focused primarily on K_2O/Na_2O ratios could provide a method of mapping areas of cryptic adularia alteration that may be associated with gold mineralization. This method could potentially be applied to mine-level sampling and

drilling. Analyses for gold, silver, Na_2O, and K_2O in conjunction with geologic mapping could provide useful information for extending ore zones and alteration patterns within the mine area.

2) Hematite, goethite, and jarosite are often found with gold and adularia. Detailed mapping of hematite, goethite, and jarosite proportions in conjunction with adularia zones could provide a means of delineating areas where abundant jarosite is a result of adularia + jarosite alteration, rather than supergene weathering of pyrite.

3) On Shell Butte, there is a well-defined increase in grade between elevations of 5,300 and 5,000 feet. The implication is that although gold mineralization occurs in vertical veins near the surface, gold mineralization may also be localized within a certain depth interval, perhaps due to rapid mixing or boiling of hydrothermal fluids. Thus, the configuration of ore on Shell Butte may be a horizontally-defined ore horizon; and the best means of testing and delineating ore would be to drill holes at low angles to intercept the projections of east-west veins exposed on the surface at an elevation of roughly 5,300 to 5,000 feet.

4) Although areas of propylitic alteration appear to be low in gold, they tend to be more anomalous in base-metals than areas affected by adularia alteration. This may indicate that the propylitized exposures of Alder Gulch syenodiorite are just the top of a much larger zone of

base-metal-rich mineralization. The best way to test this would be to drill several deep holes on the mapped outcrops of Alder Gulch syenodiorite.

GEOGRAPHIC INFORMATION SYSTEM ANALYSIS

Introduction

A geographic information system (GIS), as defined by D.J. Cowen, is "A decision support system involving the integration of spatially referenced data in a problem solving environment" (Cowen, 1988). This compact, yet functional, definition includes two of the characteristics which make GIS computer programs a useful tool in mineral exploration, namely, the ability to aid in decision making based on spatial data, and a capacity to integrate many different data sets into derivative plots. A GIS is a tool, and as such deserves no more or less consideration than any other tool at the geologist's disposal. A GIS will never be able to formulate appropriate questions; however, it does have the ability to speed up and streamline the process of answering questions posed by a competent geoscientist. It also enables assessment of prospective ground in a systematic way, enabling exploration geologists to continuously monitor and develop exploration targets.

Exploration geology deals with a vast amount of spatially referenced data and often requires effective manipulation of these data to delineate mineral deposits and prospects. For this reason, it is an ideal application of GIS technology. One such application, undertaken by the United States Geological Survey (USGS), assessed the mineral potential of the Butte 1° X 2° sheet in Montana by combining geologic, geochemical, geophysical, and remote sensing data to produce maps showing high,

moderate, and low potential for several different deposit types (Elliot et al., 1989). The relative ease of applying geologic models, and their ability to be progressively developed and modified within a company or government agency, enable a level of assessment impractical using non-computerized assessment techniques. As a result, a better estimation of the potential of a given mineral prospect or region can be made, regardless of the immediate exploration target.

The present study utilized a GIS to analyze data from the area surrounding the Zortman Mine area in Montana. It includes three levels of resolution, progressing from small areas with the most complete data, to larger areas with less complete data. The three areas (see Figure 26) are 1) Antoine Butte, an area of less than one square mile encompassing an advanced gold prospect near the mine (4000E, 8000N to 8000E, 14000N); 2) the five square mile area encompassed by thesis mapping (4000E, 4000N to 16000E, 16000N); and 3) the roughly 30 square mile area encompassing both the Landusky and the Zortman mines (-12000E, -6000N to 22000E, 22000N), the area which was grid soil sampled. All three areas were georeferenced to the local grid system used by the mine. Data originally in Universal Transverse Mercator (UTM) units, such as Landsat data, were converted to Zortman coordinates by resampling the Landsat imagery.

Detailed geologic mapping was performed at a scale of 1 inch = 400 feet in order to obtain accurate geologic data for GIS analysis. Field data were recorded on field sheets and subsequently digitized into AutoCAD, a computerized drafting program. Mappable outcrops were given unique numerical identifiers such as

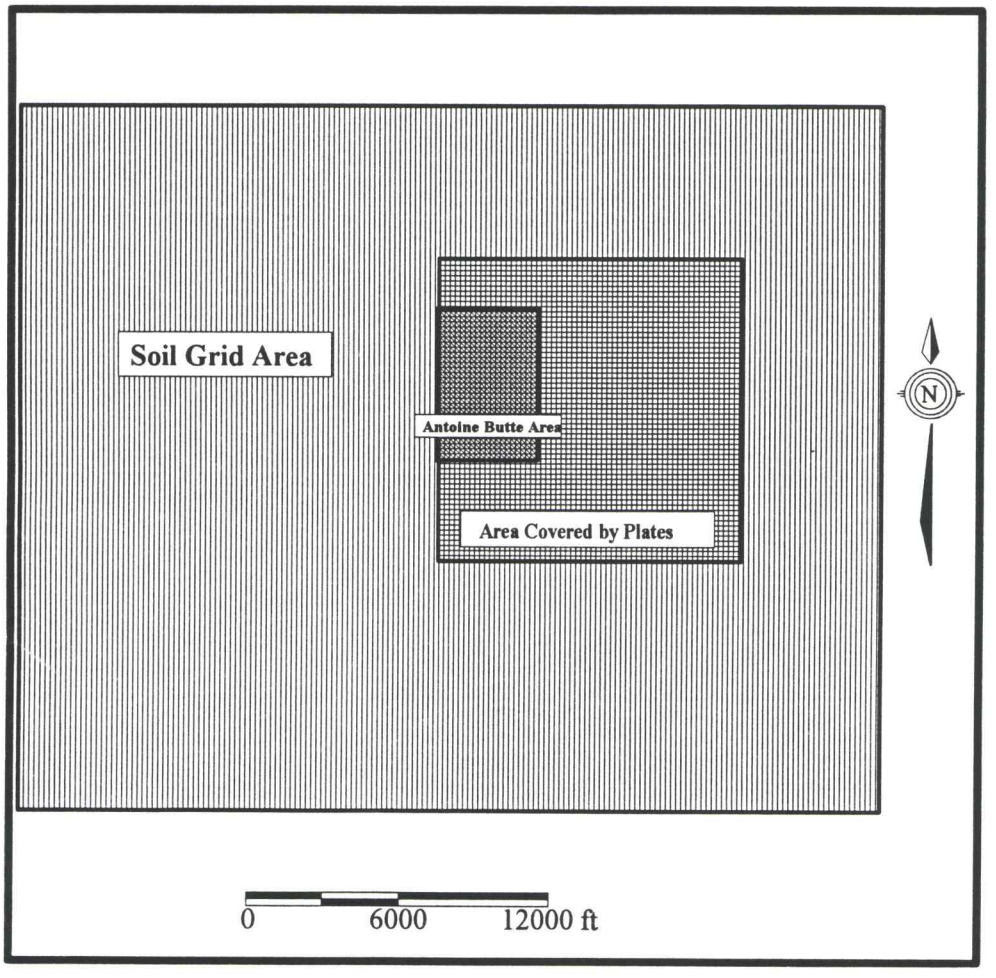

Figure 26. Relative sizes and locations of GIS study areas.

OC001. All notes and outcrop samples are referenced to these outcrop numbers. Geological samples, beginning with PW001, were taken of key outcrops and lithologies for later petrographic examination and geochemical analysis. AutoCAD was utilized as a graphical database. The ATTEXT command was used within AutoCAD to output easting and northing coordinates for sample locations. A database named Dbase IV was used for manipulating and storing attribute data.

Data from AutoCAD and Dbase IV were imported into IDRISI, a raster-based GIS produced by Clark University in Worcester, Massachusetts. All GIS analyses and manipulations were carried out using IDRISI. Final analysis images were exported as TIFF images and edited in Picture Publisher, an image editing program. Final image preparation was completed in a computer drafting program named Micrografx Designer 3.1. This author found the least expensive and perhaps the most useful means of output to be slide photographs taken directly of the computer monitor. This method does not require a significant investment of money, as would be the case for a color printer, and it is much faster. It has the additional advantage of being an efficient way of communicating information to a group. Black and white printouts were done on a Hewlett Packard Laserjet IIIP. Color plots were done on either a Hewlett Packard Paintjet or a Hewlett Packard Paintjet XL-300. The Hewlett Packard Paintjet XL-300 produced the most appealing output.

Hardware used for the analyses were as follows:

80486 IBM compatible computer (EISA) with an Intel 33Mhz DX microprocessor

8 Mb of RAM

NEC Multisync 3D monitor and 8514-compatible graphics card with 1 Mb RAM

120 Mb IDE hard drive with disk compression software (Stacker 2.0)

Calcomp DrawingBoard II 12- X 12-inch digitizing tablet

Objectives

The primary objective of this portion of the study was to integrate the data sets provided by the mining staff with data obtained through detailed mapping and sampling to produce derivative maps. The summary of the study which follows is organized into three main sections. The first section describes the data sets available for GIS analysis, how they were obtained, and their level of accuracy. This is followed by a section summarizing the GIS analyses performed on the data sets applicable to each of the three subareas as described above. The GIS analyses included in the report are a sampling of many analyses that were performed. It is clear from the present work that the best environment for GIS analysis is in direct contact with an ongoing exploration program. This allows for data to be exchanged and updated as needed, and exploration models to be modified as results are

obtained. The final section is an assessment of the effectiveness of the GIS as an exploration tool, and recommendations for further work.

Data Sets used for GIS Analysis

Several different data sets were compiled for use in GIS analysis. These data sets are summarized in Table 5.

Soil Data

Soil samples were collected by Zortman Mining Inc. exploration personnel at 200-foot intervals and analyzed for gold, silver, arsenic, copper, lead, and zinc by Silver Valley Geochemical Laboratories. Zinc values were not obtained for all samples. The raw data were stored, manipulated, and queried using Dbase IV. The data were subdivided into three groups; one encompassing a rectangle from 4000E, 8000N to 8000E, 14000N; the second encompassing the areas mapped for the thesis work from 4000E, 4000N to 16000E, 16000N, and the third including all available soil data. Each element was imported into the IDRISI GIS and a distance-weighted interpolation (THIESSEN polygon creation) was performed to produce a continuous surface of each element. Since the THIESSEN command in IDRISI can only operate on integer values, it was necessary to use the SCALAR function to convert from decimal to integer format. The resulting Thiessen polygons were then subjected to a low pass (mean) filter four times in order to smooth the data and create a more continuous surface. An image of 200 X 200 pixels was chosen for the data, yielding

Table 5. Data sets used for GIS analysis.

Data Set	Original Units	Source	Usefulness for Exploration	Coverage	Resolution
Soil Data					
Au	ppb	Commercial geochemical laboratory	High	Moderate/Good	Sampled on 200-foot spacings.
Ag	ppm				
As	ppm				
Cu	ppm				
Pb	ppm				
Zn	ppm				
Grab Samples					
Au	opt	Zortman Mining Inc. laboratories	Moderate	Poor/Moderate (point bias)	~896 samples over 144,000,000 square feet (equivalent to 400-foot centers).
Ag	opt				
Drilling Data					
Au	opt	Zortman Mining Inc. laboratories	Low/Moderate (local bias)	Moderate (point bias)	Varies (very dense in some areas).
Ag	opt				
Geology					
Faults		Compiled and collected	Moderate	Good	Mapped at 1-inch = 400-foot scale.
Alteration					
Topography					
Mine area	feet	Horizon Aerial Photography	Low/Moderate	Good/Excellent	Constructed at 1-inch = 400-foot scale.
Zortman USGS Quad	feet	American Digital Cartography Inc.	Low/Moderate	Good/Excellent	Scanned at 1:24,000 scale.
Landsat TM Imagery					
Band 1	relative reflectance (DN)	Barringer Geoservices	Moderate (regional)	Good	30 meters (~98 feet) for Bands 1, 2, 3, 4, 5, 7; 120 meters (~394 feet) for Band 6.
Band 2					
Band 3					
Band 4					
Band 5					
Band 6					
Band 7					
Aerial Photo Lineaments	no units (binary)	Aerial photo compilation	Low/Moderate	Moderate	Digitized from 1-inch = 2,000-foot aerial photo.
Induced Polarization Data	milliseconds	Quantech Consulting, Inc.	Low/Moderate (limited coverage)	Poor/Moderate	Dipole array 100-foot sample intervals. Lines ~300 to 600-foot spacing.
Aeromagnetic Data	gammas	Meijji Resources, Ltd.	Low/Moderate (poor resolution)	Moderate	Line spacing ¼ mile; contains 200 gammas.

Abbreviations: ppb = parts per billion; ppm = parts per million; opt = ounces per ton; DN = digital number; TM = Thematic mapper

a resolution of approximately 25 feet per pixel for the first group, 60 feet per pixel for the second, and approximately 120 feet per pixel for the third. The process of Thiessen polygon creation was performed for each element and for each of the previously mentioned data subgroups (See Figures 27, 28 & 29).

Grab Samples

A total of 896 rock samples were compiled from samples taken by this author and previous workers (see Figure 30). Sample locations were compiled from several company sources with varying scales and accuracies. Each sample was compiled in AutoCAD as a BLOCK with the sample #, and gold and silver value attached as attributes. The data were then output in X, Y, Au, Ag, Sample# format for importation into IDRISI. The samples were analyzed for contained gold and silver by the Zortman Mining Inc. geochemical laboratory. The data set did not include many samples from the mine area, so data from mine drilling were used to create a more continuous data set. A Dbase QUERY was used to extract the interval between 20 and 25 feet below ground surface from the top of each drill hole. The 20- to 25-foot interval was chosen because it was deemed most similar to a surface rock sample. Although this incorporated some error due to differences in the sampling method for the drilling versus rock chip samples, it was deemed more important to be able to incorporate at least some data from an area of known mineralization. The result was not wholly satisfactory in that the drilling, being more systematic than the grab samples, appears to have lower gold content due to

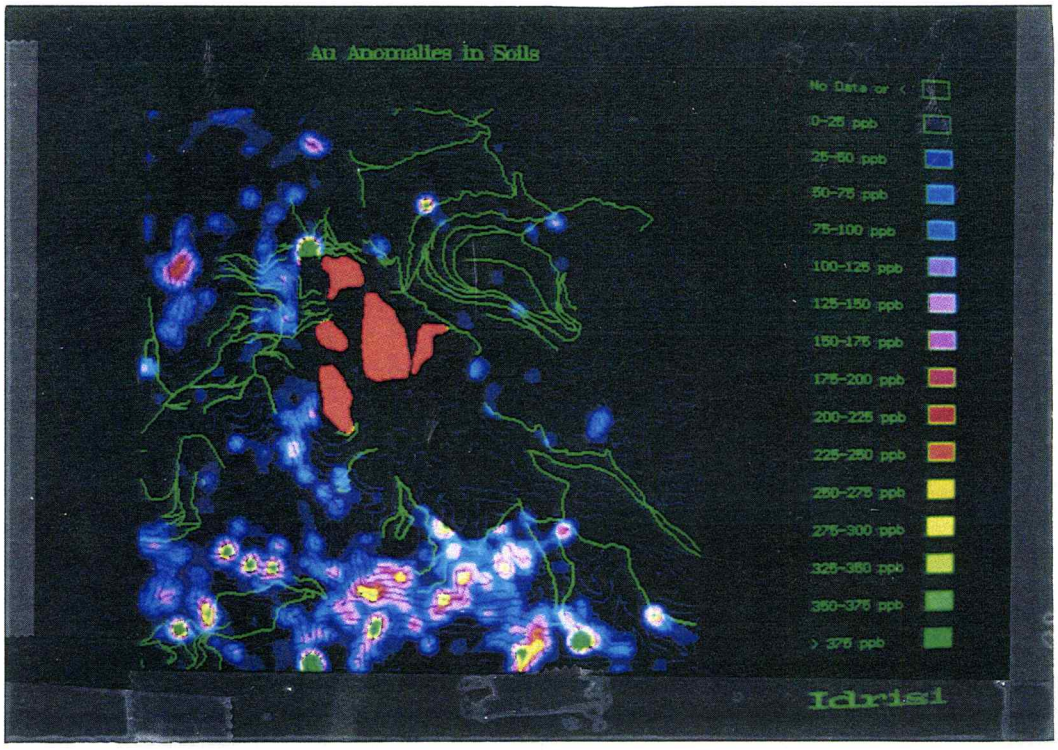

A

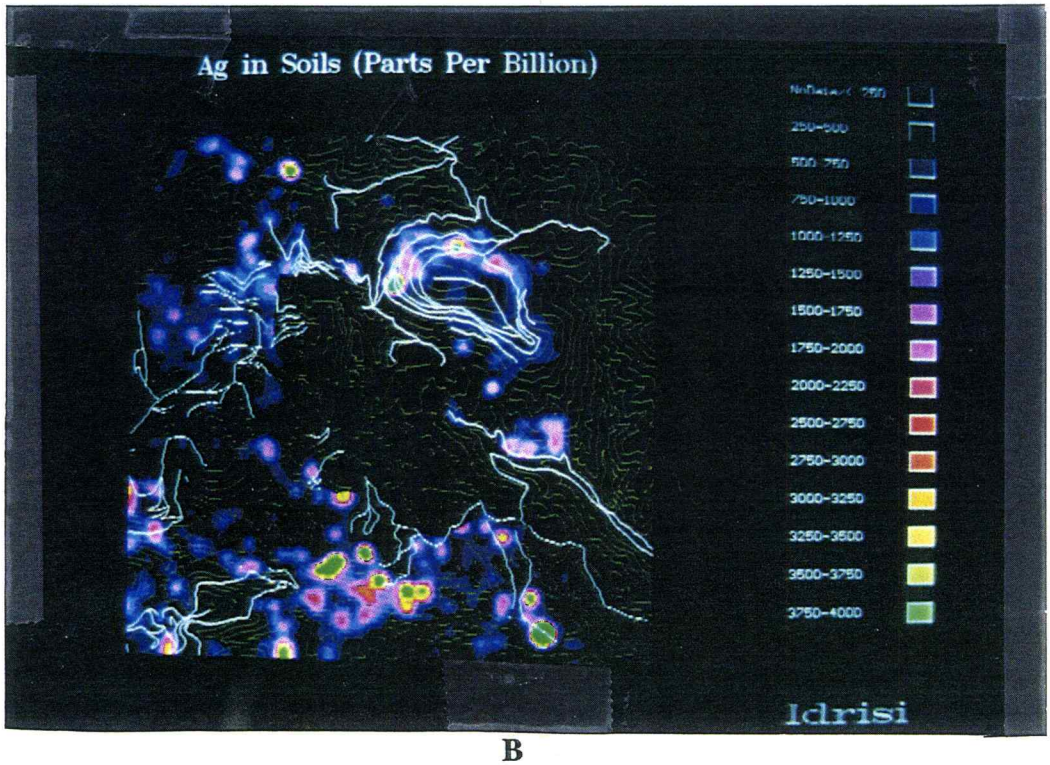

B

Figure 27. **Soil data layers (gold, sliver). A. Gold anomalies in soils. Orange area near the center of the photo is the mine area. Green lines are roads. B. Silver anomalies in soils. White lines are roads.**

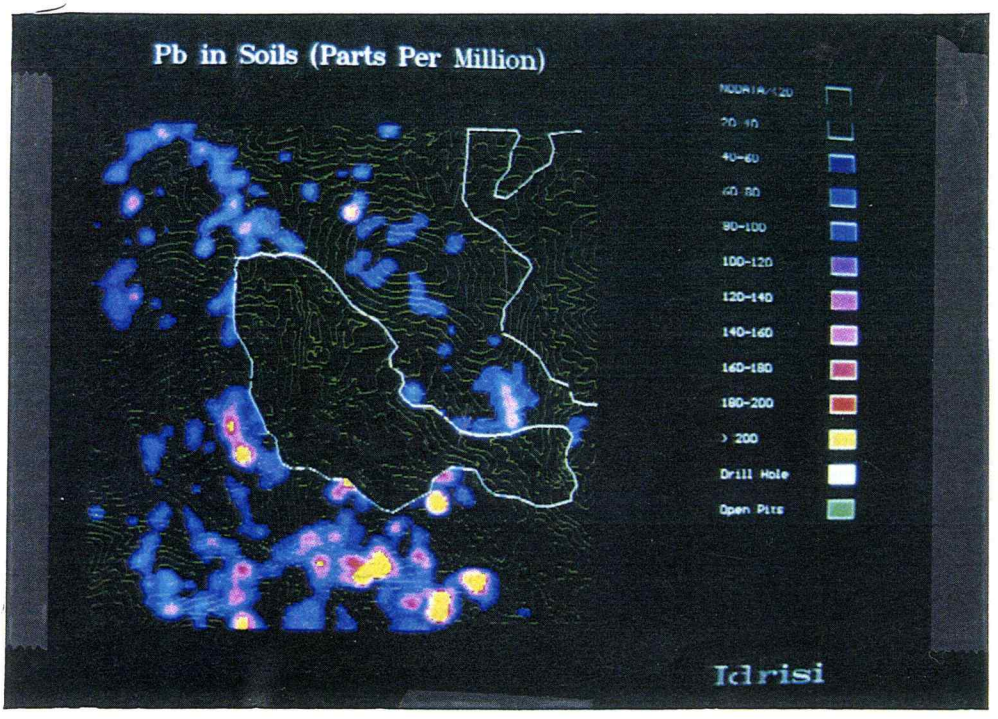

A

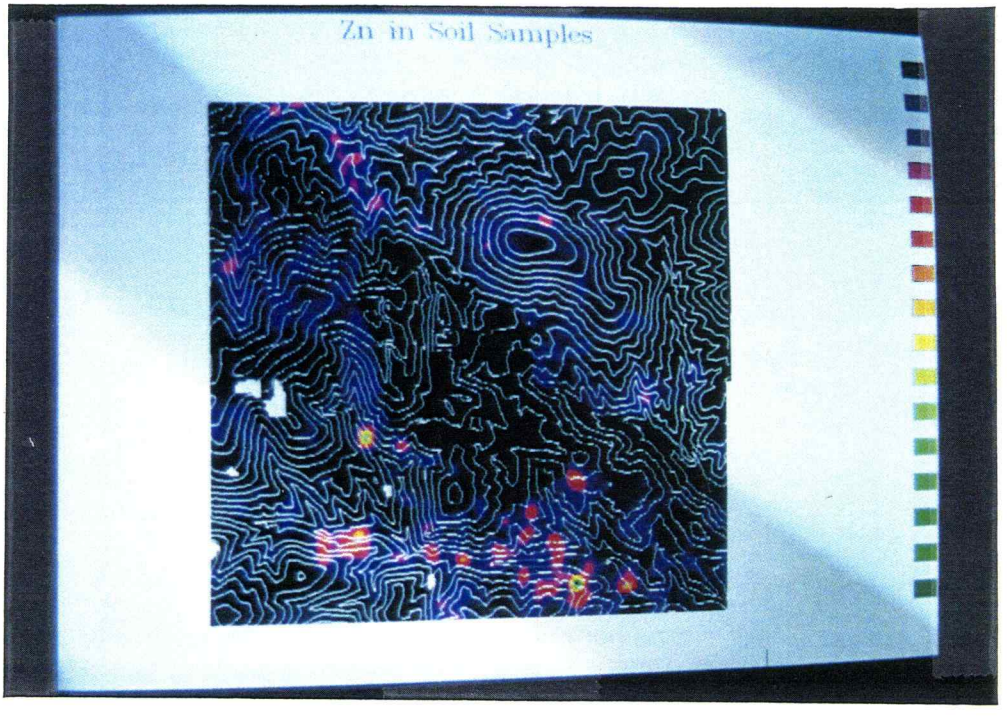

B

Figure 28. Soil data layers (lead, zinc). A. Lead anomalies in soils. White outline is the area where no soil samples were taken. B. Zinc anomalies in soil samples. The strongest anomalies are green.

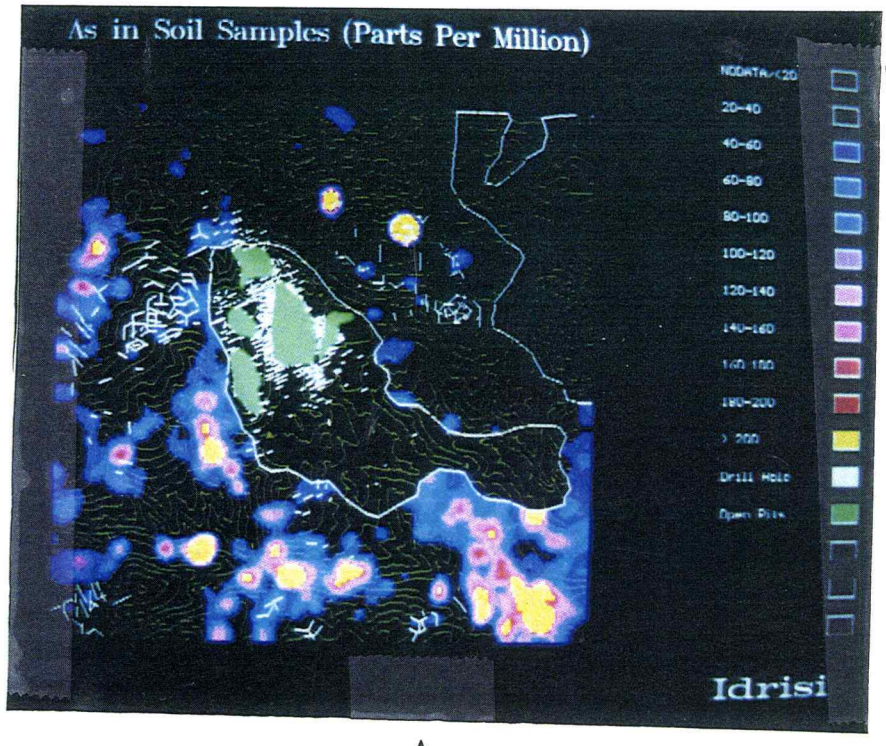

A

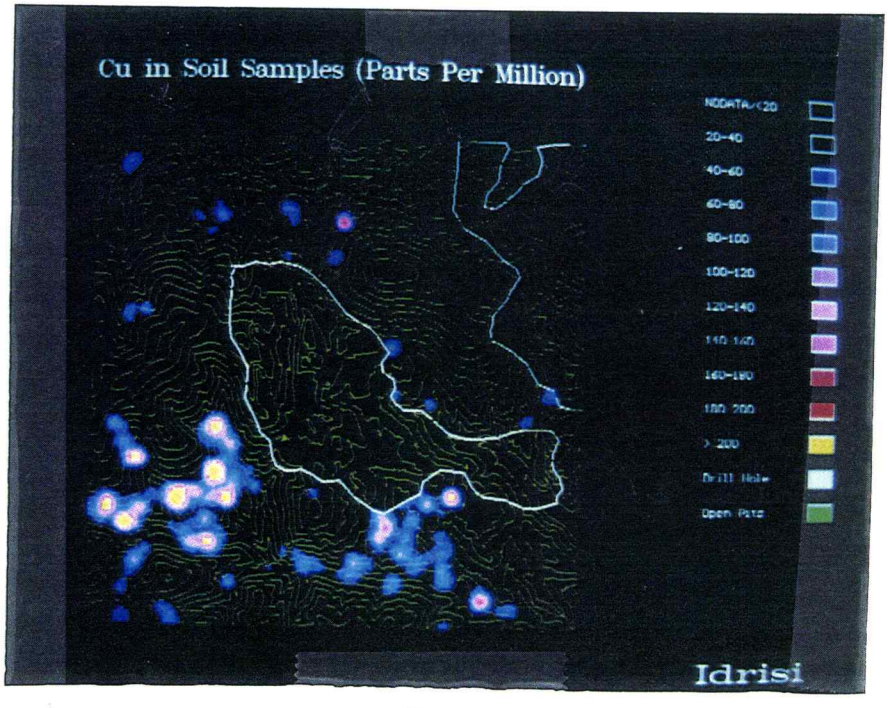

B

Figure 29. Soil data layers (arsenic, copper). A. Arsenic anomalies in soils. White lines are the horizontal projections of drill holes. Mine pits are green. B. Copper anomalies in soils. White line indicates area not sampled.

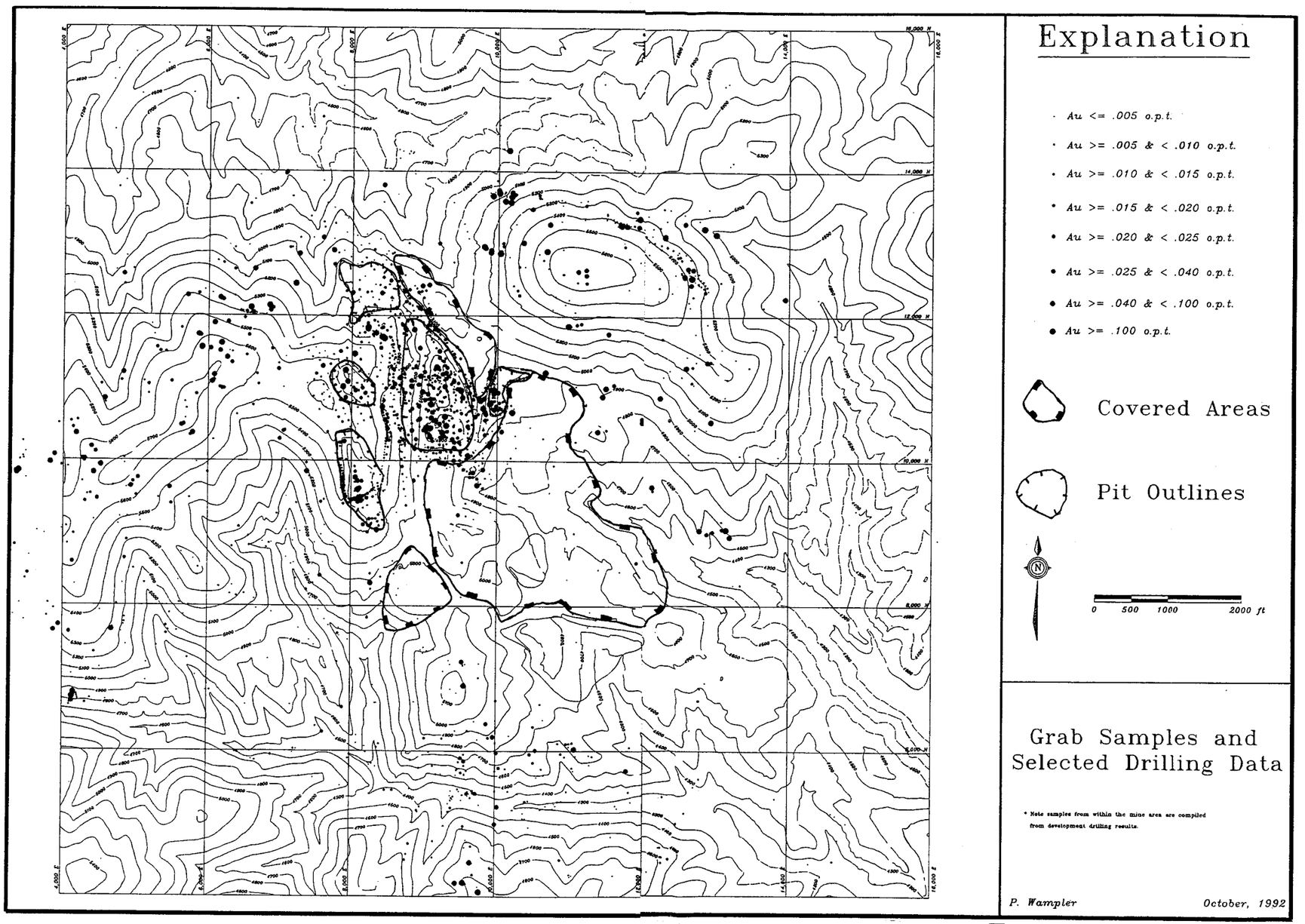

Figure 30. Grab sample point data.

the lack of the sampling bias present in the grab samples, due to "high grading". A continuous surface was created from the point data in the same manner as described above for the soil data. The resulting surface remains biased by both high grading and sample distribution (See Figure 31).

Drilling Data

Drilling data were compiled and manipulated in Dbase IV. Data included both widely spaced exploration drilling, and closely spaced development drilling, undertaken to delineate the ore body. Drilling samples were analyzed by Zortman Mining Inc. laboratory by the atomic absorption method. The easting and northing of each drill hole collar and each drill hole terminus were obtained using a Dbase IV query. These coordinates were then used to create lines, representing the horizontal projections of drill holes, with an AutoLISP program (DRILLIN.LSP). The line drawing was then imported into IDRISI using the ACDTOIDR lisp program. The gold and silver values for the drilling were utilized only on Antoine Butte since at any larger scale they represent a sample set which has a strong spatial bias. Gold and silver values for Antoine Butte were projected onto a two-dimensional data layer.

Geology

Geologic mapping at a scale of 1 inch = 400 feet was completed during summers of 1991 and 1992. The primary goal of this mapping was to define areas

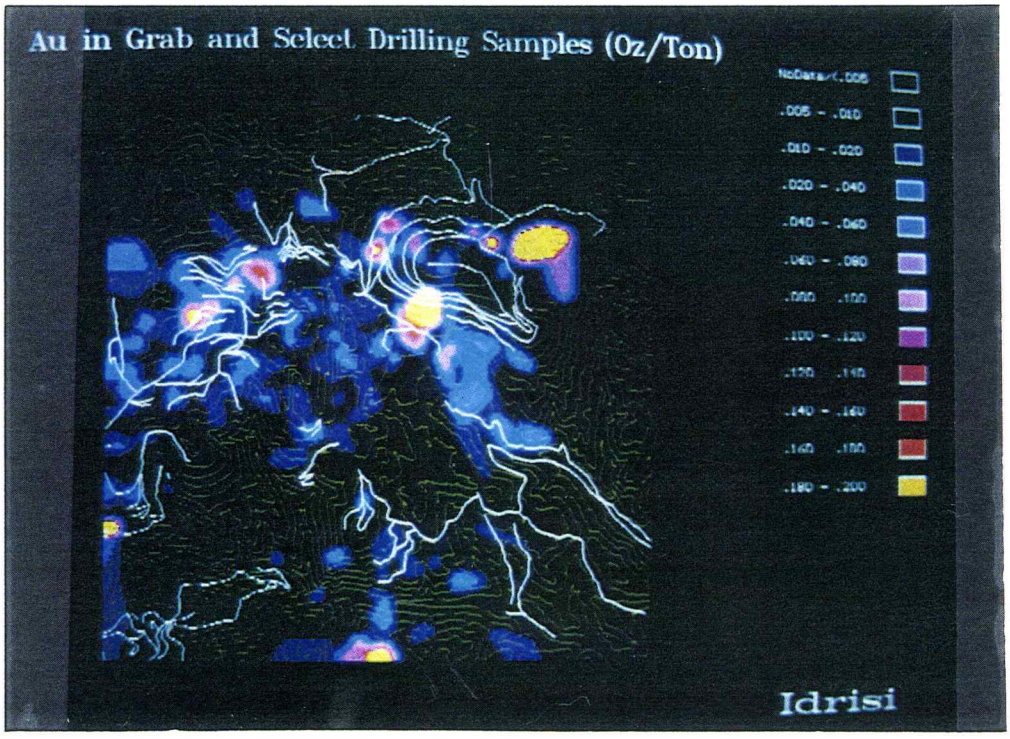

Figure 31. Grab sample data layer. White lines are roads.

of mineralization and alteration, delineate lithological boundaries and major structures, and obtain accurate geological and geochemical data. The geology was generalized to create the geology data layer for GIS analysis (see Figure 32). One hundred twenty-eight samples were taken for gold and silver analysis, using Zortman Mining Inc. laboratories. Field data were collected and compiled in both digital and manual format to expedite transfer to a GIS.

Geology data was also compiled from numerous company manuscript maps such as Gabelman, 1990; Russell, 1989b; Russell, 1989c; Brasher et al., 1983. Field data were recorded on field sheets and subsequently digitized into an AutoCAD drawing. Alteration was also compiled into an alteration data layer, using both field observations and petrologic examination of thin sections (see Figure 33). The geologic map was edited in AutoCAD for import into IDRISI as a raster image. Since the representation to be used for analysis was raster-based it was not necessary to perform rigorous topological editing.

Digital Elevation Model (Topography)

A digital elevation model (DEM) is a data matrix with each cell within the matrix representing the elevation at that point on the ground. Elevation data for the thesis area DEM were derived from Autocad 3D drawings of contour lines. A lisp program called ACDTOIDR, provided with IDRISI, was used to create IDRISI-compatible vector files of all the intermediate contours from the AutoCAD drawings provided to Zortman Mining Inc. by Horizon Aerial Photography Inc. (Horizon).

Simplified Geology Map

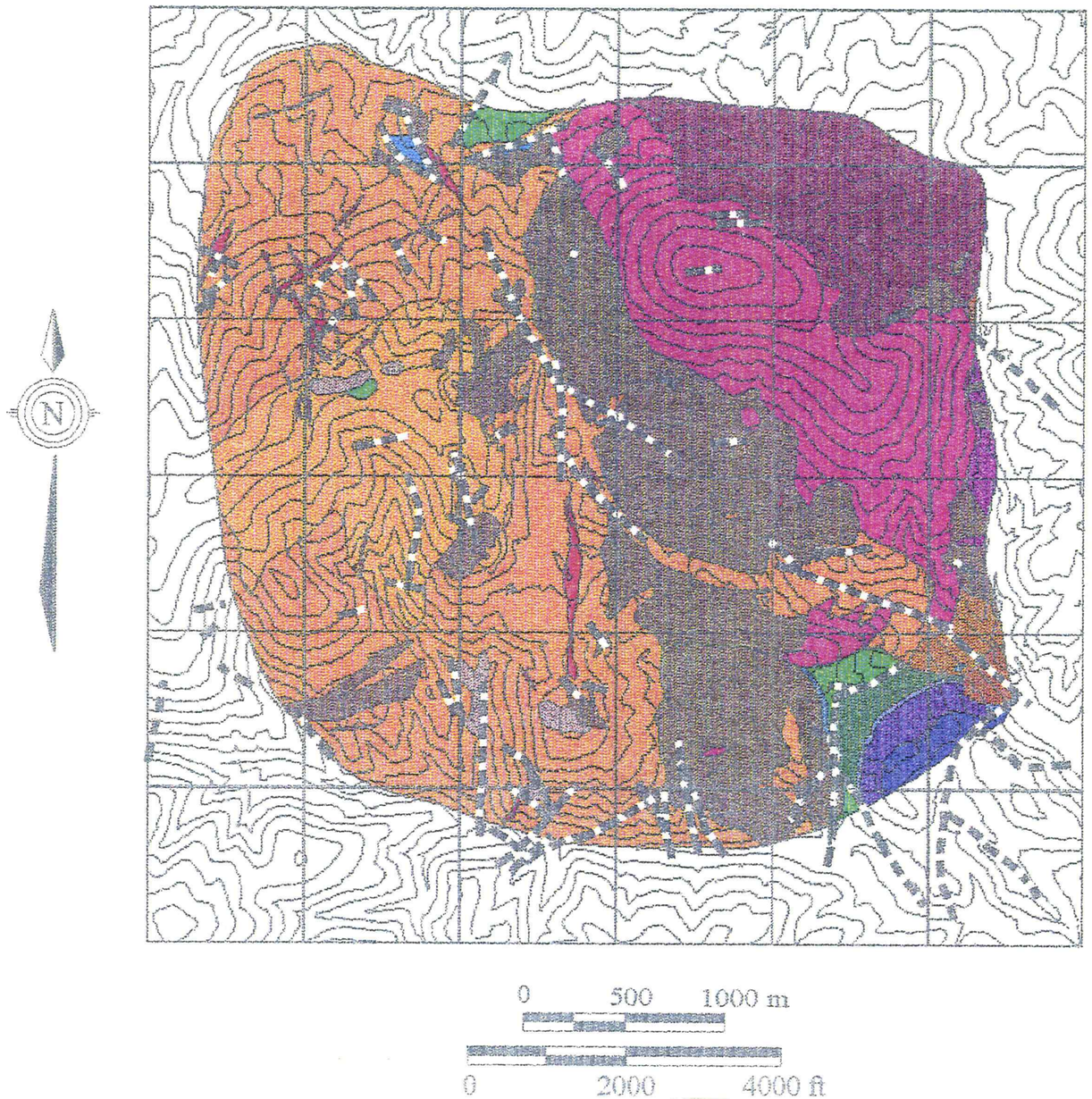

Explanation

- Dikes
- Tibx
- Tisb
- Tiss
- Tia
- Tia (c)
- Tio
- Tiof
- Tib
- Mmc
- Ml
- Dtf
- Dj
- Ob
- Coe
- Cf
- Pcu
- Pm
- Faults

P. Wampler 1993

Figure 32. Geology map data layer. Simplified raster representation of the geology surrounding the Zortman Mine.

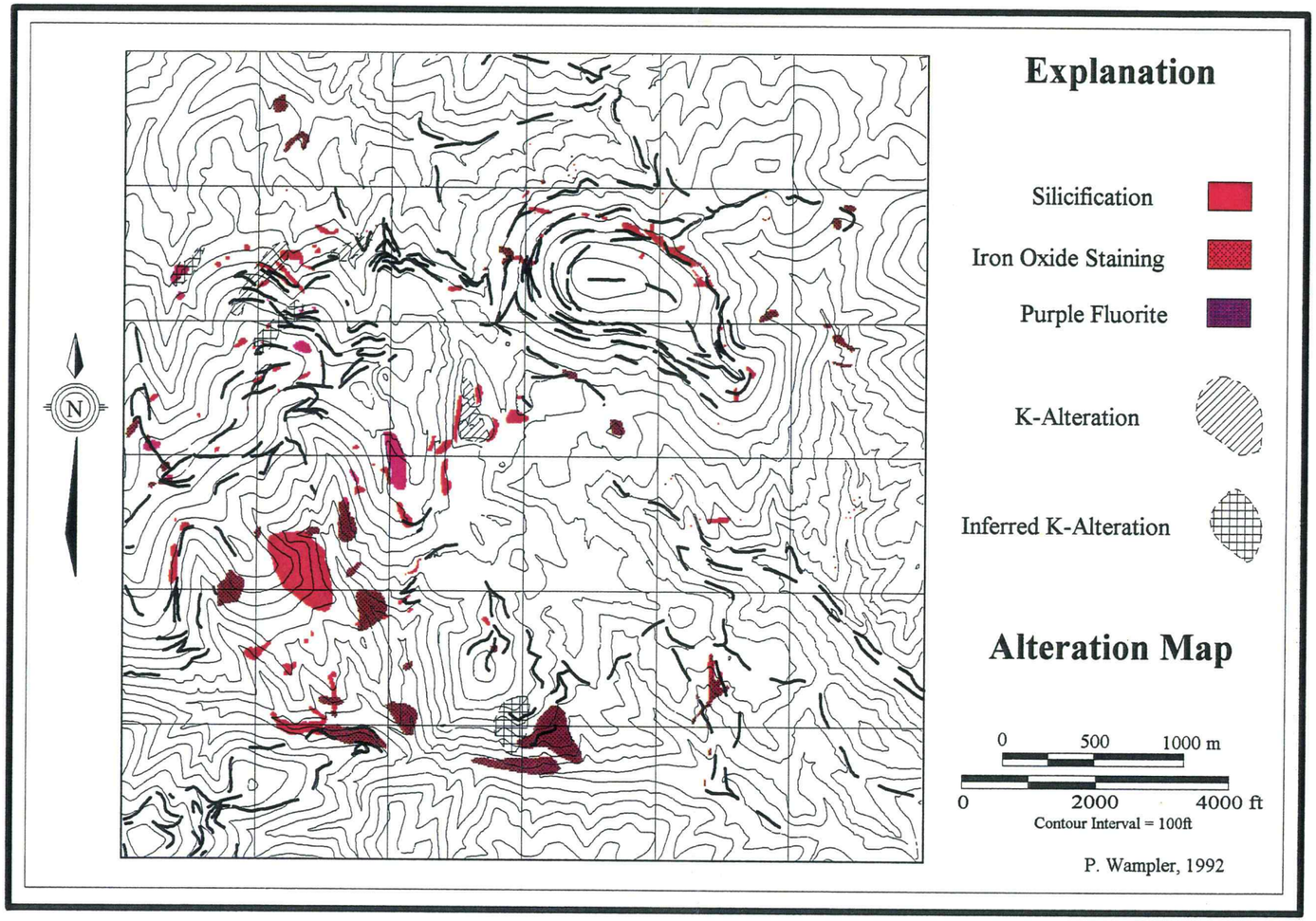

Figure 33. **Alteration data layer. Simplified raster representation of the alteration surrounding the Zortman Mine area. See Plate 2 for the detailed hydrothermal alteration map.**

The AutoCAD drawing, provided by Horizon, was created by digitizing contour lines directly from orthophotos. Several lines were found with erroneous elevations; these were corrected and the final vector IDRISI file of the contour lines was produced. The contour line files were imported in four pieces to speed up the process and to expedite error correction. The IDRISI module LINERAS was used to create a raster representation of the four areas. These areas were then merged using the CONCAT command in IDRISI. The final image is 600 X 600 pixels and has a resolution of approximately 20 feet per pixel. Once the complete image was obtained, the INTERCON routine was used to create a continuous surface from the line data. INTERCON interpolates between contour line data to produce a continuous surface. The image obtained was then smoothed several times using a low pass filter (mean filter). Once created, it was possible to create an analytical hill shading image for three-dimensional orthographic viewing. The hill shading image was reclassed to 255 classes to facilitate viewing with a 256 color palette (see Figure 34). The three-dimensional shaded relief images would be especially useful in visualizing proposed mine plans and presenting the plans to state and federal agencies.

A digital elevation model of the USGS Zortman 7½ minute topographic quadrangle was purchased from American Digital Cartographic Inc., and was originally digitized at a 1:250,000 scale. The DEM was purchased already georeferenced to UTM coordinates, and required minimal manipulation before importation into IDRISI (See Figure 35).

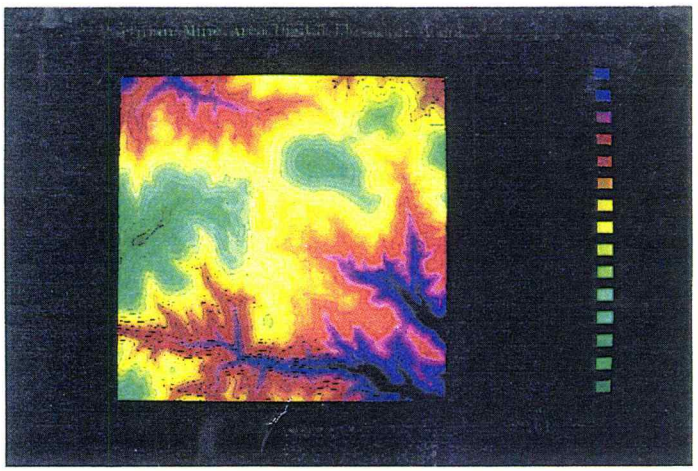

A

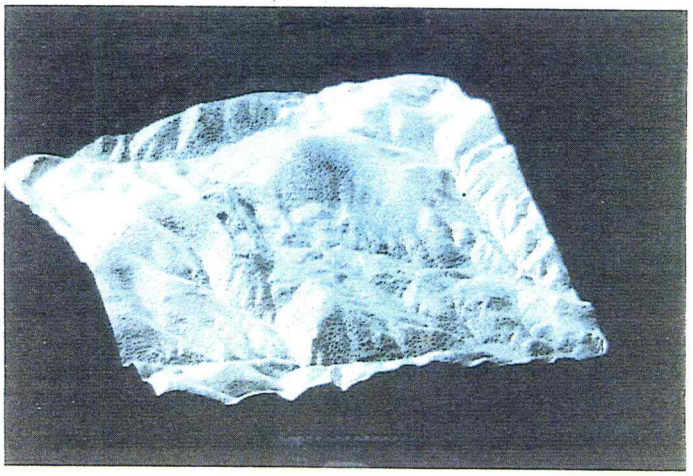

B

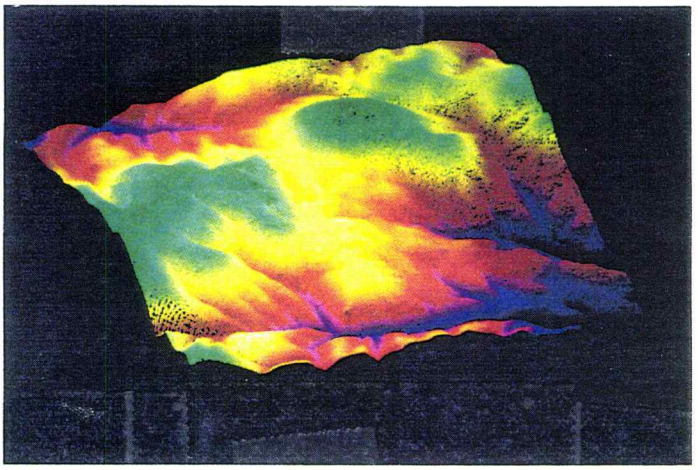

C

Figure 34. DEM of thesis area. A. Plan view; color indicates elevation. B. 3D shaded relief view of the same area. C. 3D color representation of the DEM.

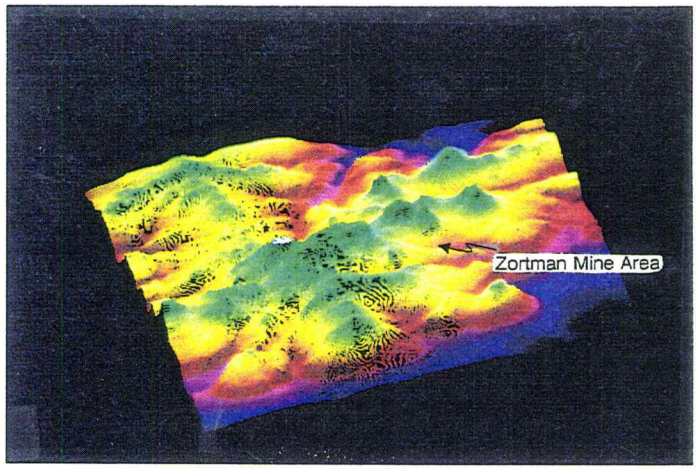

A

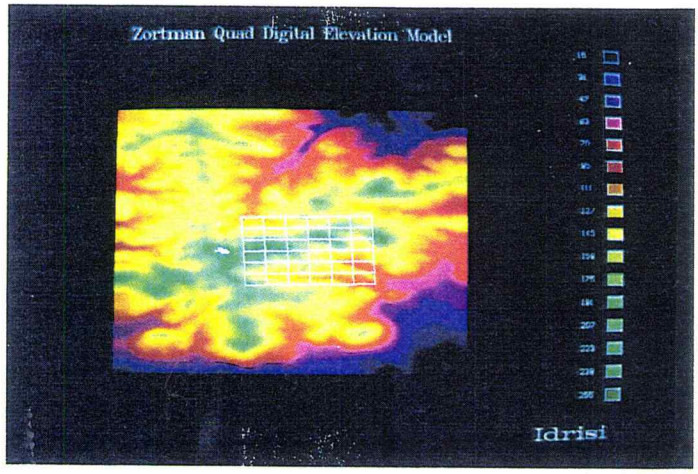

B

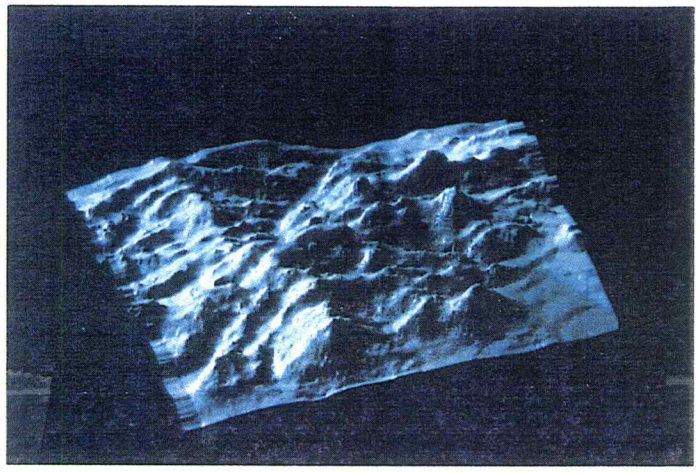

C

Figure 35. **DEM of Zortman quad. A. 3D color representation of the DEM. B. Plan view; color indicates elevation. C. 3D shaded relief view of the DEM.**

Landsat Thematic Mapper Data

A subscene of raw Landsat data was obtained from Barringer Geoservices Inc. in band interleaved (BIL) format on floppy disks. The data were imported using the BILIDRIS command in IDRISI. Georeferencing of the Landsat data to the local Zortman grid was accomplished using the RESAMPLE module of IDRISI. Ten points were chosen for georeferencing. These points are summarized in Table 6. There was a translation error between the Landsat image and the Zortman grid; this was corrected by modifying the correlation matrix. The source of the discrepancy is still unknown. The mine area was then extracted from each image using the WINDOW command (see Figure 36A and B).

Air Photo Lineaments

Air photo lineaments were compiled from aerial photography and digitized into AutoCAD. The lines were imported into IDRISI as a raster-line image.

Induced Polarization Data

Induced polarization data were collected by Quantech Consulting Inc. (Quantech) using the dipole-dipole method at 200-foot intervals along lines orientated northeast-southwest. Data were digitized from plots produced by Quantech. Only IP chargeability was digitized. The data were then imported into IDRISI and a

Table 6. Control points for UTM to local coordinates translation.

			Zortman (feet)[1]		UTM (meters)[2]		"Corrected" Zortman (feet)[3]	
Point #	Quality	Description	East	North	East	North	East	North
1	Good	Antoine Steel Tower	4805	9844	680974	5311368	4592	10269
2	Good	Hawkeye "5465" Peak	4318	4234	680902	5309667	4105	4659
3	Moderate/Poor	Alder/Pony Road Junction	14650	4299	684036	5309776	14437	4724
4	Moderate	Cowboy Gulch "5176" Peak	9798	2609	682593	5309233	9585	3034
5	Good	Carter Butte "5136" Peak	9340	6869	682420	5310504	9127	7294
6	Good	North Antoine "4949" Peak	5568	13809	681166	5312589	5355	14234
7	Good	Section Corner (12,7,13,18)	7552	8486	681829	5310981	7339	8911
8	Very good	Shell Butte "5692" Peak	11066	12642	682870	5312291	10853	13067
9	Very good	Lodgepole Road Intersection	11301	15433	682933	5313137	11088	15858
10	Good	Section Corner (1,6,12,7)	7557	13737	681783	5312588	7344	14162

[1] Error in calibration for Zortman Coordinates was ± 5 feet.
[2] Error for UTM calibration was ± 5 meters
[3] Correction required subtracting 213 feet from the easting and adding 425 feet to the northing.

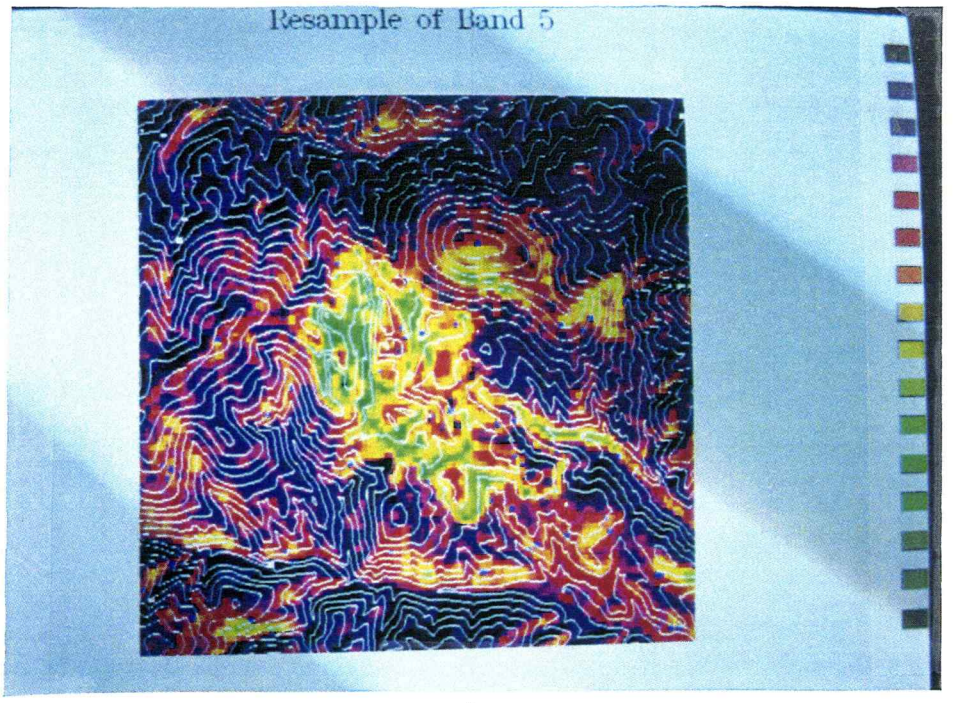

A

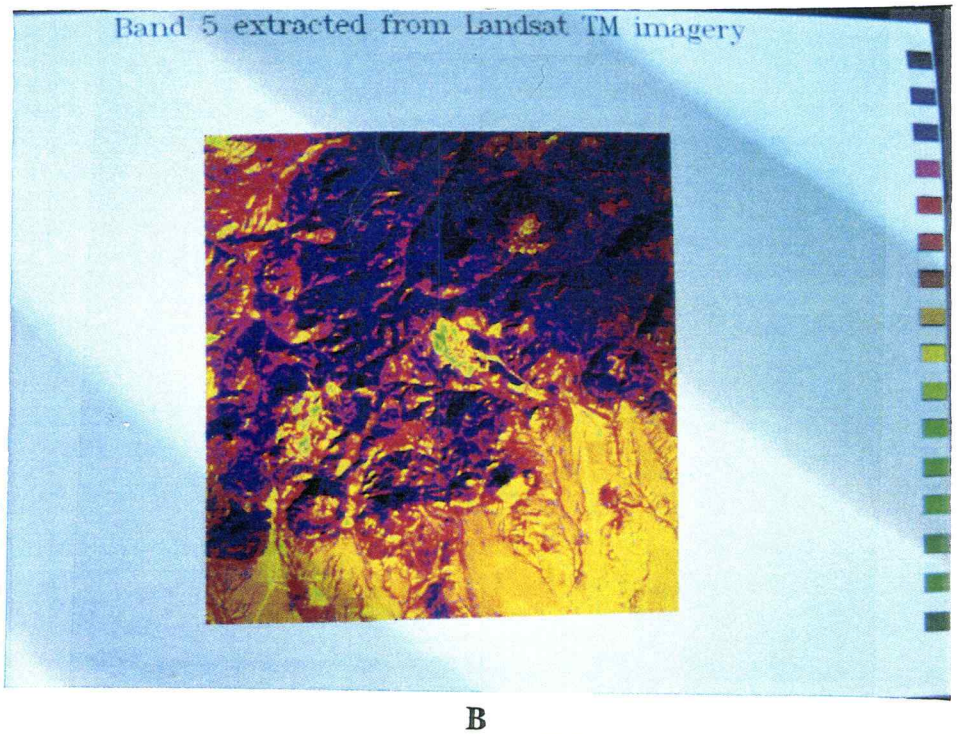

B

Figure 36. **Landsat Thematic Mapping (TM) imagery. Photo A is a subset of Photo B and corresponds to the area covered by Plate 1. Colors represent variation in relative reflectance or digital numbers (DN). Topography is shown in white. Photo B is the Landsat TM scene obtained from Barringer Geoservices Inc. The central portion of Photo B is enlarged in Photo A.**

continuous surface was created in the same manner as described for the soil samples above (see Figure 37).

Aeromagnetic Data

Aeromagnetic data were collected in 1983 by Meijji Resources Ltd. (Meijji). The maps produced by Meijji were digitized into AutoCAD (MAGNETIC.DWG). The instrument used for the survey was not specified. However, the survey elevation was 500 feet mean terrain clearance and the line spacing was one-quarter mile. The calibration error between the digital image and the map was roughly $\pm$ 5 meters. The drawing was then imported into IDRISI, and the data were interpolated and smoothed in a manner similar to the soil data. The overall error of the x-y locations in this data set is approximately $\pm$ 30 meters.

GIS Analyses

GIS analyses were performed at three scales in order to demonstrate the advantages and disadvantages of each scale. The thesis area contained the most complete data set available, and thus was given the most attention during analysis. Additionally, most areas within the thesis grid are within 4,000 feet of the Zortman Mine and could be incorporated into current and proposed mining operations. The following pages summarize each of the GIS analyses performed, including: the data layers used; the assumptions made during the analysis; the objective; and the results and conclusions derived from the analysis. Many of the analyses that follow use a

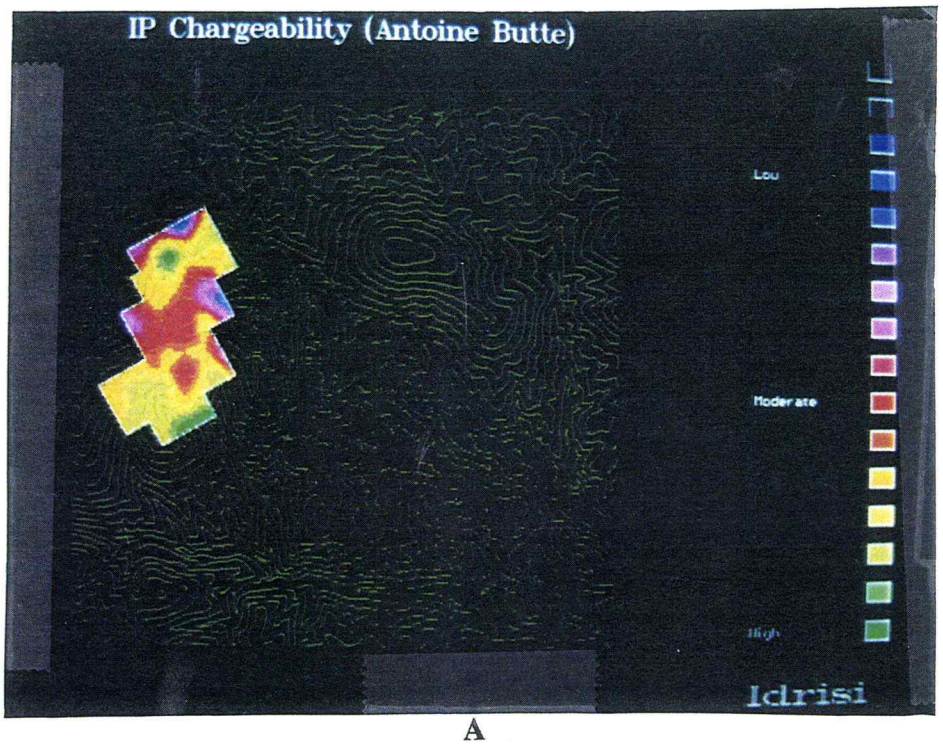

A

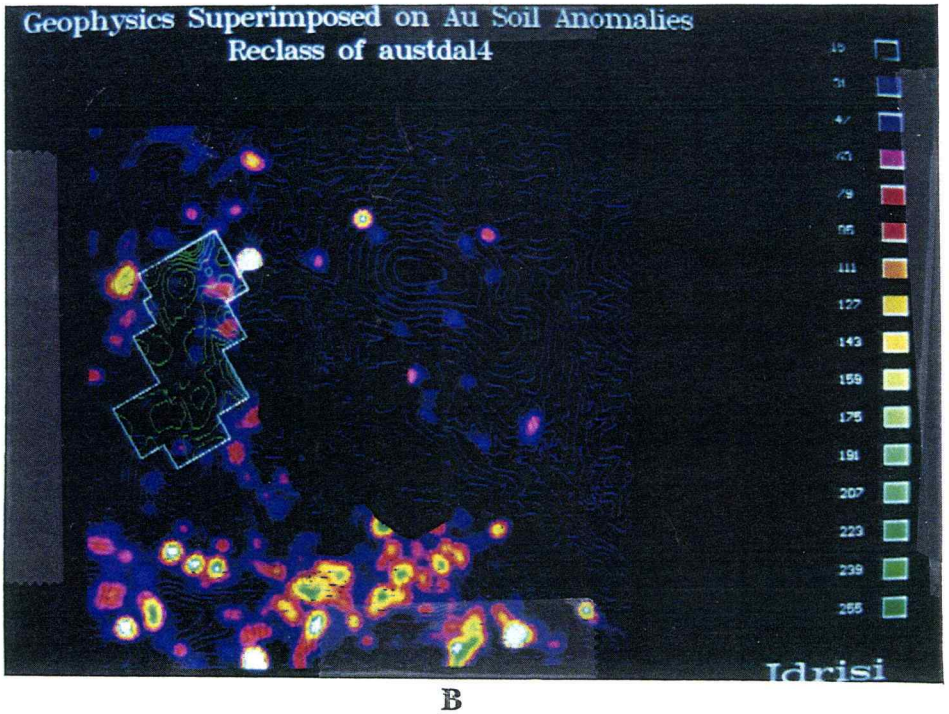

B

Figure 37. **Induced Polarization (IP) data layer. Photo A is a plan view of the Thiessen polygon created for the chargeability data layer. Areas of high chargeability are shown in green and areas of low chargeability are shown in blues. Photo B is the outline of the IP survey grid superimposed on the four times rolling average image of gold in soils. Contoured chargeability is shown in green.**

weighting method to integrate data with different units and magnitudes. For example, for the composite gold potential on Antoine Butte, the primary objective of the analysis was to highlight those areas that are most favorable for gold mineralization. Weighting, or reclassifying, each data set was used to allow each data set to contribute an amount proportional to its ability to predict gold potential on the final gold potential map. This allowed integration of data with completely different units; for example, chargeability and soil samples.

Composite Gold Potential on Antoine Butte

The data layers used were: IP chargeability; gold values from exploration drill holes; gold in soil samples; and gold in grab samples.

This analysis assumes that low chargeability correlates with gold mineralization. This assumption is based on empirical observations of the areas where mineralization was encountered in drill holes. The analysis also assumes that chargeability and gold anomalies based on exploration drilling should carry roughly the same weighting. These data sets were reclassified from 0 to 50, with 0 being the lowest value and 50 being the highest, while gold in soils is weighted 0 to 100. Gold in grab samples was considered the least accurate predictor of gold potential, with a weighting of 0 to 25 (see Figure 38).

The objective of this analysis is to delineate those areas with the highest potential for gold mineralization in a small target area. Additionally, it was meant to demonstrate the integration of geophysical data into a GIS analysis.

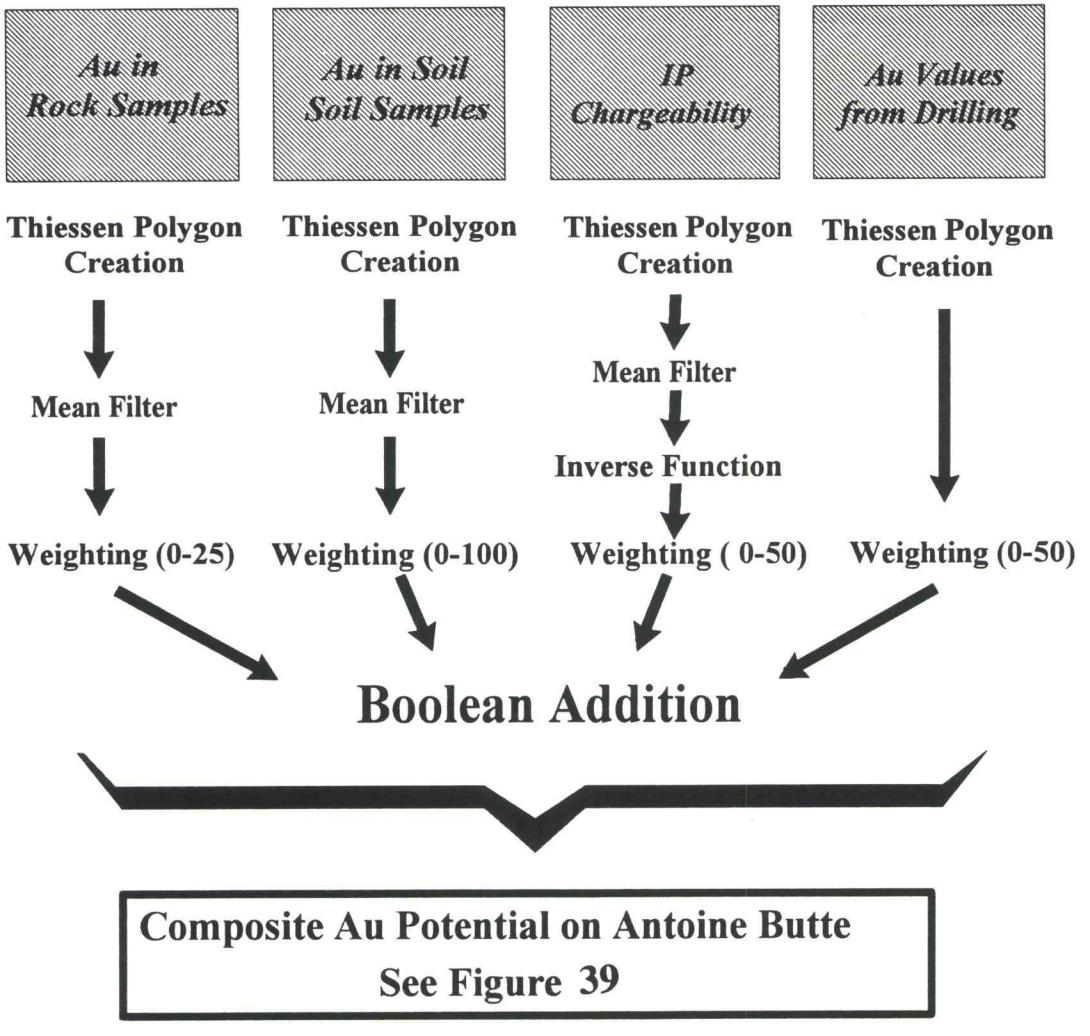

Figure 38. Flow chart for the creation of the composite gold potential on Antoine Butte GIS analysis. The boxes at the top represent raw data in original data units.

It was necessary to reclassify the chargeability data so that areas with low chargeability carried the largest values (since low chargeability was considered a positive attribute). This was done by subtracting the maximum value from all the other values and multiplying them by -1. Once the chargeability was reclassed, it was a simple matter to weight the other data layers described above by reclassifying them into 0 to 100, 0 to 50, and 0 to 25 classes. The reclassed images were then added together, using the OVERLAY command, to produce an image in which areas with the highest values were the areas of highest potential based on the criteria chosen.

Several areas were delineated by the analysis (see Figure 39). A significant northeast trend was present over the central portion of Antoine Butte. The correlation between areas of low chargeability and gold mineralization proved to be useful in delineating areas using the GIS.

Composite Gold Potential for the Map Area

The data layers used were: gold in grab samples; gold in soil samples; horizontal drill projections; and mapped faults.

It is assumed for the purposes of this analysis that the presence of gold is the best indicator of gold mineralization. Thus, only gold in soil and rock samples was considered for this analysis. It is also assumed that since most mineralization at the Zortman Mine is fault- or fracture-controlled, proximity to a mapped fault increases the potential of finding mineralization. The analysis also assumed that soil samples

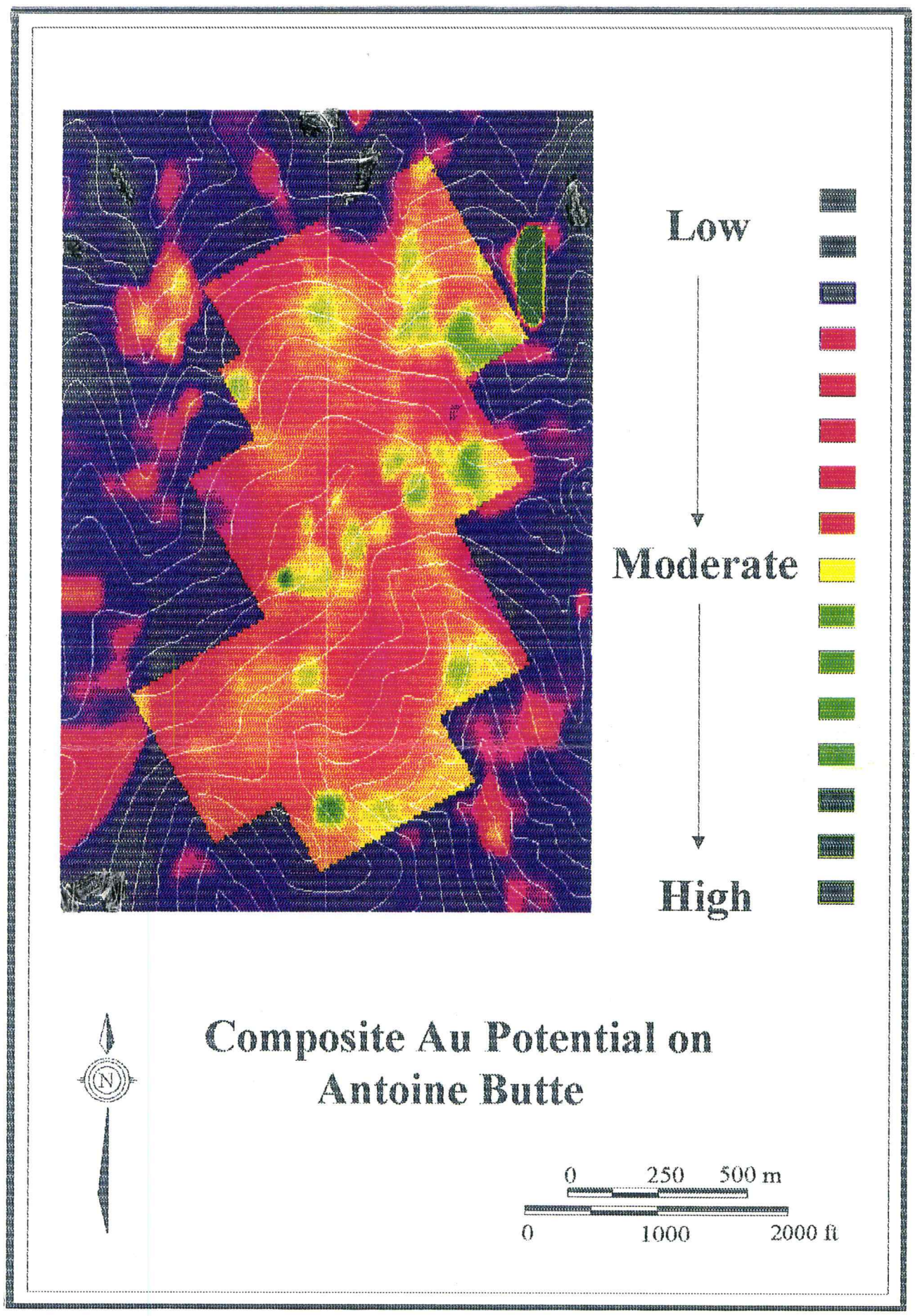

Figure 39. **Composite gold potential on Antoine Butte. Note apparent increase in potential due to availability of IP data within the irregularly-shaped polygon.**

are the most accurate data set for predicting gold potential, followed by grab samples, and lastly the proximity to drilling and faults. Additionally, it assumed that distance from an existing drill hole is proportional to the potential of finding undiscovered mineralization; the greater the distance, the greater the potential that a given area has not been tested.

The primary objective was to integrate the four data sets described above into a composite potential map delineating those areas most likely, based on the criteria, to yield undiscovered mineralization.

The first step was to reduce the four data sets into weighted data sets depending on their relative contribution to the gold potential. Gold in soil samples was most heavily weighted, with a range of 0 to 100; and gold in grab samples were weighted from 0 to 25. The distance to drilling was weighted from 0 to 10, 0 being at a drill hole and 10 being the maximum distance within the data set. The distance to a mapped fault was also weighted 0 to 10, but the values were reversed relative to the drilling, with 0 being assigned to cells farthest from mapped faults and 10 assigned to cells located on a mapped fault. Once weighted, the four data sets were added together using OVERLAY to produce the composite potential map. Thus, areas which had the highest weighted value in all four sets would have the highest overall composite value (see Figure 40).

The heavy weighting on the soil sample data set is apparent in the resulting composite (see Figure 41); however, some areas which appeared to have very high potential based on soils alone appear less interesting on the composite map. The

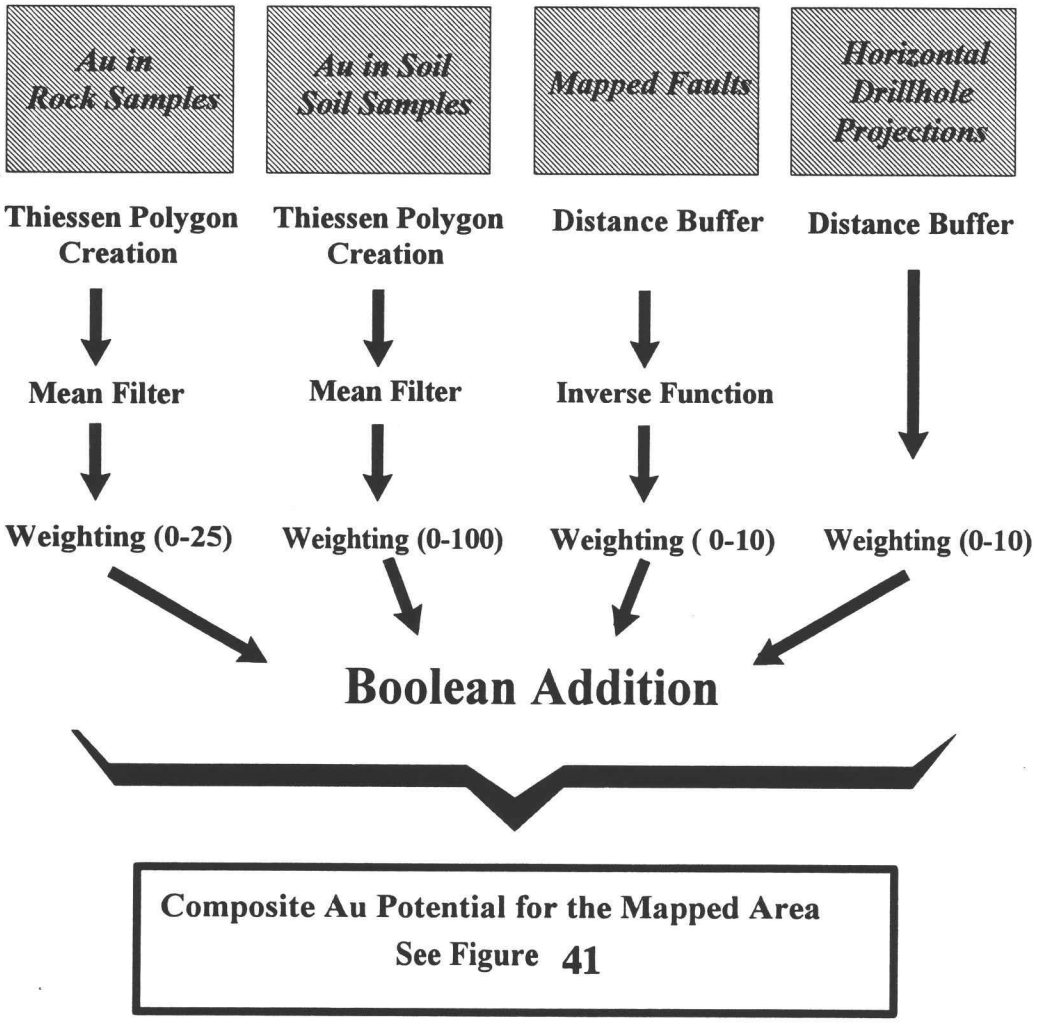

Figure 40. Flow chart for the composite gold potential for the mapped area GIS analysis. Boxes at the top represent raw data in original data units.

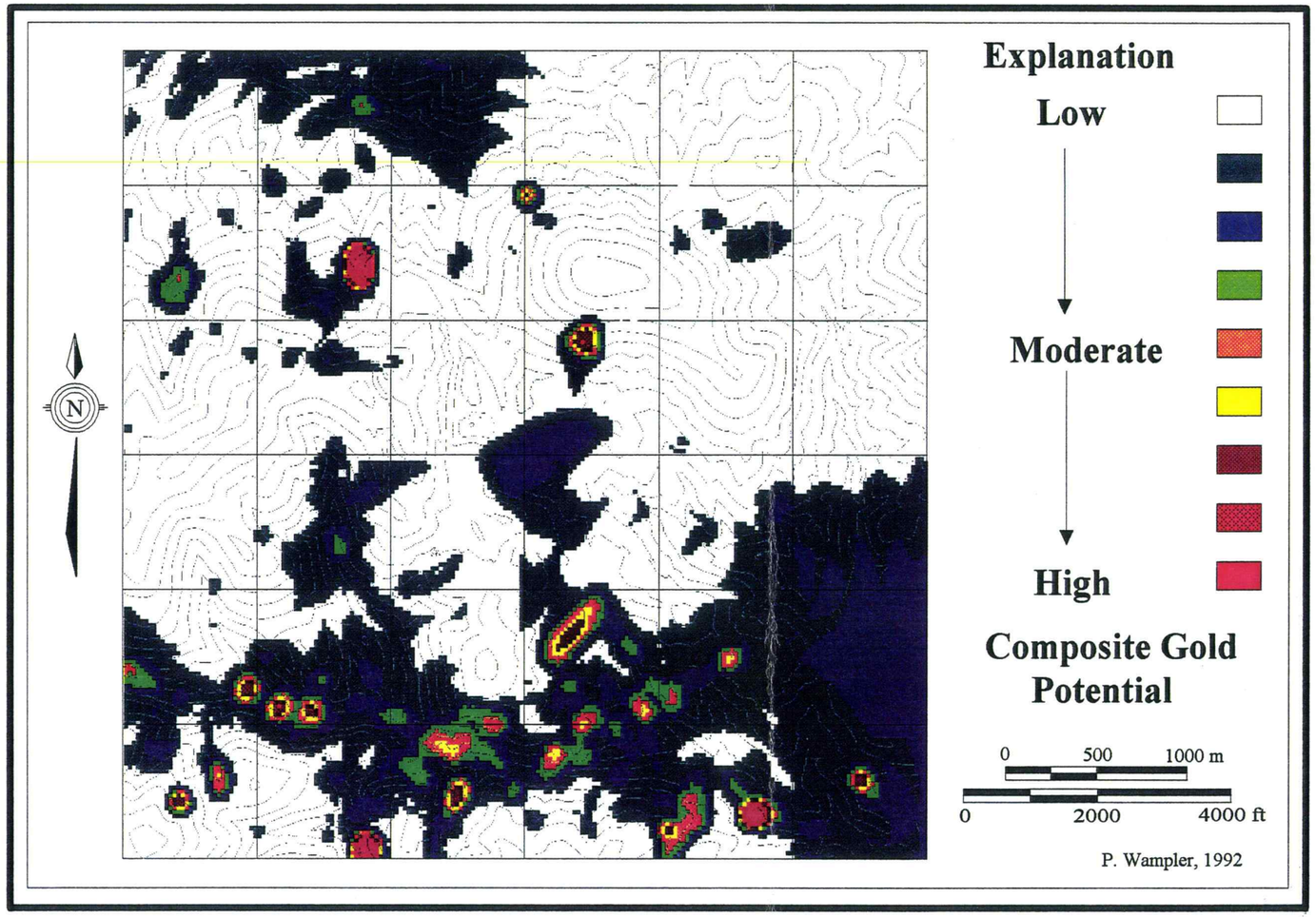

Figure 41. Composite gold potential for the mapped area. See text for description.

analysis results could be enhanced by "fine tuning" the weighting factors, and adding criteria as correlations with gold mineralization are discovered.

Iron-Oxide Anomalies Derived From Landsat Imagery

The data layers used were: resampled Zortman Landsat Band #1; resampled Zortman Landsat Band #3; and roads in the thesis area.

This analysis is based on the assumption that weathered iron-oxide minerals have strong reflectance in thematic band 3, visible red, and weak reflectance in band #1 (Sabins, 1987). Thus a ratio of band 3 to band 1 should highlight iron-oxides. It is also assumed that the observed reflectance in the Landsat 3/1 ratio is enhanced in areas where the surface talus has been disturbed by road building. Road building displaces cobbles and boulders covered with grey or green lichen, causing the oxidized undersides, which are free of lichen, to be exposed.

The main problem with looking for iron-oxides in the Landsat imagery of the Zortman area is that scree-covered areas disturbed by roads all look anomalously iron oxide-stained. The objective of this analysis is to screen out the effect of road disturbance, and delineate those areas which represent significant iron-oxide anomalies.

An image was produced using the DISTANCE module to delineate areas within 100 feet of a road. The image was reclassified using RECLASS so that areas within 100 feet of a road were assigned a value of 0.10. The value of 0.10 was determined by comparing areas of known road disturbance and areas of known iron-

oxide occurrence on the Landsat 3/1 ratio image. The value, 0.10, is an estimate of the amount of the reflectance contributed by road disturbance. This derivative image was then subtracted from the Landsat 3/1 ratio image to produce an image with some of the road disturbance effect removed.

The analysis delineated those areas known to have significant iron-oxide from field observations (see Figure 42). A few areas which showed up as having high reflectance coincide with areas of Paleozoic rocks. This is likely due to their higher overall reflectance. The results of this analysis would serve well in an area which has not been well mapped, but which requires rapid assessment. The areas outlined could be visited first to quickly assess the potential of an area.

Road Placement Accounting for Slope and Proximity to Outcrops

The data layers used were: resampled Zortman Landsat ratio 4/3 (vegetation) and slope in percent.

This analysis assumes that areas with greater slopes will be more difficult and expensive on which to build roads than areas of lesser slope. It also assumes that building roads in areas which have trees will be less expensive, since there is more soil development and usually less scree. Note that depending on the objective of the road building, for example, minimizing environmental impact versus minimizing cost, the presence of vegetation can either be a positive or a negative attribute.

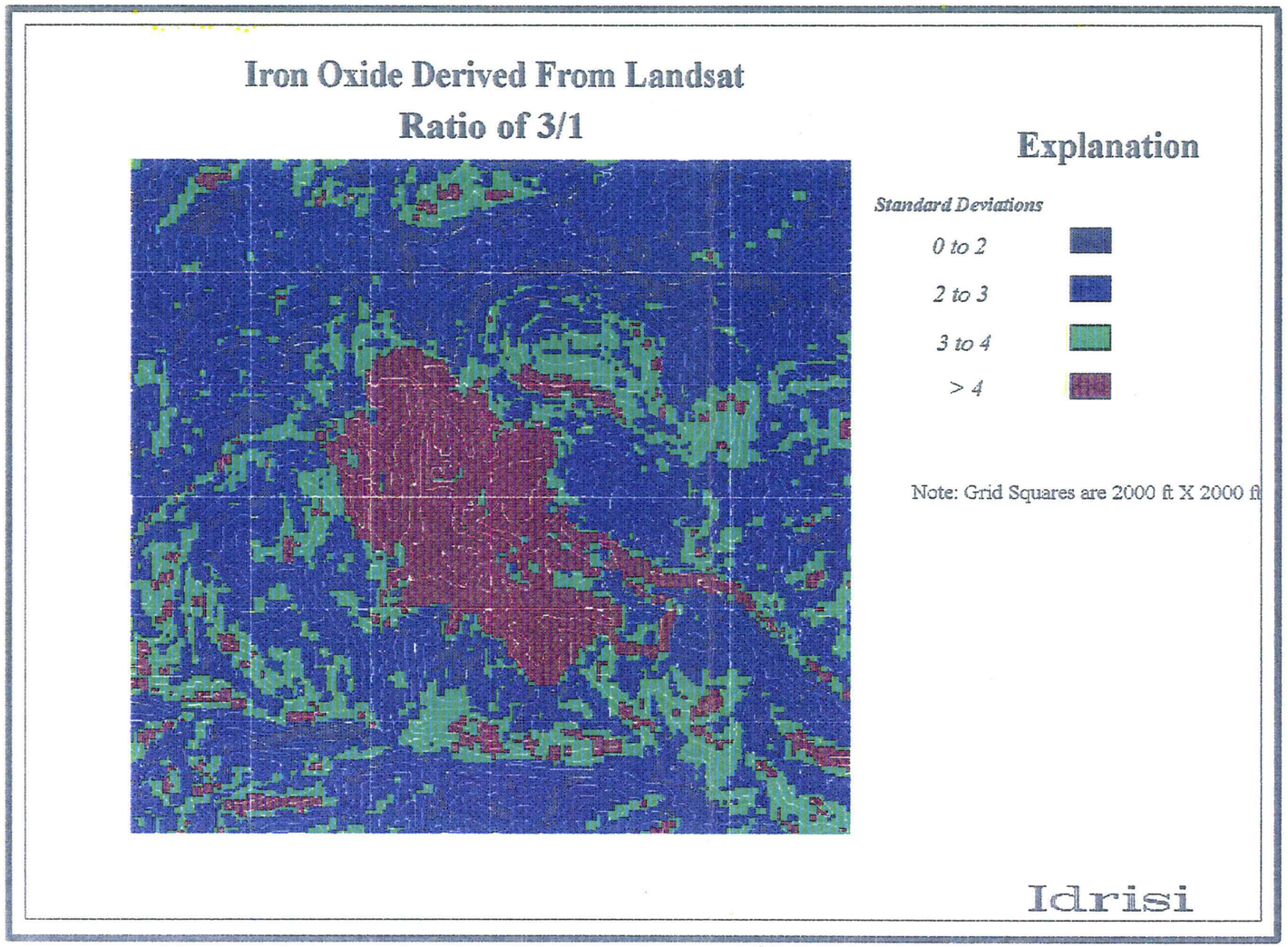

Figure 42. Areas of iron oxide derived from Landsat Thematic Mapper imagery. Red areas are areas with abundant iron-oxides based on the GIS analysis.

The main objective is to create a derivative map which could be used in the planning and placement of drilling roads, either to minimize environmental impact or reduce construction costs.

First a Landsat ratio image was created using the ratio of band 4 to band 3 in order to highlight vegetation (see Figure 43). This ratio was then reclassified to create a binary image of areas with vegetation and those without vegetation. Next, a slope map was created using the IDRISI command SURFACE on the digital elevation model. The slope map was then reclassified into four classes: 1 for slopes 0 to 30 percent; 2 for slopes 30 to 50 percent; 3 for slopes 50 to 80 percent; and 4 for slopes >80 percent. The two layers were then intersected to find areas with vegetation and various slope classes. The resulting map contains eight classes, 1 to 4 being varying slope amounts with no vegetation and 5 to 8 the same slope classes but areas that have vegetation.

The final map clearly shows those areas which should be avoided when planning roads (see Figure 44). It would prove especially useful in communicating with federal and state agencies about the placement of roads and the environmental impact they would cause. This sort of map has potential uses in many departments within a mining operation. Engineers could use it to place new access roads, explorationists could use it to plan drilling roads, and environmental supervisors could use it to communicate to state and federal agencies.

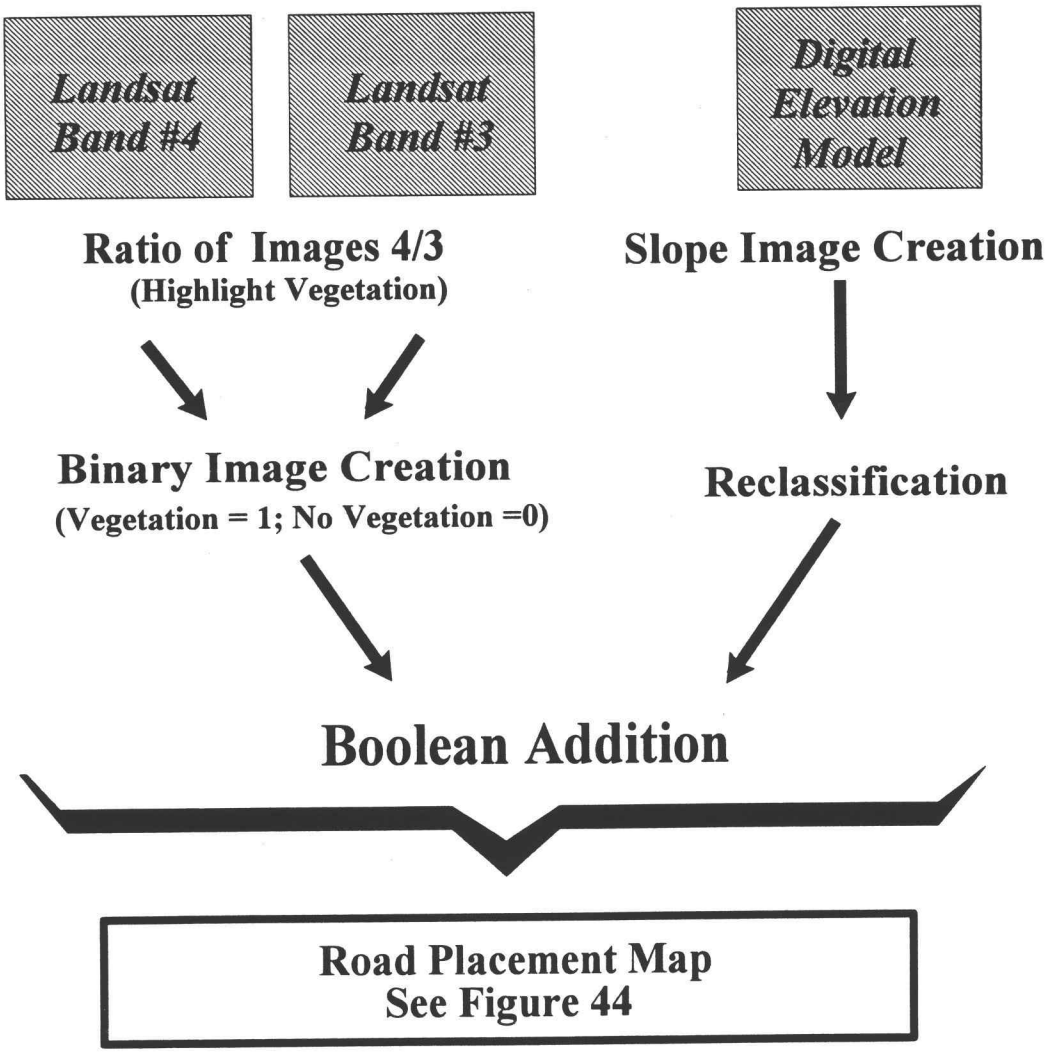

Figure 43. Flow chart for the road placement map GIS analysis. Boxes at the top represent raw data sets in original data units.

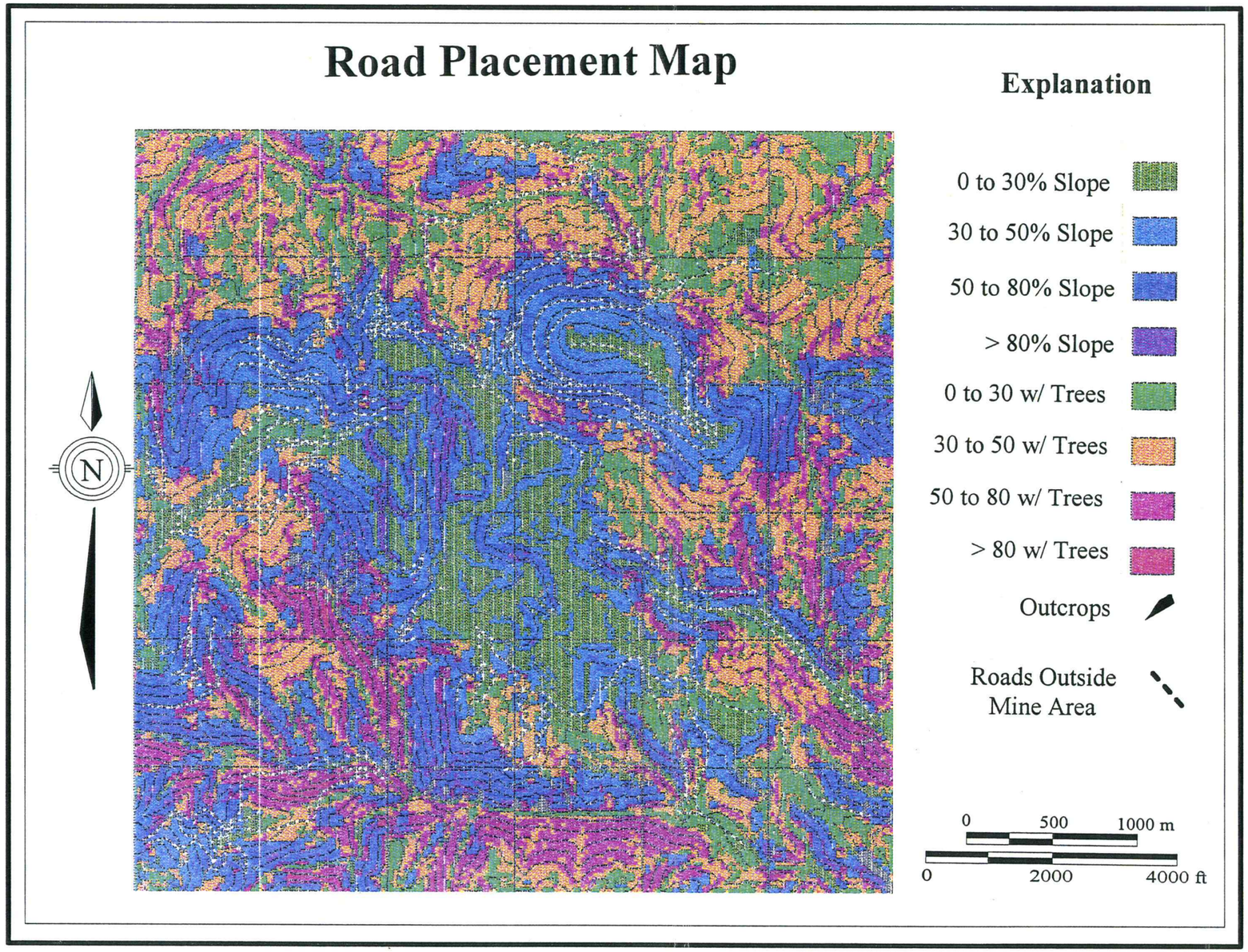

Figure 44. **Road placement map. Green areas represent those areas that are favorable for road building based on the GIS analysis criteria.**

Drill Testing of Gold Soil Anomalies

The data layers used were a raster image of gold in soil samples and distance buffers around drill hole projections.

The basic assumption made by this analysis is that an area 100 feet around a horizontal drill hole projection is adequately tested by a given drill hole. This assumption is probably a good one in areas where mineralization is predominantly controlled by vertical faults, and is not covered by surficial deposits. It is not a good assumption, however, in areas where there is either significant horizontal or low angle control to mineralization, or where surface cover is extensive. Mineralization is predominantly controlled by vertical faulting and surficial cover is minimal surrounding the Zortman Mine area.

The main objective of this analysis is to highlight those areas that have anomalous amounts of gold in soil samples but have not been adequately tested by current exploration drilling.

The gold in the soils Thiessen polygon layer was reclassified into five categories based on the number of standard deviations of each cell within the image (different than the standard deviation of the point data set due to mean filter smoothing). This resulted in an image with values between 1 and 5, with 1 equal to 1 standard deviation and 5 equal to 5 standard deviations. An image representing the horizontal projections of drill holes was then reclassified into a binary image with 1 representing areas within 100 feet of a drill hole projection and 0 representing those

areas greater than 100 feet from a drill hole. The binary image was reclassified so that cells on the drill hole layer with a value of 1 were assigned an arbitrary value of 20. The gold standard deviation image was then added into the reclassified binary drilling image to produce a composite image in which values greater than 20 represented areas with various gold anomalies which were within 100 feet of a drill hole. These values were considered "tested" and assigned a value of 6. The untested areas retained their original values of 1 to 5, since the value of 0 was added from the binary drilling image. The final image then consisted of cells with values between 1 and 6; with 6 representing "tested areas" and 1 through 5 representing areas with "untested" gold anomalies, with values of 5 representing highly anomalous areas which are untested (Figure 45).

Several areas were delineated which have not been adequately tested by current drilling based on the criteria used.

Combined Metals in Soil Samples

The data layers used were the binary images representing areas with >1 standard derivation for each element in soil samples.

It is assumed for this analysis that areas with different combined metals represent some difference in geologic or geochemical environment. The complexity of the interactions of the combined metals makes this analysis subject to bias. For instance, if an area of elevated copper is subjected to a gold- and silver-rich mineralizing event, the result may appear to be a copper, silver, and gold

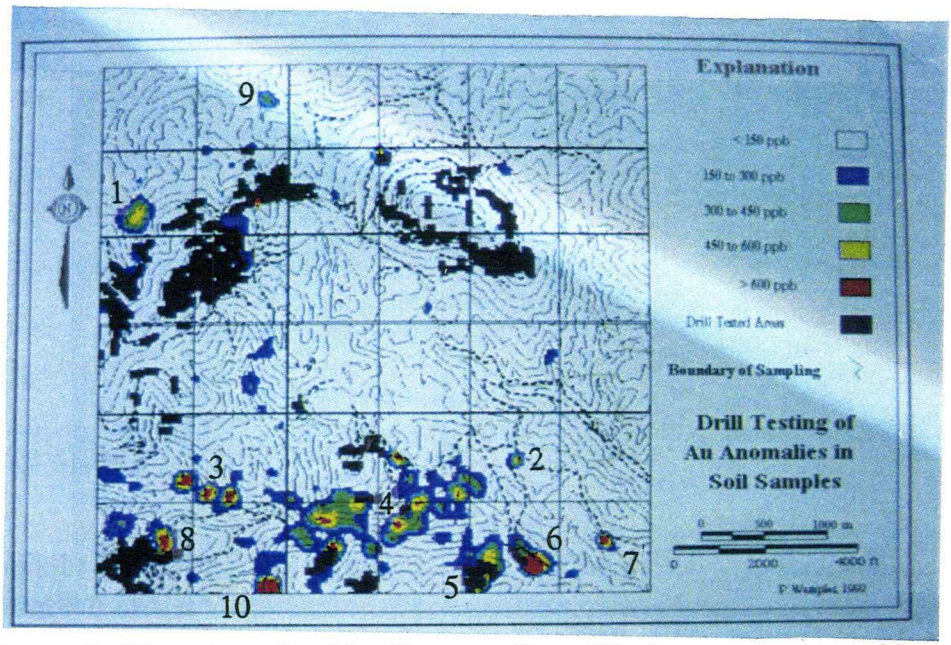

Figure 45. Drill testing of gold soil anomalies. Black areas are considered "tested". Numbers indicate the ten areas defined by this analysis.

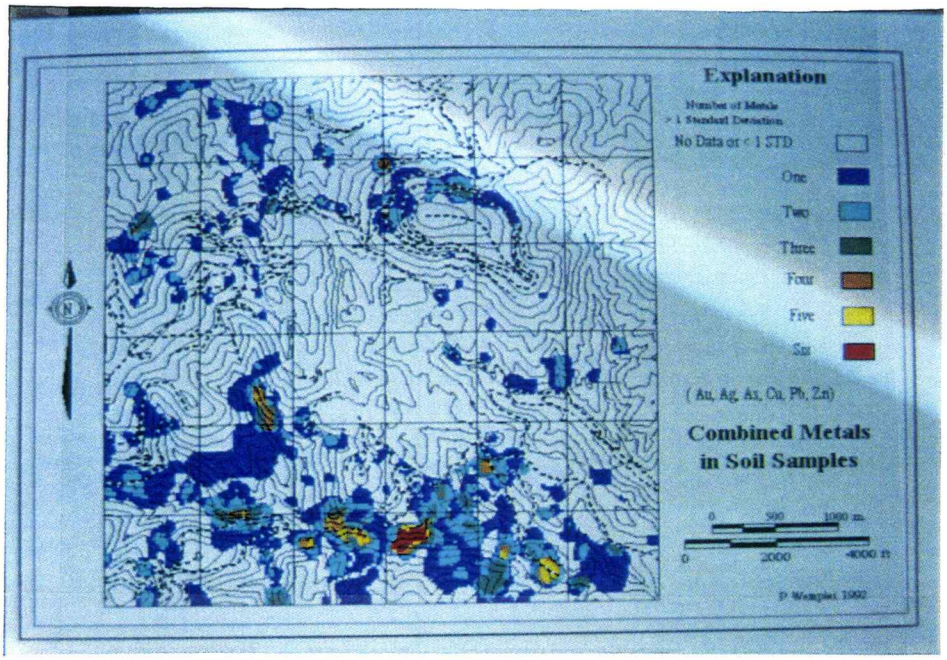

Figure 46. Combined metals in soil samples. Note the red area on the lower portion of the photo (south Carter Butte).

mineralizing event. There is really no way to avoid this dilemma except to consider the local geology before making any conclusions.

The objective of this analysis is to define areas of increasing metallogenic complexity to help in defining areas which have been subjected to different mineralizing events.

The method was simply to add together binary representations of each element analyzed in soil samples, which represent areas with greater than 1 standard deviation of a given element. The result is a very simplified measure of the metallogenic complexity of various areas. A severe limitation to this analysis is that it does not yield any information on specific metal associations. This limitation will be addressed in the analysis which follows.

Only one area, southeast Carter Butte, was anomalous in all six elements (see Figure 46). All but two of the metalogenically complex areas (those with more than four anomalous elements) were located in Alder Gulch. One possible explanation for the large areas of metallogenic complexity near Carter Butte is that this area was the locus of a metalogenically complex mineralizing event, or alternatively, several superimposed events. Another possible explanation is that there is simply a sampling bias in this area. The former is consistent with propylitic alteration in the Alder Gulch area.

(Gold + Zinc + Lead)/Arsenic in Soil Samples

The data layers used were: lead in soil samples; gold in soil samples; zinc in soil samples; and arsenic in soil samples. All values were in ppm.

A basic assumption upon which this analysis is based is that there will be a distinct geochemical signature in soil samples which records the mineralizing event responsible for producing the Zortman deposit.

This analysis was based on the empirical observation, derived from previous analyses that lead, zinc, and gold appear to all occur along a roughly north-northwest-trending zone which seems to coincide with the trace of the Ruby shear zone. Additionally, arsenic was observed to be negatively correlated with the same north-northwest trend. So by dividing gold + lead + zinc by arsenic, it should be possible to highlight the areas affected by this particular geochemical signature.

The method was to add the gold, lead, and zinc values together to produce a summation of these three elements, then divide the result by the arsenic values in soils.

Results from this analysis were very interesting (see Figure 47). The north-northwest trend which coincides with the Ruby shear zone is quite obvious, extending some distance to the southeast of the mine area, far beyond any known mineralization. There is potential for a buried extension of the Ruby shear zone mineralization in this area.

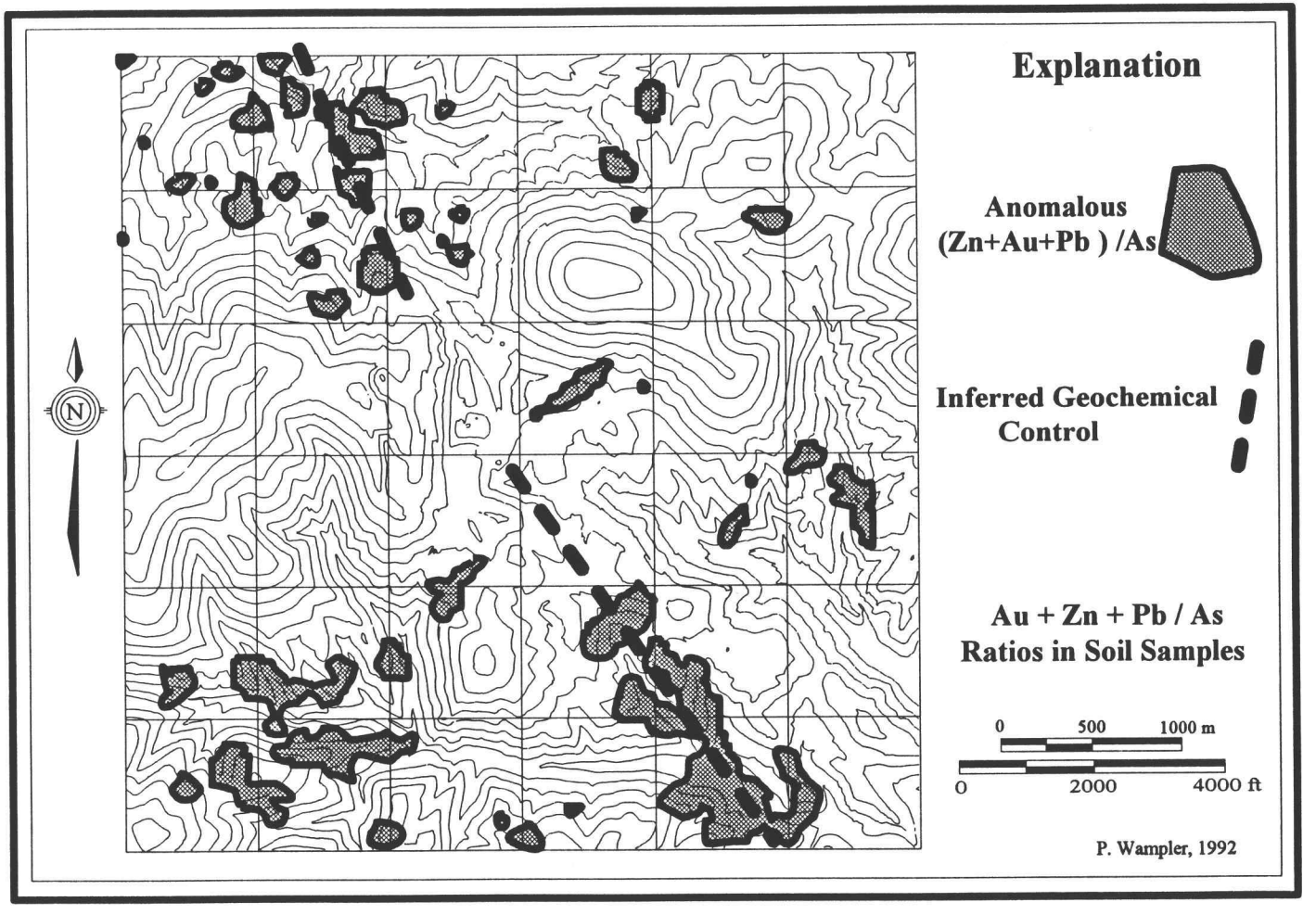

Figure 47. Gold + zinc + lead ratioed with arsenic in soil samples.

Air Photo Lineaments Associated with Gold in Soil Samples

The data layers used were air photo linears and gold in soil samples.

The assumption is made that if gold is consistently associated with a particular air photo lineament, it lends support for designating the lineament an actual fault, or at least a locus of hydrothermal fluids.

The objective of this analysis is to determine which photo lineaments, if any, are likely to represent mineralized structures on the ground.

The DISTANCE module of IDRISI was run on lines representing the air photo lineaments. The distance image was then reclassified into a binary image with a value of 1 for all areas within 100 feet of an air photo lineament. This image was then multiplied by the binary gold greater than 1 standard deviation image to produce a map of only those areas which contained anomalous gold in soil samples and were located within 100 feet of an air photo lineament.

Results were not significantly different than expected (see Figure 48). The east-west lineament in Alder Gulch is spatially associated with abundant gold soil anomalies. Additionally, the north-northwest-trending lineament south of the mine area has good spatial correlation with gold anomalies in soil samples. This sort of analysis would serve well as an early step in the exploration of a new area to generate initial exploration targets.

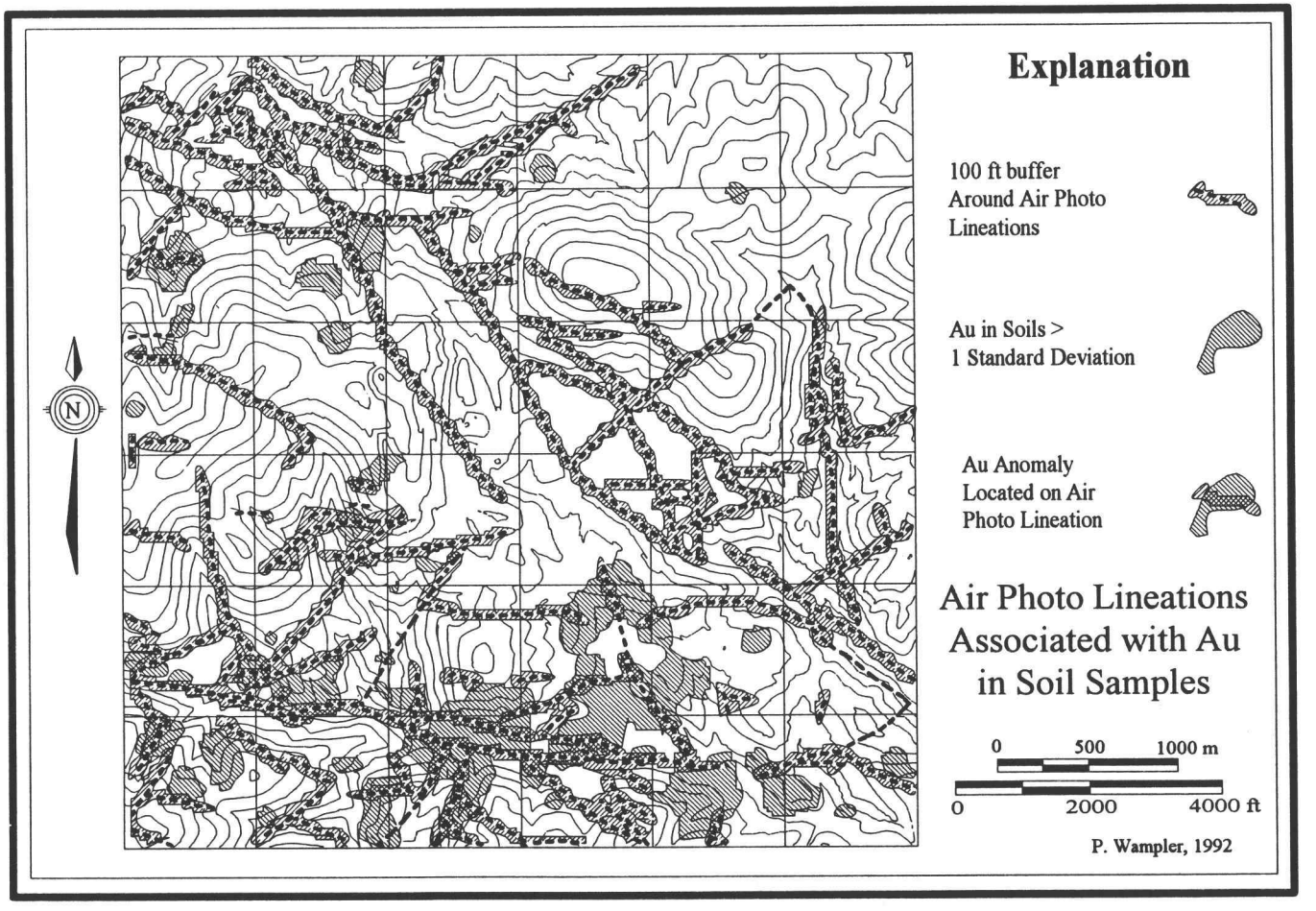

Figure 48. **Air photo lineations which correlate with gold anomalies in soil samples.**

Composite Gold Potential (Soil Grid Area)

The data layers used were: aeromagnetic data; Landsat bands 3 and 1; and gold in soils.

This analysis assumes that aeromagnetic lows are more likely to be associated with Zortman-style gold mineralization than aeromagnetic highs. It also assumes that areas highlighted by a Landsat data ratio of bands 3 and 1 will highlight areas of iron-oxide, and by association, areas with gold mineralization. Lastly, the analysis assumes that gold in soil samples is the most accurate predictor of gold mineralization (weighted 0 to 100), followed by Landsat data (weighted 0 to 40), and finally by aeromagnetic data (weighted 0 to 20).

The primary objective is to delineate areas of high potential for gold mineralization based on the criteria used. The secondary objective is to demonstrate the ability of GIS to predict areas of high gold potential on a regional scale.

The method is similar to that described for the other gold potential analyses. The only data sets available at this scale were the aeromagnetics, Landsat, and soil samples; so the resulting potential map is limited (as all GIS analyses are) by its parent data sets. Since areas of low magnetic signature were desired, it was necessary to create an inverse of the image. The three images were then weighted and added together to produce the final composite map.

The results from this analyses yielded several apparent regional trends (see Figure 49). The large-scale structural trends are well highlighted and the several

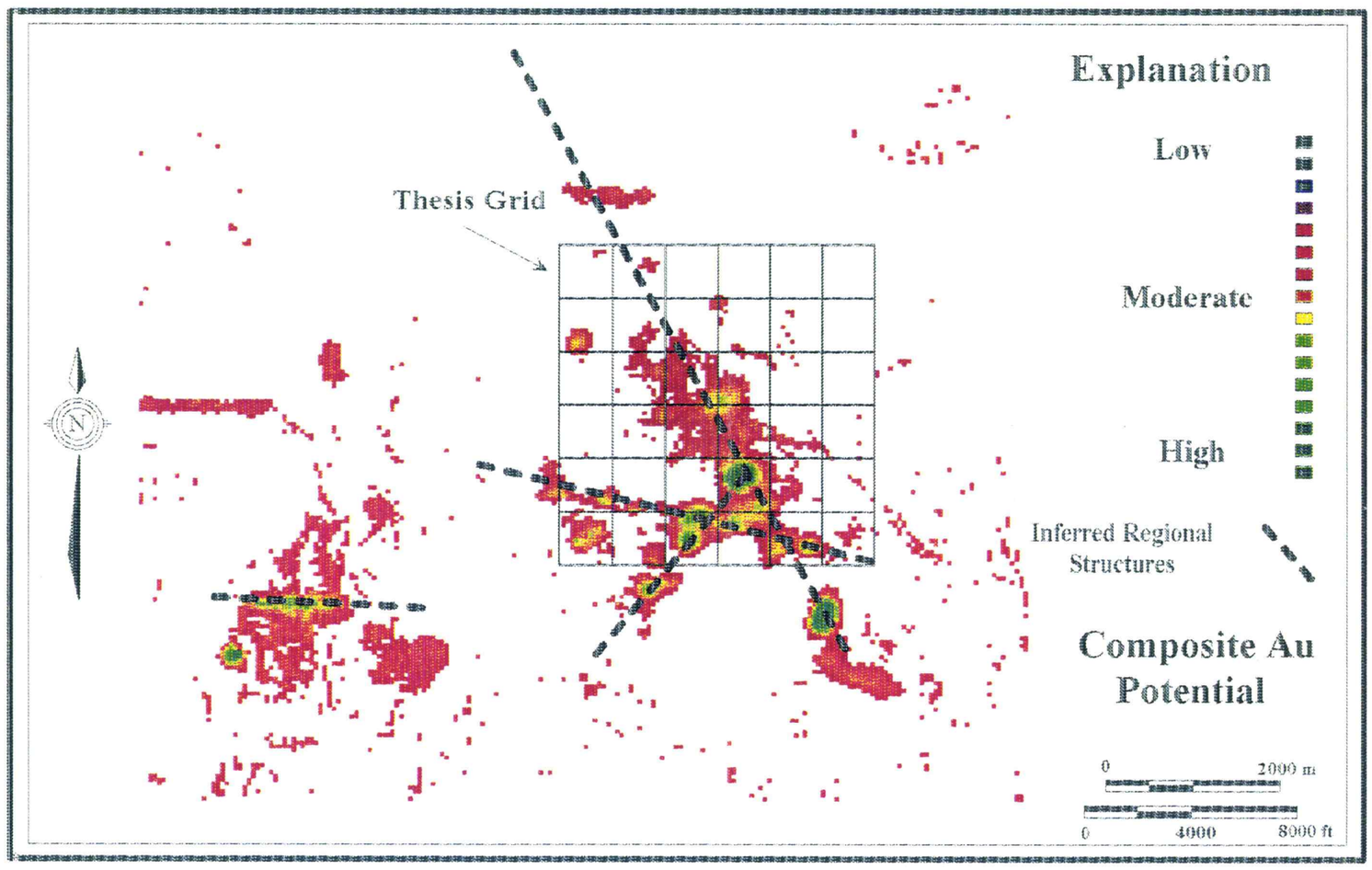

Figure 49. Composite gold potential on a regional scale. Green indicates areas of high potentiatial based on the GIS analysis.

areas of potential along those trends are apparent. Four obvious trends were observed. The north-northwest trend which goes directly through the Zortman deposit appears to continue to the southeast at least another 4,000 to 6,000 feet outside the area mapped for this study, and perhaps a similar distance to the north-northwest, although the north-northwest extension is very weak. The Alder Gulch lineament also showed up as a potential mineralization-controlling structure. The south Carter structure which trends roughly east-northeast extends 2,000 to 4,000 feet beyond the thesis area. The south Carter Butte area is at the intersection of these three structures, which may explain some of the metallogenic complexity observed.

GIS Conclusions and Recommendations

IDRISI was chosen as the geographic information system for this study for several reasons. Below is a summary of the advantages and disadvantages of using IDRISI.

Advantages of IDRISI

1) It can handle both raster and vector data.
2) It is an effective remote sensing tool, and manipulates Landsat images well.
3) The raster data model is simple and intuitive to use.
4) The software is very inexpensive.

5) The low cost and ease of use make it an easy first step into GIS technology.

6) Output is quick, versatile, and easily exchanged with other graphics programs.

7) Data can be imported and exported in several standard formats.

Disadvantages of IDRISI

1) Database functions are not directly linked to graphic objects.

2) Some vector functions are not possible or are very difficult using IDRISI.

3) Large outputs, greater than 11 X 17 inches, are difficult and expensive.

4) Topology is not rigorously defined as in other vector-based GIS programs.

Other programs considered for this study included ARCINFO, marketed by ESRI, and SPANS, a software package marketed by Tydac Inc. (Tydac). SPANS was the author's first choice of a GIS. It has the advantage of being able to deal with both raster and vector data, and is unique in its application of the quadtree data structure for raster data encoding. SPANS was eventually rejected after several weeks of working with it due to bugs in the programming. The author considers SPANS a capable piece of software; however, Tydac needs to spend more time beta-

testing the program. It is possible that some of the bugs would not be encountered if the OS/2 rather than the DOS version of the program were used. ARCINFO has the advantage of being one of the first GIS programs to be marketed, and thus has a very large installed user base. ARCINFO was rejected mainly due to its lack of support for raster data in the DOS version of the program, as well as the difficulty of use, and inadequate output options.

GIS and Exploration Geology

At this time most GIS programs are too complex and expensive to be feasible for a small mining company such as Zortman Mining Inc. There are, however, cheap and quite adequate programs such as IDRISI which can fulfill many of the needs of a property-scale exploration program. IDRISI costs roughly $300 and is capable of working with both vector- and raster-based files. It is also capable of importing and exporting several standard GIS formats as well as AutoCAD drawings. IDRISI is particularly useful in the integration of Landsat imagery. Since Landsat MSS three band imagery is now available at very little cost, this would be an inexpensive, and potentially quite useful, first step in a new exploration program. IDRISI is sold through: The IDRISI Project, Clark University, Graduate School of Geography, 950 Main Street, Worcester, Massachusetts 01610.

Output Options

A brief note on output options seems appropriate in that it often occupies a significant portion of the time in GIS analysis. This author found the least expensive and perhaps the most useful means of output to be slide photographs taken directly off the computer monitor. It does not require a significant investment of money as the alternative, a color printer, and it is much faster. It has the additional advantage of being an efficient way of communicating geologic information to a group. It would be especially useful in planning meetings in which slides could be projected onto a "dry erase board" and annotated and discussed directly. Care must be taken in choosing exposure times for photographing the screen. An exposure time too short ($< 1/30$ second) will result in bands across the image; exposure times too long will result in images too bright and fuzzy (> 1 second). Images were also exported and manipulated in other software packages. Images were exported as TIFF images and edited in Picture Publisher, an image editing program. Final image preparation was completed in Micrografx Designer 3.1. Black and white printouts were done on a Hewlett Packard Laserjet IIIP. Color plots were done on either a Hewlett Packard Paintjet or a Hewlett Packard Paintjet XL-300. The Hewlett Packard Paintjet XL-300 produced the most appealing output.

GIS Organizational Strategy

Perhaps the best organizational strategy for GIS in mineral exploration is one in which a central GIS department staffed by one or two GIS technicians, preferably with geological training, and a geologist supervisor provide technical support to site-based, inexpensive, GIS programs such as IDRISI. The central GIS department could send technicians to sites in order to assist personnel in creating and maintaining local geographic databases. A more powerful GIS such as SPANS or ARCCAD (New version of ArcINFO), running on a large computer could be maintained by the central GIS office and provide technical support for regional exploration programs and acquire data for use in regional exploration strategies.

Conclusions

It is essential that the end user be familiar with the area being analyzed by the GIS in order to make valid assumptions about the data. The geologist, environmental supervisor, or engineer must be able to manipulate and analyze the data themselves on a system which is not complex or expensive. Expecting geologists to learn all the information necessary to build a GIS just so they can use it as a tool is a bit like expecting a them to be able to build a Brunton compass. Instruction in the use of a Brunton compass is essential geological training, however it would be a waste to train geologists in their construction. In a similar manner it is essential that geologists obtain training in the use of GIS, however, this author does

not believe it is essential that most exploration geologists be able to build one. It is more important that they devote their time to understanding the geological data rather than the data structures of a GIS.

The use of IDRISI allowed rapid integration of the data sets, and the ability to modify analyses based on the results obtained. It is clear from this study that creating gold potential maps from numerous data sets is much easier using a GIS than conventional, non-computerized techniques. Several areas of high potential were delineated through the use of the GIS. Most of these areas were described in a separate report provided to Zortman Mining Inc. (Wampler, 1992).

Future work using a GIS on the Zortman deposit should focus on: 1) drill testing the anomalies already delineated; 2) collecting and compiling Na_2O/K_2O ratio data to be used as a means of delineating alteration; 3) combining more rigorous statistical techniques with the GIS analyses to produce more refined potential maps; and 4) compilation of a thin section alteration database to track the alteration types identifiable only in thin section.

REFERENCES

Bailey, R. L., 1974, Geology and ore deposits of the Alder Gulch area, Little Rocky Mountains, Montana: Unpub. M.Sc. thesis, Montana State Univ., 81 p.

Bonham-Carter, G. F., Agterberg, F. P., and Wright, D. F., 1988, Integration of geological data sets for gold exploration in Nova Scotia: Photogrammetric Engineering and Remote Sensing, v. 54, p. 1585-1592.

Brasher, G.K., Coolbaugh, M.R., and Disbrow, A.E., 1983, Reconnaissance geologic mapping and sampling for Zortman-Landusky Mining Company, Little Rocky Mountains, Montana: Unpublished consulting report, 16 p. (plus sample appendix and four plates).

Bryant, D. G., and Metz, H.E., 1966, Geology and ore deposits of the Warren Mining district, in S.T. Titley and C.L. Hicks eds., Geology of the Porphyry Copper Deposits, Southwestern North America, University of Arizona Press, Tuscon, p. 189-203.

Buchanan, L. J., The las Torres mine, Guanajuato, Mexico, ore controls of a fossil geothermal system: Unpublished Doctoral thesis, Colorado School of Mines, Golden, Colorado, 138 p.

Busenberg, E., and Clemency, C. V., 1976, The dissolution kinetics of feldspars at 25°C and 1 atm CO_2 partial pressure: Geochemica et Cosmochima Acta, v. 40, p. 41-49.

Carten, R. B., 1986, Sodium calcium metasomatism: chemical, temporal, and spatial relationships at Yerington, Nevada, porphyry copper deposit: Economic Geology, v. 81, p. 1495-1519.

Coolbaugh, M.R., and Disbrow, A.E., 1984, Geology of Antoine Butte for Zortman Mining Inc., Little Rocky Mountains, Montana: Unpublished company report.

Deer, W. A., Howie, R. A., and Zussman, J., 1963, Rock Forming Minerals - Volume 4 Framework Silicates: Longmans, Green and Co. Ltd., London, p. 36-45.

Dyson, J. L., 1938, Ruby Gulch gold mining district, Little Rocky Mountains, Montana: Economic Geology, v. 34, p. 201-213.

Emmons, W. H., 1908, Gold deposits of the Little Rocky Mountains, Montana: U.S. Geol. Survey Bull. 340, p. 96-116.

Enders, M. S., and Rogers, L. M., 1983, Design of the geologic program at the Zortman and Landusky mines, Little Rocky Mountains, Montana: Soc. Mining Engineers AIME, Preprint 83-373, 9 p.

Gabelman, J. L., 1990, Shell Butte geologic map: unpublished company map, 1:2400-scale, Zortman Mining Inc., Zortman, Montana.

Hastings, J. S., 1988, Gold deposits of the Little Rocky Mountains, Montana, in Schafer, R. W., Cooper, J. J., Vikre, P. G., eds, Bulk mineable precious metal deposits of the Western United States, Symposium Proceedings: Geol. Soc. Nevada, Reno, p. 187-205.

Heald, P., Foley, N. K., and Hayba D. O., 1987, Comparative anatomy of volcanic-hosted epithermal deposits: acid-sulfate and adularia-sericite types: Economic Geology, v. 82, p. 1-26.

Jacob, J. P., 1988, 1988 Exploration Drilling, Zortman Mining Inc.: Unpublished company report, Zortman Mining Inc, Zortman, Montana, 13 p.

Jensen, M. L., Ashley, R. P., and Albers, J. P., 1971, Primary and secondary sulfates at Goldfield, Nevada, Economic Geology, v. 72, p. 618-626.

Keller, W. D., 1957, Principals of chemical weathering: Lucas Brothers Publishing, Columbia, Missouri, 111 p.

Kents, P., 1964, Special breccias associated with hydrothermal developments in the Andes: Economic Geology, v. 59, p. 1551-1563.

Knechtel, M. M., 1959, Stratigraphy of the Little Rocky Mountains and encircling foothills, Montana: U.S. Geol. Survey Bull. 1072-N, p. 723-749.

Larsen, E. S., 1940, Petrographic province of central Montana: Geol. Society of America Bull., v. 51, p. 888-948.

MacKevett, E. M. Jr, and Radtke, A. S., 1966, Hydrothermal alteration near the Kennecott copper mines, Wrangell mountains area, Alaska -- a preliminary report: U.S. Geol. Survey Professional Paper 550-B, p. B165-B168.

Marvin, R. F., Hearn, B. C., Mehnert, H. H., Naeser, C. W., Zartman, R. E., and Lindsey, D. A., 1980, Late Cretaceous-Paleocene igneous activity in north-central Montana: Isochron/West, no. 29, p. 5-25.

O'Niell, J. M., and Lopez, D. A., 1985, Character and significance of the Great Falls tectonic zone, east-central Idaho and west-central Montana: American Association of Petroleum Geologists Bulletin, v. 69, p. 437-447.

Pegasus Gold Corporation, 1993, 1992 annual report, Pegasus Gold Corporation, 54 p.

Ramsay, J. G., and Huber, M. I. 1987, The techniques of modern structural geology, volume 2 folds and fractures: Academic Press Limited, San Diego, 462 p.

Reed, M. R., Spycher N. F., 1985, Boiling cooling and oxidation in epithermal deposits: a numerical modelling approach in Berger, B. R. and Bethke, P. M. eds., Geology and Geochemistry of Epithermal Systems: Society of Economic Geologists, Reviews in Economic Geology v 2., p. 249-270.

Reed, M. R., Spycher N. F., 1989, SOLTHERM: database of equilibrium constants for aqueous-mineral-gas equilibria: Department of Geological Science, University of Oregon, Eugene, Oregon, 25 p.

Reynolds, T. J., 1991, Reconnaissance fluid inclusion survey of samples from Zortman-Landusky area, Montana: Unpublished company report, Zortman Mining Inc., Zortman, Montana, 8 p.

Richardson, G. L., 1973, Geology and ore deposits of the Landusky mining district, Phillips County, Montana: M.Sc. thesis, Univ. Arizona, 64 p.

Russell, C. W., 1984, Geology of the central portion of the Little Rocky Mountains, Phillips County, Montana: Unpub. M.Sc. thesis, Univ. Idaho, 92 p.

Russell, C. W., 1989b, Geologic map of eastern Antoine Butte, 1:4800-scale: Unpublished company report, Zortman Mining Inc., Zortman, Montana.

Russell, C. W., 1989c, Geologic cross section for a portion of Antoine Butte: Unpublished company report, Zortman Mining Inc., Zortman, Montana.

Russell, C. W., 1991, Gold mineralization in the Little Rocky Mountains Phillips County, Montana in Montana Bureau of mines Special Publication No. 100, Guidebook 1991 - Central Montana Alkalic Province, p. 1-18.

Sabins, F. F. Jr., 1986, Remote Sensing - Principles and Interpretation 2nd Edition: New York, W. H. Freeman and Company, 449 p.

Sander, M. V., and Einaudi, M. T., 1990, Epithermal deposition of gold during transition from propylitic to potassic alteration at Round Mountain, Nevada: Economic Geology, v. 85, p. 285-311.

Scott, K. M., 1990, Origin of alunite- and jarosite-group minerals in the Mt. Leyson epithermal gold deposit, northeast Queensland, Australia: American Mineralogist, v. 75, p. 1176-1181.

Stoffregen, R.,1986, Observations on the behavior of gold during supergene oxidation at Summitville, Colorado, U.S.A., and implications for electrum stability in the weathering environment: Applied Geochemistry, v. 1, p. 549-558.

Wampler, P. J., 1990, Geology on Antoine Butte: Unpublished company report, Zortman Mining Inc., Zortman, Montana, 7 p.

Wampler, P. J., 1992, Geographic information system analysis of the area surrounding the Zortman Mine: Unpublished company report, Zortman Mining Inc., Zortman, Montana, 20 p.

Watson, G. P., Rencz, A. N., Bonham-Carter, G. F., 1989, Computers assist prospecting: Geologic Survey of Canada, Mineral Resource Division, GEOS (Ottowa), v. 18, p. 8-15.

Weed, W. H., and Pirsson, L. V., 1896, The geology of the Little Rocky Mountains: Journal of Geology, v. 4, p. 399-428.

Wilson, M. R., 1987, Petrogenesis of fluids associated with unconformity-type Uranium deposits in Saskatchewan, and the Zortman-Landusky Au-Ag deposits in Montana: Unpub. Ph.D., University of Saskatchewan, Saskatoon, Saskatchewan, 158 p.

Wilson, M. R., and Kyser, T. K., 1988, Geochemistry of porphyry-hosted Au-Ag deposits in the Little Rocky Mountains, Montana: Economic Geology, v. 83, p. 1329-1346.

Wolery, T. J., and Jackson, K. J., Bourcier, W. L., Bruton, C. J., Viani, B. E., Knauss, K. G., Delany, J. M., 1990, Current status of the EQ3/6 software package for geochemical modeling, in Chemical modeling of aqueous systems II, p. 104-116.

APPENDICES

Appendix A. Major element analyses of rock samples[1].

Sample No.	PW007	PW018	PW024	PW040	PW043	PW077	PW123	PW144	PW173A	PW182	PW186C	PW186D	PW802	PW803	PW804
Easting	15352	13903	12762	14622	13912	9538	7441	5382	4861	5693	10413	10413	9399	9379	9360
Northing	7634	9234	9884	11085	13305	14823	13587	14594	12835	12329	8580	8580	10202	10206	10210
Elevation (ft)	4300	4550	4800	4600	5100	4600	4700	4820	4900	5380	4900	4900	4900	4900	4900
Description[2]	Tio	Tiof	Tib	Tid(2)	Tiss	Tisb	Tia	Tid(1)	Tid(3)	Tibq	Pc Gneiss	Pc basalt	O.K. Pit[3]	O.K. Pit	O.K. Pit
Alteration	unaltered[4]	unaltered	unaltered[5]	unaltered	unaltered	unaltered	unaltered	unaltered	AO altered[6]	AO altered	unaltered	unaltered	K-altered[7]	K-altered	K-altered
SiO_2	66.26	64.49	66.55	67.45	66.95	68.87	68.91	61.34	68.94	68.61	47.36	62.02	67.63	68.20	67.37
Al_2O_3	17.72	18.00	17.58	17.60	17.98	17.72	17.32	19.67	15.59	17.34	11.95	10.76	15.35	14.94	15.96
Fe_2O_3[8]	1.10	3.02	2.17	1.40	1.87	1.27	0.82	1.90	1.00	0.82	15.56	8.85	0.81	1.18	0.73
MgO	0.04	0.08	0.44	0.18	0.08	0.02	0.12	0.17	<0.01	0.17	9.17	6.51	0.03	0.00	0.03
CaO	0.89	1.94	2.37	1.19	1.61	0.79	0.01	0.77	0.01	0.01	9.82	6.41	0.11	0.05	0.05
Na_2O	6.11	5.12	4.39	5.25	5.05	5.78	4.99	7.22	1.40	1.63	2.61	3.53	0.92	1.14	1.38
K_2O	4.83	5.34	3.59	3.95	4.21	4.99	5.71	6.54	10.78	10.77	0.82	0.56	12.25	11.52	11.82
TiO_2	0.09	0.29	0.21	0.13	0.17	0.11	0.14	0.20	0.13	0.13	1.18	0.58	0.15	0.15	0.16
P_2O_5	0.05	0.08	0.10	0.11	0.09	0.07	0.05	0.08	0.05	0.01	0.06	0.03	0.06	0.07	0.08
MnO	0.04	0.10	0.07	0.03	0.07	0.04	<0.01	0.06	0.03	<0.01	0.32	0.20	0.00	0.00	0.00
LOI	0.83	1.98	3.28	2.19	1.62	1.33	0.83	1.39	0.84	1.04	1.88	1.35	1.45	0.98	1.10
TOTAL	97.96	100.44	100.77	99.48	99.70	100.99	98.89	99.34	98.56	100.52	100.73	100.80	98.76	98.23	98.68

[1] Analyses were performed by Bondar-Clegg Ltd., Vancouver, B.C., Canada, using the DC plasma emmision method.
[2] See text for lithologic abbreviations
[3] O.K. Pit samples are located on Figure 10.
[4] The term "unaltered" is used to describe the least altered example of a given porphyry
[5] Weak sericite + pyrite alteration
[6] Adularia overgrowth alteration
[7] Pervasive adularia alteration
[8] All iron reported as Fe_2O_3

Appendix A. Major element analyses of rock samples (continued).

Sample No.	PW805	PW806	PW807	PW808	PW809	PW811	PW814	PW816	PW817	PW818	PW821	PW822	PW823	PW824	PW825	PW826
Easting	9350	9340	9331	9321	9311	9290	9183	9164	9306	9510	9350	9296	9207	9204	9200	9198
Northing	10212	10213	10214	10214	10214	10215	10197	10192	10212	10161	10212	10213	10204	10203	10201	10202
Elevation (ft)	4900	4900	4900	4900	4900	4900	4900	4900	4900	4900	4900	4900	4900	4900	4900	4900
Description[1]	O.K. Pit[2]	O.K. Pit	O.K. Pit	O.K. Pit	O.K. Pit	O.K. Pit	O.K. Pit	O.K. Pit	O.K. Pit	O.K. Pit	O.K. Pit	O.K. Pit	O.K. Pit	O.K. Pit	O.K. Pit	O.K. Pit
Alteration	K-altered[3]	K-altered	K-altered	K-altered	K-altered	K-altered	K-altered	K-altered	K-altered	K-altered	K-altered	K-altered	K-altered	K-altered	K-altered	K-altered
SiO_2	69.99	68.06	68.07	67.91	69.75	65.80	64.78	67.16	66.61	57.41	69.82	67.67	69.87	66.78	63.97	66.98
Al_2O_3	15.64	15.86	15.18	15.87	14.97	15.43	17.88	18.05	15.22	19.73	13.02	13.18	14.86	12.60	11.36	15.58
Fe_2O_3[4]	0.83	0.91	1.09	0.78	1.18	2.33	1.07	0.69	1.52	4.03	1.60	2.40	0.76	4.48	9.21	1.51
MgO	0.05	0.01	0.00	0.02	0.00	0.19	0.10	0.10	0.01	0.02	0.00	0.00	0.12	0.36	0.20	0.05
CaO	0.03	0.03	0.00	0.03	0.03	0.02	0.06	0.05	0.02	0.07	0.05	0.02	0.00	0.09	0.06	0.02
Na_2O	1.13	1.30	0.98	1.13	1.03	0.20	0.35	0.40	0.90	0.13	0.98	0.59	0.19	0.15	0.15	0.36
K_2O	11.46	12.20	12.10	12.34	12.05	12.45	10.37	9.38	12.38	12.79	10.98	11.39	10.37	9.21	9.16	11.97
TiO_2	0.19	0.15	0.14	0.14	0.14	0.65	0.18	0.19	0.14	0.33	0.14	0.15	0.17	0.40	0.88	0.17
P_2O_5	0.08	0.03	0.06	0.07	0.03	0.05	0.06	0.07	0.02	< .03	0.01	0.04	0.07	0.02	0.09	0.09
MnO	0.00	0.00	0.00	0.00	0.00	0.00	0.00	0.00	0.00	< .01	0.00	0.00	0.00	0.00	0.00	0.00
LOI	1.23	1.09	1.19	1.07	1.23	2.41	3.75	3.32	1.41	5.45	1.83	2.61	2.01	4.79	3.07	1.37
TOTAL	100.63	99.64	98.81	99.36	100.41	99.53	98.60	99.41	98.23	100.05	98.43	98.05	98.42	98.88	98.15	98.10

[1] See text for lithologic abbreviations
[2] O.K. Pit samples are located on Figure 10.
[3] Pervasive adularia alteration
[4] All iron reported as Fe_2O_3

Appendix A. Major element analyses of rock samples (continued).

Sample No.	PW829	PW828	PW830	PW827
Easting	9008	9044	9112	9136
Northing	10138	10156	10176	10183
Elevation (ft)	4900	4900	4900	4900
Description[1]	O.K. Pit[2]	O.K. Pit	O.K. Pit	O.K. Pit
Alteration	K-altered[3]	K-altered	K-altered	K-altered
SiO_2	69.64	67.74	65.85	67.49
Al_2O_3	16.82	17	17.92	15.47
Fe_2O_3[4]	0.9	0.65	0.87	0.95
MgO	0.06	0.05	0.05	0.04
CaO	0.16	0.05	0.03	0.01
Na_2O	4.47	0.38	0.32	0.77
K_2O	6.75	12.06	11.01	11.37
TiO_2	0.17	0.17	0.19	0.16
P_2O_5	0.04	0.06	<0.03	0.07
MnO	<0.01	<0.01	<0.01	0.00
LOI	0.8	1.37	2.39	1.27
TOTAL	99.92	99.71	98.83	97.60

[1] See text for lithologic abbreviations
[2] O.K. Pit samples are located on Figure 10.
[3] Pervasive adularia alteration
[4] All iron reported as Fe_2O_3

Appendix B. Sample locations.

Sample No.	Easting	Northing	Outcrop No.	Sample Type	Field Designation	Date Taken
PW001	16044	6516	OC001	Outcrop	PCa	6/21/91
PW002	15790	6814	OC001	Outcrop	Scraggy	6/22/91
PW003	15436	7074	OC002	Outcrop	Calcite Vein	6/22/91
PW004	15825	7412	OC003	Outcrop	Scraggy	6/22/91
PW005	15821	7680		Subcrop	Emerson	6/22/91
PW006	15826	7752	OC004	Outcrop	Scraggy	6/22/91
PW007	15352	7634	OC006	Outcrop	Scraggy	6/23/91
PW008	15942	8384	OC009	Outcrop	Scraggy	6/23/91
PW009	16284	9068	OC010	Float	Dike/Tiof?	6/23/91
PW010	14606	8447	OC014	Subcrop	Dike	7/4/91
PW011	14450	9154		Subcrop	Beaver?????	7/4/91
PW012	14014	9490	OC017	Subcrop	Shell Butte	7/4/91
PW013	13838	10012		Float	Shell Butte	7/4/91
PW014	14047	8609	OC018	Outcrop	Fine Scraggy	7/4/91
PW015	14106	8417	OC019	Outcrop	PCi?	7/4/91
PW016	14240	8855	OC021	Outcrop	Fine Scraggy	7/5/91
PW017	13890	9176	OC022	Outcrop	Dike	7/5/91
PW018	13903	9234	OC022	Outcrop	Fine Scraggy??	7/5/91
PW019	12961	10506		Subcrop	Shell Butte	7/5/91
PW020	13120	9046		Adit	Tertiary?? Tia?	7/5/91
PW021	13036	8724	OC027	Outcrop	Tertiary?? Tia?	7/5/91
PW022	13079	8687	OC027	Outcrop	Tia/Altered??	7/5/91
PW023A	13040	9233	OC026	Outcrop	Precambrian Intrusive	7/5/91
PW023B	12963	9014	OC029	Outcrop	Tertiary?? Tia?	7/5/91
PW024	12762	9884	OC031	Outcrop	Beaver/Tid	7/5/91
PW025	12089	9719		Subcrop	Beaver/Tid????	7/5/91
PW026	11365	10422	OC035	Prospect	PC/Sil. Vein	7/5/91
PW027	12770	8757		Outcrop	Tia????	7/10/91
PW028	14836	9143	OC041	Outcrop	Beaver/Tid????	7/10/91
PW029	14917	9316	OC042	Outcrop	Contact Zone	7/10/91
PW030	14628	11749	OC046	Outcrop	Son of Scraggy	7/12/91
PW031	14640	11740	OC046	Outcrop	Contact Zone	7/12/91
PW032	14590	11410	OC048	Outcrop	Son of Scraggy	7/12/91
PW033	14493	9537	OC049	Outcrop	Precambrian	7/23/91
PW034	14786	9434	OC050	Outcrop	Beaver Porphyry?	7/23/91
PW035	14902	9645	OC051	Outcrop	Dike/Contact	7/23/91
PW036	14904	9648	OC051	Outcrop	Breccia	7/23/91
PW037	14900	9647	OC051	Outcrop	Beaver Porphyry	7/23/91
PW038	14907	9648	OC051	Outcrop	Beaver Porphyry	7/23/91
PW039	14710	10576	OC052	Outcrop	Beaver Porphyry	7/24/91
PW040	14622	11085	OC053	Outcrop	Beaver(?) Porphyry	7/24/91
PW041	14620	11083	OC053	Outcrop	Breccia	7/24/91

Appendix B. Sample locations (continued).

Sample No.	Easting	Northing	Outcrop No.	Sample Type	Field Designation	Date Taken
PW042	13916	13608	OC054	Outcrop	Mouse Porphyry	7/25/91
PW043	13912	13305	OC056	Outcrop	Mouse Porphyry	7/25/91
PW044	13711	13227	OC058	Outcrop	Mouse Porphyry	7/25/91
PW045	13381	13059	OC063	Outcrop	Mouse Porphyry	7/25/91
PW046A	13652	12868	OC064	Outcrop	Mouse Porphyry	7/26/91
PW046B	14432	12203	OC066	Outcrop	Shell Butte	7/26/91
PW047	14410	12256	OC067	Outcrop	Precambrian	7/26/91
PW048	14347	12204	OC069	Outcrop	Mouse Porphyry(?)	7/26/91
PW049	13650	12134	OC070	Outcrop	Unknown (TIMP)	7/26/91
PW050	14424	12848	OC073	Outcrop	Precambrian	7/30/91
PW051	13498	12526		Float	Scraggy/Shell	7/30/91
PW052	12788	13333	OC076	Outcrop	Scraggy/Shell	7/30/91
PW053	15093	15355	OC081	Outcrop	Scraggy/Shell	7/30/91
PW054	13249	14648	OC082	Outcrop	Scraggy/Shell	7/31/91
PW055	13187	15242	OC086	Outcrop	Scraggy/Shell	7/31/91
PW056	12317	15810	OC087	Outcrop	Scraggy/Shell	7/31/91
PW057	12200	15208	OC090	Outcrop	Scraggy/Shell	7/31/91
PW058	13236	14130	OC093	Outcrop	Scraggy/Shell	7/31/91
PW059	13103	14054	OC094	Outcrop	Scraggy/Shell	7/31/91
PW060	12535	15339	OC097	Outcrop	Scraggy/Shell	7/31/91
PW061	12196	13236	OC100	Prospect	Scraggy/Shell?	8/3/91
PW062	12036	13465	OC101	Outcrop	Scraggy/Shell	8/3/91
PW063A	12003	13512	OC101	Outcrop	Scraggy/Shell	8/3/91
PW063B	8611	14352	OC102	Outcrop	Emerson	8/5/91
PW064	8614	14351	OC102	Outcrop	Emerson	8/5/91
PW065	8620	14175		Prospect	Skarn!	8/5/91
PW066	8805	14164		Float	Precambrian	8/5/91
PW067	9997	13780	OC103	Outcrop	Precambrian	8/5/91
PW068	9977	13743	OC103	Outcrop	Precambrian	8/5/91
PW069	11426	15228	OC104	Outcrop	Scraggy/Shell	8/6/91
PW070	11338	15046	OC109	Outcrop	Scraggy/Shell	8/6/91
PW071	11290	14806	OC110	Outcrop	Scraggy/Shell	8/6/91
PW072	10619	14350	OC111	Outcrop	Shell Butte	8/6/91
PW073	10482	14534	OC112	Outcrop	Scraggy/Shell	8/6/91
PW074	10037	14402	OC113	Outcrop	Precambrian	8/7/91
PW075	10058	14438	OC	Float	Precambrian	8/7/91
PW076	10329	14850	OC115	Outcrop	Scraggy/Shell	8/7/91
PW077	9538	14823	OC116	Outcrop	Shell Butte	8/7/91
PW078	10161	13644		Prospect	Shell Butte	8/7/91
PW079	9515	14710	OC117	Outcrop	Shell Butte	8/8/91
PW080	9249	14123	OC118	Outcrop	Shell Butte	8/8/91
PW081	8639	13700	OC119	Outcrop	Shell Butte	8/8/91
PW082	8618	13767	OC120	Outcrop	Precambrian	8/8/91
PW083	8677	14326		Float	Emerson	8/9/91

Appendix B. Sample locations (continued).

Sample No.	Easting	Northing	Outcrop No.	Sample Type	Field Designation	Date Taken
PW084	8697	14337		Outcrop	Emerson	8/9/91
PW085	8658	14282		Float	Porphyry? (Tia)	8/9/91
PW086	8842	14282	OC123	Outcrop	Quartzite	8/9/91
PW087	8817	14251	OC122	Outcrop	Marble	8/9/91
PW088	8581	14185	OC124	Outcrop	Precambrian	8/9/91
PW089	8632	14075		Outcrop	Precambrian	8/9/91
PW090	8928	6037	OC125	Outcrop	Pebble BXA	8/19/91
PW091	8903	6011	OC125	Outcrop	Pebble Breccia	8/19/91
PW092A	8762	5968	OC125	Outcrop	Dike (Tid)	8/19/91
PW092B	8887	12465	OC126	Outcrop	Antoine Porphyry?	8/20/91
PW093	8872	12474	OC126	Outcrop	Ti??	8/20/91
PW094	8982	12686	OC128	Outcrop	Precambrian	8/20/91
PW095	8964	12849	OC129	Outcrop	Augen Gneiss	8/20/91
PW096	8779	13011	OC130	Outcrop	Precambrian	8/20/91
PW097	8783	13013	OC130	Outcrop	Contact Zone	8/20/91
PW098	8782	13012	OC130	Outcrop	Antoine Porphyry(?)	8/20/91
PW099	8491	12907	OC131	Outcrop	Skarn(?)	8/20/91
PW100	9686	12493	OC135	Outcrop	Precambrian	8/21/91
PW101	9759	12925	OC138	Outcrop	Precambrian	8/21/91
PW102	8761	13330	OC144	Outcrop	Shell Butte	8/21/91
PW103	8799	13267	OC145	Outcrop	Antoine Porphyry	8/21/91
PW104	8474	13888	OC146	Outcrop	Precambrian	8/21/91
PW105	8121	12961	OC148	Outcrop	Antoine Porphyry	8/22/91
PW106	8063	12968	OC149	Outcrop	Antoine Porphyry(?)	8/22/91
PW107	8065	12965	OC149	Outcrop	Breccia	8/22/91
PW108	7861	13363	OC150	Outcrop	Antoine Porphyry	8/22/91
PW109	7872	13719	OC152	Outcrop	Antoine Porphyry(?)	8/22/91
PW110	7584	14743		Float	Breccia (Sil.)	8/22/91
PW111	7429	14939	OC154	Outcrop	Antoine	8/22/91
PW112	7443	14777	OC155	Outcrop	Antoine Porphyry	8/22/91
PW113	7451	14603	OC156	Outcrop	Emerson	8/22/91
PW114	7372	14264	OC157	Outcrop	PC Marble	8/22/91
PW115	7484	14218	OC158	Outcrop	Dike Sanidine	8/22/91
PW116	7260	13044	OC159	Outcrop	Dike (F.G.)	8/23/91
PW117	7316	13067	OC160	Outcrop	Dike (F.G.)	8/23/91
PW118	7401	13102	OC161	Outcrop	Dike (F.G.)	8/23/91
PW119	7593	13093	OC162	Outcrop	Dike (F.G.)	8/23/91
PW120	7616	13226	OC163	Outcrop	Dike (F.G.)	8/23/91
PW121	7635	13289	OC163	Outcrop	Breccia (Sil.)	8/23/91
PW122	7615	13229	OC163	Outcrop	Contact	8/23/91
PW123	7441	13587	OC165	Outcrop	Antoine Porphyry	8/23/91
PW124	7590	13869	OC167	Outcrop	PC Marble	8/23/91
PW125	7138	13708	OC168	Outcrop	Antoine Porphyry	8/23/91
PW126	7091	13976	OC169	Outcrop	Contact Zone	8/23/91

Appendix B. Sample locations (continued).

Sample No.	Easting	Northing	Outcrop No.	Sample Type	Field Designation	Date Taken
PW127	7090	13975	OC169	Outcrop	Contact Zone	8/23/91
PW128	7069	14015	OC170	Outcrop	Precambrian	8/23/91
PW129	7196	14786	OC171	Outcrop	PC Marble	8/24/91
PW130	7212	14628		Float	Contact Zone	8/24/91
PW131	7267	14589		Float	Antoine Porphyry	8/24/91
PW132	6841	14992	OC172	Outcrop	Antoine Porphyry	8/24/91
PW133	6677	14688	OC174	Outcrop	Antoine Porphyry	8/24/91
PW134	6671	14659	OC175	Outcrop	Antoine Porphyry	8/24/91
PW135	6616	13411	OC177	Outcrop	Bipyramidal Dike	8/24/91
PW136	6585	13315	OC178	Outcrop	Antoine Porphyry	8/24/91
PW137	6638	13470	OC179	Outcrop	Antoine Porphyry	8/24/91
PW138	6853	13819	OC181	Outcrop	Antoine Porphyry	8/24/91
PW139	6896	14004	OC182	Outcrop	Contact Zone	8/24/91
PW140	6970	14046	OC183	Outcrop	Precambrian	8/24/91
PW141	6896	14004	OC181	Outcrop	Chill Margin?	8/24/91
PW142	5507	14826	OC184	Outcrop	Antoine Porphyry	8/25/91
PW143	5376	14775	OC185	Outcrop	Antoine (C)	8/25/91
PW144	5382	14594	OC186	Outcrop	Green Dike	8/25/91
PW145	4779	13868	OC188	Outcrop	Antoine Porphyry	8/25/91
PW146	4753	13763	OC189	Outcrop	Pebble Dike	8/25/91
PW147	4797	13747	OC190	Outcrop	Skarn????	8/25/91
PW148	6276	14942	OC191	Outcrop	Antoine Porphyry(?)	8/26/91
PW149	6131	15240	OC192	Outcrop	Antoine Porphyry(?)	8/26/91
PW150	13342	8296	OC194	Outcrop	Tiof???????	9/4/91
PW151	13249	8284	OC195	Outcrop	Antoine Porphyry	9/4/91
PW152	13292	8165				9/4/91
PW153	9997	10717	OC197	Outcrop	Precambrian	9/6/91
PW154	9725	7277	OC201	Outcrop	Antoine	9/7/91
PW155	9723	7279	OC201	Outcrop	Fault Gouge	9/7/91
PW156	9492	6815		Float	Pebble BXA??	9/7/91
PW157	9472	7508	OC202	Outcrop	Ti???	9/7/91
PW158	9436	7547	OC203	Outcrop	Dike Sanidine	9/7/91
PW159	9389	7554	OC203	Outcrop	Dike????	9/7/91
PW160	8556	8539	OC204	Outcrop	Antoine??	9/8/91
PW161	8435	8423	OC205	Outcrop	Ti??	9/8/91
PW162	8310	8189	OC206	Outcrop	Antoine??	9/8/91
PW163	8229	8070	OC206	Outcrop	Antoine?	9/8/91
PW164	8105	7907	OC207	Outcrop	Antoine(C)	9/8/91
PW165	4905	12170	OC208	Outcrop	Antoine	9/11/91
PW166	4844	12359	OC209	Outcrop	Fluorite BXA	9/11/91
PW167	4796	12723	OC210	Outcrop	F.G. Dike	9/11/91
PW168	4734	12620	OC210	Outcrop	Antoine??	9/11/91
PW169	4881	12703	OC212	Outcrop	Dike??	9/12/91
PW170	4810	12730	OC213	Outcrop	Antoine	9/12/91

Appendix B. Sample locations (continued).

Sample No.	Easting	Northing	Outcrop No.	Sample Type	Field Designation	Date Taken
PW171	4819	12732	OC213	Outcrop	Contact BXA	9/12/91
PW172	4818	12732	OC213	Outcrop	Dikeing Phase	9/12/91
PW173A	4861	12835	OC214	Outcrop	F.G. Dike	9/12/91
PW173B	6008	13722	OC215	Outcrop	Antoine (C)	9/12/91
PW174	6155	14159	OC216	Outcrop	Antoine (C)	9/12/91
PW175	6359	14573	OC217	Outcrop	Antoine	9/12/91
PW176	6546	13665	OC218	Outcrop	Antoine	9/12/91
PW177	7163	12936	OC219	Outcrop	Fluorite BXA	9/12/91
PW178	7161	12936	OC219	Outcrop	Fluorite BXA	9/12/91
PW179	7120	12957	OC220	Outcrop	Antoine	9/12/91
PW180	6513	12517	OC221	Outcrop	Antoine (C)	9/12/91
PW181	6345	12625	OC222	Outcrop	Antoine Stockwork	9/12/91
PW182	5693	12329	OC223	Outcrop	Bipyramidal Dike	9/12/91
PW183	10563	8436	OC224	Outcrop	Precambrian	9/16/91
PW184	10437	8563	OC225	Outcrop	Antoine Porphyry	9/16/91
PW185	10400	8592		Subcrop	Skarn-like Rock	9/16/91
PW186	10413	8580	OC225	Outcrop	Basaltic? Dike	9/16/91
PW187	12447	6222	OC238	Outcrop	Antoine Porphyry?	6/20/92
PW188	12532	5205	OC247	Outcrop	Antoine Porphyry?	6/20/92
PW189	10902	5315	OC256	Outcrop	Antoine Porphyry	6/22/92
PW190	10811	5613	OC258	Outcrop	Tid(f)????	6/22/92
PW191	10500	5834	OC259	Float	Precambrian??	6/22/92
PW192	10513	5819	OC259	Subcrop	Breccia	6/22/92
PW193	9920	5720	OC261	Outcrop	Antoine Porphyry?	6/22/92
PW194	10079	5730	OC261	Outcrop	Antoine Porphyry?	6/22/92
PW195	10458	5307	OC263	Outcrop	Unknown Porphyry	6/22/92
PW196	10040	5357	OC265	Outcrop	Ti?? (Dike?)	6/22/92
PW197	11179	5252	OC267	Outcrop	Antoine Porphyry?	6/22/92
PW198	11675	5212	OC270	Outcrop	Diabase-like??	6/22/92
PW199	9378	5386	OC271	Outcrop	Antoine Porphyry?	6/23/92
PW200	9264	5476	OC273	Outcrop	Antoine Porphyry	6/23/92
PW201	9135	5488	OC274	Outcrop	Vein Material	6/23/92
PW202	8973	5465	OC275	Outcrop	Antoine Porphyry	6/23/92
PW203	8819	5485	OC276	Outcrop	Unknown "Porphyry"	6/23/92
PW204	8708	5505	OC277	Outcrop	Unknown "Porphyry"	6/23/92
PW205	7700	6148	OC283	Outcrop	Antoine Porphyry	6/23/92
PW206	7426	6093	OC284	Outcrop	Antoine Porphyry	6/23/92
PW207	7298	6109	OC285	Outcrop	Antoine Porphyry	6/23/92
PW208	8167	6027	OC287	Outcrop	Antoine Porphyry	6/25/92
PW209	8116	6090	OC288	Outcrop	Antoine Porphyry	6/25/92
PW210	7768	6802	OC289	Outcrop	Antoine Porphyry	6/25/92
PW211	7496	7476	OC290	Outcrop	Quartz Stockwork	6/25/92
PW212	7258	7702	OC291	Outcrop	Antoine Porphyry	6/25/92
PW213	7108	7858		Float	Antoine Porphyry	6/25/92

Appendix B. Sample locations (continued).

Sample No.	Easting	Northing	Outcrop No.	Sample Type	Field Designation	Date Taken
PW214	6405	8141	OC292	Outcrop	Antoine Porphyry	6/25/92
PW215	6280	8266	OC293	Outcrop	Antoine Porphyry	6/25/92
PW216	6383	8455	OC294	Outcrop	Antoine Porphyry	6/25/92
PW217	7103	8640	OC295	Outcrop	Antoine Porphyry	6/25/92
PW218	9654	5358	OC297	Outcrop	Antoine Porphyry	6/25/92
PW219	9695	5420	OC298	Outcrop	Antoine Porphyry	6/26/92
PW220	9606	5730	OC299	Outcrop	Antoine Porphyry	6/26/92
PW221	9577	5894	OC300	Outcrop	Stockwork Veins	6/26/92
PW222	9788	6164	OC310	Outcrop	Antoine Porphyry	6/26/92
PW223	9832	6134	OC302	Outcrop	Antoine Porphyry	6/26/92
PW224	9897	6094	OC303	Outcrop	Antoine Porphyry	6/26/92
PW225	10632	6556	OC304	Outcrop	Precambrian	6/26/92
PW226	11025	6195	OC305	Outcrop	Precambrian	6/26/92
PW227	6819	7356	OC310	Outcrop	Antoine Porphyry?	6/29/92
PW228	6974	7041	OC311	Outcrop	Antoine Porphyry?	6/29/92
PW229	6971	6814	OC312	Outcrop	Antoine Porphyry?	6/29/92
PW230	8273	8312	OC314	Outcrop	Antoine (C)	7/2/92
PW231	7735	8589	OC316	Outcrop	Antoine (C)	7/2/92
PW232	7743	8872	OC322	Outcrop	Antoine (C)	7/4/92
PW233	7469	9257	OC328	Outcrop	Antoine (C)	7/6/92
PW234	7329	9305	OC330	Outcrop	Antoine (C)	7/6/92
PW235	7468	9642	OC332	Outcrop	Breccia Tia(C)	7/6/92
PW236	7475	9650	OC332	Outcrop	Fluorite BXA	7/6/92
PW237	12763	5212	OC334	Outcrop	Cambrian Flthd	8/6/92
PW238	12720	5503	OC335	Outcrop	Precambrian	8/6/92
PW239	12601	5538	OC336	Outcrop	Skarn-like	8/6/92
PW240	12498	5787	OC337	Outcrop	Precambrian	8/6/92
PW241	12315	5917	OC339	Outcrop	Antoine Porphyry	8/6/92
PW242	5899	6949	OC340	Outcrop	PC/Porphyry Contact	8/7/92
PW243	6563	6746	OC341	Outcrop	Late Dike??	8/7/92
PW244	6507	6745	OC341	Outcrop	Quartz Veins	8/7/92
PW245	6489	6796	OC342	Outcrop	Antoine Porphyry	8/7/92
PW246	6900	8866	OC343	Outcrop	Antoine Porphyry	8/10/92
PW247	6772	8876	OC344	Outcrop	Antoine (C)	8/10/92
PW248	6052	9733	OC347	Outcrop	Antoine (C)	8/10/92
PW249	6994	9255	OC349	Outcrop	Antoine (C)	8/7/92
PW250	10381	6997	OC353	Outcrop	Unknown Porphyry	8/11/92
PW251	11992	6070	OC356	Outcrop	Shell Butte??	8/11/92
PW252	11916	6519	OC362	Outcrop	Precambrian	8/12/92
PW253	12264	7771	OC370	Outcrop	Shell Butte	8/12/92
PW254	9146	6918	OC377	Outcrop	Intrusive BXA	8/13/92
PW255	8916	6981	OC378	Outcrop	Unknown Porphyry	8/13/92
PW256	5063	8979	OC389	Outcrop	Antoine Porphyry	8/14/92
PW257	5757	8356	OC390	Outcrop	Antoine Porphyry	8/14/92

Appendix B. Sample locations (continued).

Sample No.	Easting	Northing	Outcrop No.	Sample Type	Field Designation	Date Taken
PW258	8168	7222	OC401	Outcrop	Antoine (C)?	8/18/92
PW259	8087	7350	OC402	Outcrop	Antoine (C)?	8/18/92
PW260	7823	7620	OC404	Outcrop	Antoine Porphyry	8/18/92
PW261	7503	8035	OC407	Outcrop	Antoine (C)	8/18/92
PW262	7215	8482	OC408	Outcrop	Antoine Porphyry??	8/18/92
PW263	7238	8367	OC409	Outcrop	Precambrian??	8/18/92
PW264	12875	6940	OC419	Outcrop	Breccia (L.S.)	8/20/92
PW265	6799	9201	OC425	Outcrop	Dike	8/21/92
PW266	9640	9935	OC432	Outcrop	Antoine Porphyry	8/24/92
PW267	9706	9997	OC437	Outcrop	Dike??	8/24/92
PW268	10068	8951	OC440	Outcrop	Precambrian ??	8/24/92
PW269	10054	8877	OC440	Outcrop	Intrusive Breccia???	8/24/92
PW270	8918	9211	OC441	Outcrop	Dike?	8/24/92
PW271	8634	10413	OC443	Outcrop	Antoine Porphyry??	8/25/92
PW272	7608	10529	OC449	Outcrop	Antoine (C)	8/25/92
PW273	6887	11537	OC456	Outcrop	Antoine (C)	8/27/92
PW274	7081	11504	OC457	Outcrop	Medusa Breccia	8/27/92